DESIGN OF A NOVEL NON-CONTACT TEMPERATURE CONTROLLED SURGICAL LASER SYSTEM

by

Özgür Kaya

B.S., in Electrical & Electronics Engineering, Koç University, 2004

M.S., in Biomedical Engineering, Delft University of Technology, 2009

Submitted to the Institute of Biomedical Engineering

in partial fulfillment of the requirements

for the degree of

Doctor

of

Philosophy

Boğaziçi University

2023

PREFACE

It is not easy to conduct a graduate study in Turkey. Funding is scarce, resources and infrastructure are limited. Ph.D. candidates are viewed first as students and then as quasi-researchers. If you are lucky/unlucky enough to get a position as a research assistant, then you can get compensation for your efforts. Even so, you are expected to do a multitude of tasks depending on your talents that are not related to your or any other research. These tasks can include secretarial and administrative duties, organization of conferences, or being a computer technician, electrician, lathe operator, construction worker, photographer, videographer, graphic designer, qualified slave, unqualified laborer, and all around problem solver.

Even when you successfully dodge or overcome these obstacles, there is always the ever-present turmoil within the country that takes your focus away from your research. Political and intellectual conflicts may cause grant applications to be refused, independent of their scientific merit. The struggle for power and control over all institutions and values affects your intellectual mind and psychological wellbeing. You feel obliged to resist against cutting down trees in a park as a symbol of protecting your ideology, meanwhile risking your health, life and putting your research aside. You feel obliged to express that people have certain basic rights only to become the target of a country wide witch-hunt. It is not easy to be an independent, intellectual, freethinker in this country where you are expected to be just an ignorant and mindless follower.

As you can imagine, this dissertation is the result of several years of hard work spent in an obstacle course. Occasionally, it also felt like swimming against the stream. You can practically consider the text itself as an "end of level boss." Now, it is time for overcoming new and bigger bosses.

ACKNOWLEDGMENTS

To my amazing family, for providing me with all kinds of support throughout this madness called the Ph.D. study. Especially, my mother, Dr. Güner Kaya, and my cousin, Dr. Mehmet Emre Hatipoğlu, acted as devil's advocates and unofficial academic & research advisors for me. You guys are my role model for an excellent academician, life-long student, researcher, activist, rebel, altruist, and more importantly, a good human being. I hope to live up to the example you have set up.

To my wonderful ex-partner, Beria Elif Ökçün, for providing me with emotional support throughout my Ph.D. journey. Thank you for being a constant cheerleader for me. You are my role model for being a lovely wise-ass and a polymath.

I am grateful to my advisor, Dr. Murat Gülsoy, for his kind and sincere guidance and support on all aspects of my Ph.D. journey. He enabled me to see the big picture and focus back on to what matters when I lost myself in the details as an OCD-prone person. He is a multifaceted, multitalented person whom I look up to. I would like to thank my co-advisor, Dr. İnci Çilesiz, for sharing her expertise on my research subject and on being an academician. Her perfectionist yet positive and supportive attitude helped me to grow into a better researcher. I am also thankful to Dr. Adnan Kurt for guiding me regarding optics and IR temperature sensors.

I can never sufficiently express my gratefulness to İpek Düzgören for assisting me with the arduous experiments, and Dr. Bora Büyüksaraç for helping out with CAD drawings of custom-designed parts required for my device.

I also want to thank Dr. Hamdi Torun for giving me the last push I needed to get my manuscript published. His support replenished my resolve to complete this dissertation, as well.

A very special gratitude goes out to my fellow lab rats, friends, in the Biophotonics Research Group and the rest of the members of the Institute of Biomedical Engineering for providing perspective to scientific subjects when I needed one. We shared a lot. I especially appreciated our barbecue dinners at the terrace, lunches at the seaside, and of course, the drinks that went with them. You have made this long struggle a lot more fun than any Ph.D. candidate can expect to experience.

And last but not least, I would like to thank the Institute staff, Çiğdem Günsur Çelik and Ayşegül Ünal, for always looking out for me.

This thesis study was financially supported by a matching grant (BAP-8500 14XM2) provided by the Boğaziçi University Research Fund.

ACADEMIC ETHICS AND INTEGRITY STATEMENT

I, Özgür Kaya, hereby certify that I am aware of the Academic Ethics and Integrity Policy issued by the Council of Higher Education (YÖK) and I fully acknowledge all the consequences due to its violation by plagiarism or any other way.

Name :

Signature:

Date:

ABSTRACT

DESIGN OF A NOVEL NON-CONTACT TEMPERATURE CONTROLLED SURGICAL LASER SYSTEM

Achieving repeatable and successful results without causing excessive collateral damage is of paramount importance for photothermal laser applications. Conventionally, dosimetry studies are conducted on laboratory animals to determine ideal laser parameters. Unfortunately, these predetermined parameters cannot ensure patient safety and treatment success in the clinic due to variance between optical and thermal characteristics among subjects. Controlling laser irradiation with tissue temperature feedback is the current gold standard for various photothermal treatments. In this dissertation, I present the development of a compact and easy to use non-contact radiometric temperature measurement and laser control system based on a commercial, inexpensive IRt/c sensor. This thesis study establishes the validity of my design that potentially makes temperature control more accessible in clinical environments. I have shown the ability of this system to maintain tissue temperature at a set value over extended durations (60 s) using *ex vivo* Wistar albino rat skin. Additionally, I evaluated the practical performance of this system by *ex vivo* photocoagulation of bovine liver using two independent variables: laser power and target temperature. Temperature-time responses of samples varied significantly, in agreement with our expectations, confirming a wide range of optical and thermal coefficients. Using target temperature as an independent variable, this system was successful in regulating the coagulation zone. Moreover, it was able to prevent undesired thermal damage in all but two samples (out of 144). I have also shown that this system can produce scientifically valuable information for photothermal characterization of tissues.

Keywords: Temperature Regulation, Laser Control, Medical Laser Treatment, Photothermal Interactions.

ÖZET

ÖZGÜN TEMASSIZ SICAKLIK KONTROLLÜ CERRAHİ LASER SİSTEMİ TASARIMI

Isıl-ışıl laser uygulamaları için aşırı çevresel hasar oluşturmadan tekrarlanabilir ve başarılı sonuçlar elde etmek büyük önem taşır. Geleneksel olarak, ideal laser parametrelerinin belirlenmesi için laboratuvar hayvanları üzerinde dozimetri çalışmaları yapılır. Ancak, önceden belirlenmiş olan parametreler kişiler arası optik ve ısıl karakteristiklerin farklı olması nedeniyle hasta güvenliğini ve uygulama başarısını garanti edemez. Laser ışımasını doku sıcaklığı geri beslemeli olarak kontrol etmek çeşitli ısıl-ışıl tedaviler için altın standarttır. Bu tezde düşük maliyetli bir IRt/c sensörü temelli, kompakt ve kolay kullanılabilir bir temassız radyometrik sıcaklık ölçüm ve laser kontrol sisteminin geliştirilmesini sunuyorum. Bu çalışma, sıcaklık kontrolünü klinik ortamlarda daha erişilebilir kılma potansiyeline sahip olan tasarımımın geçerliliğini ortaya koymaktadır. Sistemin doku sıcaklığını uzun süre (60 s) boyunca istenilen sıcaklıkta tutabildiğini *ex vivo* Wistar albino sıçan derisinde gösterdim. Ayrıca, sistemin pratikteki performansını *ex vivo* sığır karaciğerinin iki bağımsız değişken (laser gücü ve hedef sıcaklık) kullanarak fotokoagülasyonu ile değerlendirdim. Örneklerin sıcaklık-zaman tepkilerindeki önemli derecedeki farklılık optik ve ısıl katsayıların geniş bir aralıkta değiştiğini destekledi. Hedef sıcaklığın bağımsız bir değişken olarak kullanılmasıyla bu sistem koagülasyon alanını başarıyla regüle etti. Bunun yanı sıra, sistem, istenmeyen ısıl hasarı 144 örnekten ikisi haricinde engelledi. Ayrıca, bu sistemin dokuların ısıl-ışıl karakterizasyonu için bilimsel değeri olan veriler üretebildiğini gösterdim.

Anahtar Sözcükler: Sıcaklık Regülasyonu, Laser Kontrolü, Medikal Laser Uygulaması, Isıl-ışıl Etkıleşimler.

TABLE OF CONTENTS

PREFACE . . . iii
ACKNOWLEDGMENTS . . . iv
ACADEMIC ETHICS AND INTEGRITY STATEMENT . . . vi
ABSTRACT . . . vii
ÖZET . . . viii
LIST OF FIGURES . . . xiii
LIST OF TABLES . . . xvi
LIST OF SYMBOLS . . . xviii
LIST OF ABBREVIATIONS . . . xx
1. OVERVIEW . . . 1
2. INTRODUCTION . . . 2
3. THEORETICAL BACKGROUND . . . 8
3.1 Photothermal Interactions . . . 8
3.2 Thermo-Physiological Effects . . . 15
3.3 Temperature Dependence of Tissue Properties . . . 18
3.4 IR Radiometric Temperature Measurement . . . 19
4. MATERIALS & METHODS: DESIGN & DEVELOPMENT OF THE TEMPERATURE CONTROLLED MEDICAL LASER SYSTEM . . . 27
4.1 Temperature Measurement System . . . 29
4.1.1 IRt/c Sensor . . . 30
4.1.2 Electronic Design . . . 36
4.1.3 Optical & Mechanical Design . . . 36
4.2 Laser System . . . 43
4.2.1 Laser Source . . . 43
4.2.2 Laser Irradiation Control Methods . . . 43
4.2.3 Beam Delivery Optics . . . 44
4.3 Temperature Controlled Medical Laser System . . . 46
4.3.1 Microcontroller Development . . . 47
4.3.2 Communication . . . 48

4.3.3 Noise, Power Source, and Bluetooth Connection 49
4.3.4 IRt/c Sensor Readout 50
4.3.5 Control of Laser Irradiation 52
5. STUDY 1: MEASUREMENT OF SYSTEM SPECIFICATIONS 53
5.1 Materials & Methods 53
5.1.1 Microcontroller Techniques 53
5.1.2 Calibration & Accuracy 54
5.1.3 Spatial Resolution 54
5.1.4 Temporal Response 55
5.2 Results & Discussion 56
5.2.1 Accuracy 56
5.2.2 Spatial Resolution 57
5.2.3 Temporal Response 57
6. STUDY 2: TEMPERATURE CONTROLLED IRRADIATION ON WISTAR ALBINO RAT SKIN 59
6.1 Study 2 Materials & Methods 59
6.1.1 Non-contact Temperature Controlled Medical Laser System . . 59
6.1.2 Temperature Controlled Laser Irradiation Procedure 62
6.2 Study 2 Results & Discussion 62
7. STUDY 3: CONTROLLED THERMAL DENATURATION ON BOVINE LIVER TISSUE 65
7.1 Study 3 Materials & Methods 66
7.1.1 Non-contact Temperature Controlled Medical Laser System . . 66
7.1.2 Thermal Denaturation of Bovine Liver Tissue 68
7.1.3 Evaluation of Thermal Denaturation Area & Statistical Analysis 69
7.2 Study 3 Results & Discussion 71
7.2.1 Temperature-Time Response 71
7.2.2 Thermal Denaturation 79
8. CONCLUSION 90
8.1 Future Research & Development Options 91
APPENDIX A. ADJUSTING IRt/c SENSOR SETTINGS 93
A.1 PC to I^2C Adaptor (I2C2PC) Terminal Settings using Realterm 94

A.2 IRt/c Sensor Settings . . . 94
A.2.1 Read Settings . . . 94
A.2.2 Original Settings . . . 95
A.2.3 Normal Operation & Response Time Measurement(Fast) . . . 95
A.2.4 Spot Size Measurement (Moderate) . . . 95
A.2.5 Accuracy Measurement & Calibration (Slow) . . . 96
A.2.6 Change IIR & FIR Settings . . . 96
A.2.7 Change Sensor SMBus Address to B4 (5A in 7bit notation) . . . 96
APPENDIX B. MICROPROCESSOR CODES . . . 97
B.1 Watchdog Timer (WDT) Pushbutton Debouncing . . . 97
B.1.1 Initiate Watchdog Timer . . . 97
B.2 UART . . . 98
B.2.1 UART Baudrate Settings Registers . . . 98
B.2.2 UART Buffer Settings and Variable Initializations . . . 100
B.2.3 USCI_A1 Interrupt Service Routine for UART . . . 101
B.2.4 Watchdog Timer Interrupt Service Routine . . . 102
B.3 Hardware Stopwatch . . . 102
B.3.1 Initial TIMERA2 Setup . . . 103
B.3.2 `tic()` . . . 103
B.3.3 `toc()` . . . 103
B.4 Readout from MLX90614 Sensor . . . 104
B.4.1 Initialize I^2C for SMBus Operation . . . 104
B.4.2 Raw Data Readout . . . 104
B.4.3 “Divide & Conquer” Temperature Conversion . . . 106
B.5 Moving Window Average . . . 107
B.5.1 Variable Initializations . . . 107
B.5.2 Averaging Function . . . 107
B.5.3 Window Size Selection . . . 108
B.6 Periodic Sensor Readout . . . 110
B.6.1 TIMERA0 Settings . . . 110
B.6.2 Readout Interval Selection . . . 111
B.7 Laser Control Signal (TTL) . . . 112

B.8 Continuous Temperature Controlled Operation 113
B.8.1 TIMERA0 Interrupt Service Routine 113
B.9 5 s Temperature Controlled Operation 114
B.9.1 Main Code 114
B.9.2 TIMERA0 Interrupt Service Routine 115
B.10 Temperature Monitored Fixed-Dose Operation 117
B.10.1 Main Code 117
B.10.2 TIMERA0 Interrupt Service Routine 119
APPENDIX C. CONFERENCE PRESENTATION 122
APPENDIX D. PUBLISHED CONFERENCE PROCEEDING 132
APPENDIX E. PUBLISHED ARTICLE 142
REFERENCES 159

LIST OF FIGURES

Figure 3.1	Flow chart with important parameters and processes for photothermal interactions.	8
Figure 3.2	Propagation of light for biological tissues.	9
Figure 3.3	The Jablonski diagram describing the possible fates of excitation.	11
Figure 3.4	Critical temperatures for the occurrence of cell necrosis.	16
Figure 3.5	Location of thermal effects inside biological tissue.	17
Figure 3.6	Characteristic emission spectrum for black bodies at various absolute temperatures.	21
Figure 4.1	Schematic of the Temperature Controlled Medical Laser System.	28
Figure 4.2	Initial design of the beam delivery optics.	29
Figure 4.3	Melexis IRt/c Sensor Chips in Mini TO-46 & TO-39 Housing.	31
Figure 4.4	Block Diagram of Texas Instruments TMP006 IR MEMS Sensor.	31
Figure 4.5	Melexis IRt/c Sensor MLX90614ESF-BCC.	32
Figure 4.6	Block Diagram of the Melexis IRt/c Sensor Chips [62].	32
Figure 4.7	Accuracy of MLX90614 except for xCK type (Ta: ambient temperature, To: object temperature) [62].	33
Figure 4.8	Field of View of MLX90614ESF-BCC [62].	34
Figure 4.9	IIR & FIR Filter Settings and Corresponding Settling Times for MLX90614 Series Sensors [62].	35
Figure 4.10	Electronic Circuit for SMBus communication of MLX90614ESF-BCC [62].	36
Figure 4.11	Transmission Spectra of Various Materials and Corresponding Temperatures.	39
Figure 4.12	Crystran 3 µm to 11 µm AR Coated ZnSe Lens.	39
Figure 4.13	SM05–10 mm Lens Adapter.	39
Figure 4.14	Ray Tracing Analysis of Melexis 90614ESF-BAA IRt/c Sensor & Thorlabs C036TME-F IR Lens Combination.	40
Figure 4.15	Ray Tracing Analysis of Melexis 90614ESF-BCC IRt/c Sensor & Crystran ZnSe10 IR Lens Combination 1.	40

Figure 4.16	Ray Tracing Analysis of Melexis 90614ESF-BCC IRt/c Sensor & Crystran ZnSe10 IR Lens Combination 2.	40
Figure 4.17	Thorlabs SM05 Lens Tubes and A Retaining Ring ($\varnothing = 12.7\,\mathrm{mm}$) [64].	41
Figure 4.18	Technical Drawing of the MLX90614XCC package (all dimensions in mm) [62].	42
Figure 4.19	Bare Singlemode Fiber Coupler (F-91-C1, Newport Corp., USA) & Focusing Objective (Plan-Neofluar 10x/0.30 M27, Zeiss, Germany).	45
Figure 4.20	Thorlabs Bare Fiber Terminator [64].	45
Figure 4.21	MSP430 F5529 Launchpad Microcontroller.	47
Figure 4.22	Fuel Tank, BOOSTXL-BATPAKMKII, Texas Instruments.	49
Figure 4.23	Bluetooth SSP (Standard Serial Port) Adapter, HC06, Generic.	50
Figure 4.24	Calibration Data & Linear and 2^{nd} Order Polynomial Trendlines (x-axis: RAW data [int], y-axis: temperature [℃]).	51
Figure 4.25	Calibration Data & Bi-Linear Trendlines (x-axis: RAW data [int], y-axis: temperature [℃]).	51
Figure 5.1	The blackbody calibrator and the knife-edge test setup.	55
Figure 6.1	Fiber coupling (top) and laser beam delivery (bottom) assemblies.	59
Figure 6.2	Temperature controlled laser irradiation setup.	61
Figure 6.3	Temperature controlled laser irradiation.	63
Figure 7.1	Experiment setup.	67
Figure 7.2	Temperature monitorization data of the temperature controlled application.	72
Figure 7.3	Temperature monitorization data of the fixed-dose application.	74
Figure 7.4	Box and whiskers plot of the tissue temperature reached at the end of exposure in the fixed-dose application.	75
Figure 7.5	Synergistic effect of measurement noise and discrete refresh time on temperature variation at target value.	77
Figure 7.6	Exemplary bovine liver photothermal denaturation photographs for temperature controlled application groups.	80

Figure 7.7 Box and whiskers plot of thermal denaturation diameters and depths of the temperature-controlled experiment. 81

Figure 7.8 Box and whiskers plot of thermal denaturation diameters and depths of the fixed-dose application. 81

Figure A.1 Settling Times of 90614-BCC Sensors for Various IIR & FIR Filter Settings. 93

Figure A.2 I2C2PC Device. 93

LIST OF TABLES

Table 3.1	Thermal effects of laser irradiation.	15
Table 3.2	IR sensor types, examples and characteristics.	23
Table 4.1	User requirements and related general specifications.	27
Table 4.2	IR Transmissive Materials [63, 64].	37
Table 5.1	Transient error (measurement noise) for thermo-physiologically important temperatures.	58
Table 5.2	Individual process durations of the temperature measurement system.	58
Table 6.1	Temperature values used for the performance evaluation of the system.	61
Table 6.2	Performance characteristics for thermo-physiologically important temperatures.	64
Table 7.1	Average dose of temperature controlled (experiment) groups and their corresponding fixed-dose (control) exposure durations.	68
Table 7.2	Descriptive temperature values for the surface temperature controlled application.	73
Table 7.3	Descriptive temperature values for the fixed-dose application.	73
Table 7.4	Temperature Controlled Application Results of Thermal Denaturation Diameters and Depths.	82
Table 7.5	Fixed-Dose Application Results: The mean (μ) and standard deviation (σ) of thermal denaturation diameters and depths.	82
Table 7.6	One-way ANOVA of thermal denaturation diameter.	83
Table 7.7	One-way ANOVA of thermal denaturation depth.	83
Table 7.8	Results of post hoc tests after one-way ANOVA of thermal denaturation diameter and depth values in the temperature-controlled experiment.	84
Table 7.9	Results of post hoc tests after one-way ANOVA of thermal denaturation diameter and depth values in the fixed-dose experiment.	85

Table 7.10 Temperature Controlled Application Results: Two-way ANOVA of thermal denaturation diameter. 87

Table 7.11 Temperature Controlled Application Results: Two-way ANOVA of thermal denaturation depth. 87

Table 7.12 Fixed-Dose Application Results: Two-way ANOVA of thermal denaturation diameter. 87

Table 7.13 Fixed-Dose Application Results: Two-way ANOVA of thermal denaturation depth. 87

Table A.1 PC to I^2C Adaptor (I2C2PC) Terminal Settings. 94

LIST OF SYMBOLS

$A_{\text{Arrhenius}}$	Arrhenius' constant
b	Wien's displacement constant
c	Specific heat capacity
$C(t)$	Concentration at a time t
C_0	Initial concentration of molecules or cells
c_{light}	Speed of light in vacuum
D_{d}	Damage degree
f	Focal length of a lens
h	Planck's constant
$I(z)$	Light intensity at propagation distance z
I_0	Initial light intensity
j_Q	Heat flow
k	Heat conductivity
k_{B}	Boltzmann's constant
L	Optical penetration depth
m	Mass [g]
n	Index of refraction before boundary surface, complex value
n'	Index of refraction after boundary surface
n_{I}	Index of refraction, imaginary component
n_{R}	Index of refraction, real component
Q	Heat [J]
R	Universal gas constant
T	Temperature [K]
t	Time [s]
$W(T)$	Radiant emittance of a blackbody at absolute temperature T
$W_\lambda(T)$	Emissive power at a specific wavelength
$z_{\text{therm}}(t)$	Time-dependent thermal penetration depth
α	Optical absorption coefficient

$\alpha_{\text{scattering}}$	Optical scattering coefficient
α_{total}	Total optical attenuation coefficient
ΔE	Specific tissue property
$\varnothing$	Diameter
$\epsilon(T)$	Emissivity at absolute temperature T
ϵ	Emissivity
$\epsilon_\lambda(T)$	Wavelength-dependant emissivity at absolute temperature T
κ	Temperature conductivity (thermal diffusivity)
λ	Wavelength
λ_{peak}	Wavelength of peak emission
Ω	Specific tissue property
ρ	Density
σ	Stefan-Boltzmann constant
τ	Laser pulse duration
τ_{therm}	Thermal relaxation time
θ	Angle of incidence [°]
θ'	Angle of refraction [°]

LIST OF ABBREVIATIONS

BNC	Bayonet Neill-Concelmann (a connector type for coaxial cables)
CW	Continuous Wave
FOV	Field-of-view
H&E	Hematoxylin & Eosin (a histological stain)
I^2C / IIC	Inter-Integrated Circuit (a serial computer bus protocol)
IC	Integrated Circuit
IR	Infrared
IRt/c	Infrared Thermocouple
ISR	Interrupt Service Routine
LiPo	Lithium Polymer
LLLT	Low Level Laser Therapy
LTW	Laser-Tissue Welding
MEMS	Micro-Electro-Mechanical Systems
MOEMS	Micro-Opto-Electro-Mechanical Systems
NBT	Nitroblue Tetrazolium Chloride (a histological stain)
PBM	Photobiomodulation
PDT	Photodynamic Therapy
PTT	Photothermal Therapy, throughout this dissertation PTT is used to describe not only nanoparticle-assisted photothermal therapy but a wider application of all thermally functional medical laser applications (photothermal laser treatments)
PWM	Pulse Width Modulation
SMA	SubMiniature version A (a connector type for optical fibers)
SMBus	System Management Bus (a subset of I^2C)
SNR	Signal to Noise Ratio
SSP	Synchronous Serial Port (a serial communication interface)
TTC	Triphenyltetrazolium Chloride (a histological stain)
TTL	Transistor-Transistor Logic

t/c	Thermocouple
UART	Universal Asynchronous Receiver/Transmitter
USB	Universal Serial Bus
WDT	Watchdog Timer (a microprocessor peripheral)

1. OVERVIEW

Introduction, Chapter 2, presents the reader with an in depth literature survey as well as the motivation behind this study and its aims. Theoretical Background, Chapter 3, provides necessary information for understanding the photothermal laser-tissue interactions, thermal tissue damage, physiological phenomena affecting tissue temperature, and physical laws governing the subjects in this thesis. Chapter 3 is essential for understanding the design limitations and engineering decisions made during the development of the temperature measurement and laser control system that is the subject of this thesis. The design and development process of this system is provided in Chapter 4, which can help developing invaluable insight for optical, opto-mechanical, opto-electronical, and microcontroller device development.

Chapters 5 to 7 cover independent experiments. Each of these chapters contain its own materials & methods and results & discussion sections for the sake of simplicity. The system characterization and measurement of its specifications is elaborated in Chapter 5. The Wistar albino rat skin study described in Chapter 6 demonstrates that our system is capable of maintaining tissue temperature at the desired level over extended periods of time. The *ex-vivo* bovine liver coagulation study detailed in Chapter 7 compares fixed-dosimetric and temperature-controlled photocoagulation and proves that our system can be used for controlling the extent of thermal tissue denaturation as well as ensuring patient safety.

The conclusion of this thesis study, improvement opportunities, and suggestions for future research are provided in Chapter 8. Appendices A and B provide the microprocessor codes composed for this thesis study and the instructions for setting IRt/c sensor parameters, respectively. Appendices C to E contain the presented or published works from this thesis project.

2. INTRODUCTION

When the first laser was invented in 1960, it was defined as a solution looking for a problem, as well as being magnificent [1]. Since then, lasers have been the solution to various problems of modern society, including scientific, military, industrial, medical, information technologies and consumer electronics applications. Shortly after their discovery, the first trials of medical applications of lasers were conducted in the field of ophthalmology, and the results were published in 1961 [2]. This trend was followed in the field of dentistry and other medical fields at the end of the decade. Today, various modalities of medical laser applications are commonly used throughout the world. Most of these applications are minimally invasive procedures, which aim to provide successful treatment with the least possible collateral damage.

Medical laser applications in photothermal region rely heavily on the realized tissue temperature to achieve desired thermo-physiological effects [*e.g.*, hyperthermia (>45 °C), reduction in enzyme activity and cell immobility (>50 °C), necrosis, denaturation of proteins and collagen (>60 °C), coagulation (>60 °C), coagulative necrosis, permeabilization of membranes (>80 °C), heat fixation, vaporization (>100 °C), decomposition/thermal-ablation (>100 °C), carbonization (>100 °C), and melting (>300 °C)] [3]. The various thermal effects of laser irradiation are provided in Table 3.1. Since thermal damage of the biological tissues are described as the first order Arrhenius rate equation, the onset of necrosis is also dependent on the temporal duration of the tissue temperature as depicted in Figure 3.4 [3].

Depending on the surgical procedure, it is necessary to ensure that some of these effects are generated while preventing some others. Laser tissue welding (LTW) [4–13], photocoagulation [14], ablation of various soft and hard tissues [15,16], angioplasty [17, 18], treatment of granulation tissues [19], treatment of hemangioma [20], cartilage regeneration [21] and reshaping [22, 23] are among the possible medical photothermal laser treatments (PTT). All of these procedures are highly temperature dependent

because thermo-physiological interactions occur within a narrow temperature range. Any deviation from this range may result in treatment failure or excessive thermal damage [10]. However, if a certain temperature value is exceeded, thermal damage is eminent in the target and proximal tissues, which causes prolongation of recovery time and in some cases even failure of the treatment [4, 7, 8, 10, 17].

For instance, photothermal treatment of granulation tissue aims to trigger apoptosis by hyperthermia (45 °C to 50 °C) induced heat shock protein production without causing necrosis (>50 °C) [19]. Another example for a highly temperature sensitive application is LTW. Optimally, LTW requires temperatures between 65 °C and 70 °C (skin tissue) [24] to ensure collagen denaturation (>63 °C for treatment success) while preventing excessive thermal damage (coagulative necrosis, heat fixation [25]) resulting in scarring and prolonged recovery time. Currently, both treatment of granulation tissue and LTW are experimental procedures, not regularly used in clinical environment due to reproducibility and safety issues.

It is important to ensure the thermal effect is limited to the region of interest in order to prevent collateral damage to the surrounding tissue. Thermo-physiological effects have a specific location inside the tissue, as elaborated in Section 3.2, analogous to the temperature distribution within the tissue as a result of laser exposure. Tissue temperature and its distribution, in turn, is a function of generated heat, laser parameters (wavelength, power, spot size, exposure time, operation mode), optical and thermal properties of the tissue including perfusion characteristics [26].

The most common method to prevent thermal damage and ensure the temperature dependent treatment success during PTT is conducting tissue and treatment specific dosimetry studies [17, 27]. The laser parameters deduced from dosimetry studies, despite being an open loop control method, provide a good starting point. Nonetheless, the temperature rise within the tissue depends on various independent parameters other than the laser parameters. Additionally, the controlled condition of the laboratory environment and uniformity of research animals can hardly be encountered in the clinic. In real life, the optical and thermal properties of subjects may not only change

interpersonally, but also within the same person depending on time, health condition, and diet [26, 28]. Even the psychological status of the patient is an important factor since the secretion of adrenaline and cortisol have a tremendous effect on tissue perfusion. In turn, tissue perfusion significantly modifies the thermal properties of the irradiated tissue because the heat transfer heavily depends on the perfusion. Thus, one cannot expect to end up with the same successful results when using laser parameters only defined by dosimetry studies. Even though dosimetry studies provide a limited safety in laboratory conditions, they are not sufficient on their own for clinical usage. A predetermined dose may result in successful treatments in the majority of subjects, but may also lead to treatment failure and/or excessive thermal damage in some subjects.

Another example of open loop control for surgical laser applications is external cooling of tissues. There are several published methods (cold saline dripping [9], cryogenic spray [20], heat sink [29]) available for this purpose. Yet, these methods provide uncontrolled cooling of only the tissue surface, thus bear the risk of unsuccessful thermal damage prevention of underlying tissue, as well as treatment failure at the surface tissue. Therefore, closed loop control systems are recommended [21].

The oldest closed loop control system is the surgeon/operator himself. In this method, the surgeon ceases the laser exposure by evaluating visual clues of thermal effects. Among those visual clues are opacification (whitening), desiccation, shrinkage, and carbonization [10]. These visual clues are vague, highly subjective, and their perception and evaluation is experience dependent. Besides, this method relies on human reflexes, which are slow when compared to the temperature rise due to laser exposure. Especially around 80 °C, the temperature increase has a time-exponential characteristic; and it is difficult to respond to, enhancing the risk of thermal damage.

Similarly, there are closed loop control systems that measure the temperature dependent optical properties of tissues (reflection and scattering coefficients) by means of opto-electronical systems [30]. However, as these temperature dependent optical property changes emerge with a slight delay, this laser control method is generally incompetent in preventing thermal damage. Therefore, conducting PTT with real-

time tissue temperature feedback control is necessary.

The measurement of tissue temperature, which is the actual cause of thermal damage, provides the most successful treatment results according to a plethora of research groups [4,7,8,10,12,18,19,24,31–34]. A tissue temperature controlled medical laser system ensures treatment success, standardization and patient safety. It also compensates for inexperienced operators increasing reproducibility of results for current PTT modalities used in the clinic. Consequently, a temperature controlled system may endorse the translation of experimental laser techniques (*e.g.*, LTW, granulation tissue treatment, cartilage reshaping), which currently are limited to the controlled environment of the laboratory, into regular clinical practice. Such a system may also be used in the research of thermal characteristics of tissues and development of new laser treatment techniques. Additionally, it can be used for preventing undesirable temperature increase during photochemical procedures (*e.g.*, photodynamic therapy and low-level laser therapy), which are non-thermal processes by nature [35,36].

There are a multitude of feasible configurations for tissue temperature feedback control of PTT. Thermocouples are not among the feasible systems, even though they are elementary among the temperature measurement techniques [37]. They are simple to implement, and cost efficient. Unfortunately, it is not feasible to use any sensor requiring physical contact, including thermocouples, for laser exposure control medical applications. Contacting an opaque object (*e.g.* thermocouple) to the treatment site may interfere with the laser irradiation by changing the beam-profile, as well as posing a risk for contamination, and adherence to tissue. Additionally, the temperature measurement will also be affected due to the absorption of the laser irradiation by the thermocouple, which may result in erroneous control of the laser exposure. A work-around for these problems is the placement of the thermocouple to the proximal periphery of the laser spot [38]. Yet, this method is incapable of measuring the actual tissue temperature at the target site.

Measurement of blackbody radiation for determination of the surface tissue temperature is a non-contact method devoid of the above mentioned drawbacks. This

method is also called the infrared (IR) thermometry/radiometry, because the blackbody radiation is mainly in the IR region of the electromagnetic spectrum. IR thermometry is the current gold-standard for non-contact temperature measurement. Various research groups exploited blackbody radiation by utilizing various types of IR radiometric sensors to design and develop temperature measurement and control systems for medical laser applications [5, 6, 8–10, 12, 15, 22, 39, 40]. These systems excel at various aspects of temperature control (*e.g.*, fast response time, small measurement region, high accuracy, high resolution) but mostly share a common drawback: the requirement of multiple costly apparatus that are complicated to use in the clinical environment. Currently, there are no systems that are low-cost, compact, and easy to operate.

Presently, there is also a growing interest for photoacoustic thermometry for the control of PTT [14, 41]. The advantage of this method is that it can provide non-contact, non-interfering and even subsurface temperature measurement. Unfortunately, this method is not easy to implement and requires multiple sophisticated and costly apparatus.

In a nutshell, current temperature measurement and laser control systems are either considerably complicated to operate and bulky to transfer to the clinic or insufficient with respect to system specifications like readout speed, accuracy and bandwidth. So far, technological limitations have prevented the development of temperature-controlled surgical laser systems that are feasible and sufficient for clinical use. There is a need for such a system both for scientific research and clinical implementation.

Therefore, the aim of this Ph.D. thesis study is to design and develop a non-contact temperature-controlled surgical laser system, characterize this system's specifications, and demonstrate its performance and feasibility by means of *ex-vivo* animal tissue experiments. This system comprises a laser source, a beam delivery optical assembly, a temperature measurement system, a feedback system, and a user interface. Recent advancements in the electronics technology provided low-cost IR thermocouple (IRt/c) sensors that are commercially available. Combining IRt/c temperature sen-

sors with a meticulously designed optical system enabled developing a state of the art temperature measurement and laser control system. The realized temperature measurement system *i*) is low-cost; *ii*) is simple to operate, requiring minimal training; *iii*) has a small form factor (compact) for less cumbersome adaptation into the clinic; *iv*) is non-contact in order to avoid contamination, mechanical damage, and interference with laser application; *v*) has a measurement spot size that is slightly smaller than the common laser spot sizes used for PTT; *vi*) has a sufficiently fast response/readout time in order to successfully provide feedback control; *vii*) has a measurement bandwidth that does not coincide with common surgical laser wavelengths.

3. THEORETICAL BACKGROUND

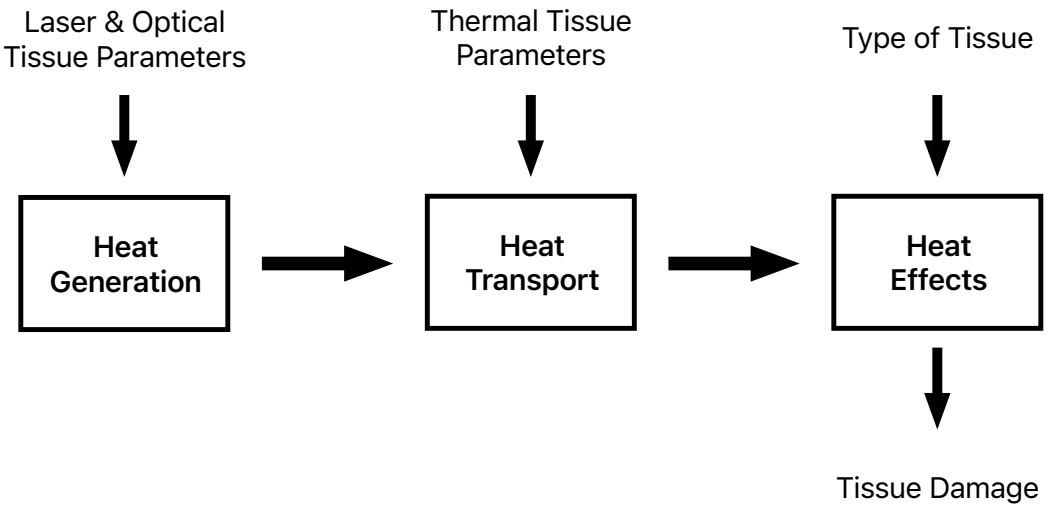


Figure 3.1 Flow chart with important parameters for photothermal interactions [3].

3.1 Photothermal Interactions

Photothermal interactions involve the interaction between laser light and biological tissues [3]. The combination of absorption and scattering processes determines the three dimensional spatial distribution of the heat generation in biological tissues during photothermal interactions [42]. The extent of these processes depends on various factors, including the optical properties (index of refraction, absorption coefficient, and scattering coefficient) and thermal properties (thermal conductivity, heat capacity, and blood perfusion) of the tissue, as well as the laser parameters (wavelength, power, exposure duration, and mode of laser irradiation). Understanding the mechanism of photothermal interactions is crucial for designing and optimising laser-based biomedical applications. The underlying mechanisms of photothermal interactions can be described as follows.

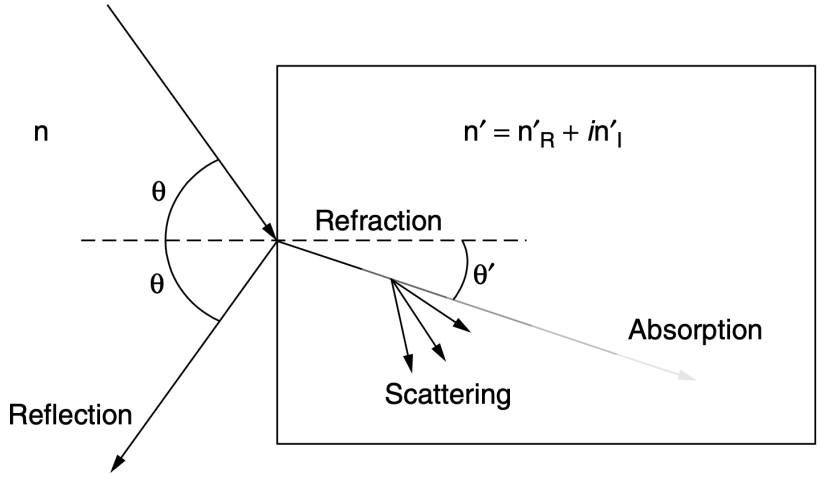


Figure 3.2 Propagation of light for biological tissues [42].

Optical Interactions and optical parameters of the tissue determine the generation and distribution of heat within the tissue [43]:

Reflection: When propagating electromagnetic radiation is incident on a boundary between two materials of different indices the returning electromagnetic radiation is defined as the reflection. The reflection is dependent on the angle of incidence, θ, of the electromagnetic radiation at the boundary, the indices of refraction, n, of the materials forming the boundary, and the polarization of the incident light. All tissues manifest diffuse reflection due to their irregular surface qualities. The reflection determines the amplitude of the electromagnetic radiation that can penetrate into the tissue. Therefore, it has an effect on the photothermal interactions.

Refraction: Any amount of light that is not reflected at the boundary between materials of different indices is refracted. The angle of the refracted light is dependent on the incident radiation angle and the indices of the two materials as defined by the Snell's law given in Eq. 3.2. The refraction affects the distribution profile of the light within the tissue. Therefore, it has an effect on the photothermal interactions.

Absorption: When laser light is incident on a biological tissue, it can be absorbed by chromophores, which are molecules that have specific absorption spectra in the wavelength range of the incident laser light. Chromophores,

such as hemoglobin, melanin, and water, absorb the laser energy and convert it into heat, leading to a localized increase in temperature in the tissue. The absorption coefficient of the tissue, α, contributes to the total attenuation, α_{total}, affecting the penetration depth of the laser irradiation within the tissue.

Scattering: Laser light can also interact with the scattering centers in biological tissues, such as cell membranes, organelles, and extracellular matrix. The scattering coefficient of the tissue, $\alpha_{\text{scattering}}$, also contributes to the total attenuation, α_{total}, affecting the penetration depth of the laser irradiation within the tissue. This scattering process results in the redirection of the incident light in different directions, leading to a diffusion of energy in the tissue and contributing to the spread of heat generation.

The refractive index, n, of the tissue given as

$$n = n_{\text{R}} + i\, n_{\text{I}} \tag{3.1}$$

plays an important role in the scattering and absorption processes of the incident light [42]. The real part, n_{R}, and the imaginary part, $i\, n_{\text{I}}$, determine scattering and absorption, respectively.

Optical refraction is described by the Snell's law given by

$$n \sin\theta = n' \sin\theta', \tag{3.2}$$

where θ is the angle of incidence, θ' is the angle of refraction, n and n' are the indices of refraction at the media before and after the boundary surface, respectively, as illustrated in Figure 3.2.

If the absorption coefficient, α, of the tissue is high, then the light energy is absorbed superficially and the penetration depth is low, and *vice versa* [43]. The mathematical relationship between the total attenuation, α_{total}, the absorption coefficient,

α, and the scattering coefficient, $\alpha_{\text{scattering}}$, is given by

$$\alpha_{\text{total}} = \alpha + \alpha_{\text{scattering}}. \tag{3.3}$$

As laser light propagates through tissue, its intensity decreases due to attenuation. The propagation distance dependent light intensity is given by the Beer-Lambert law,

$$I(z) = I_o \exp -\alpha\, z, \tag{3.4}$$

where I_0 is the initial light intensity, and z is the propagation distance [43]. Using the Beer-Lambert law we can calculate the optical penetration depth,

$$L = \frac{1}{\alpha}, \tag{3.5}$$

which is defined as the distance z where the light intensity $I(z)$ drops to $1/e$ of its incident value I_0.

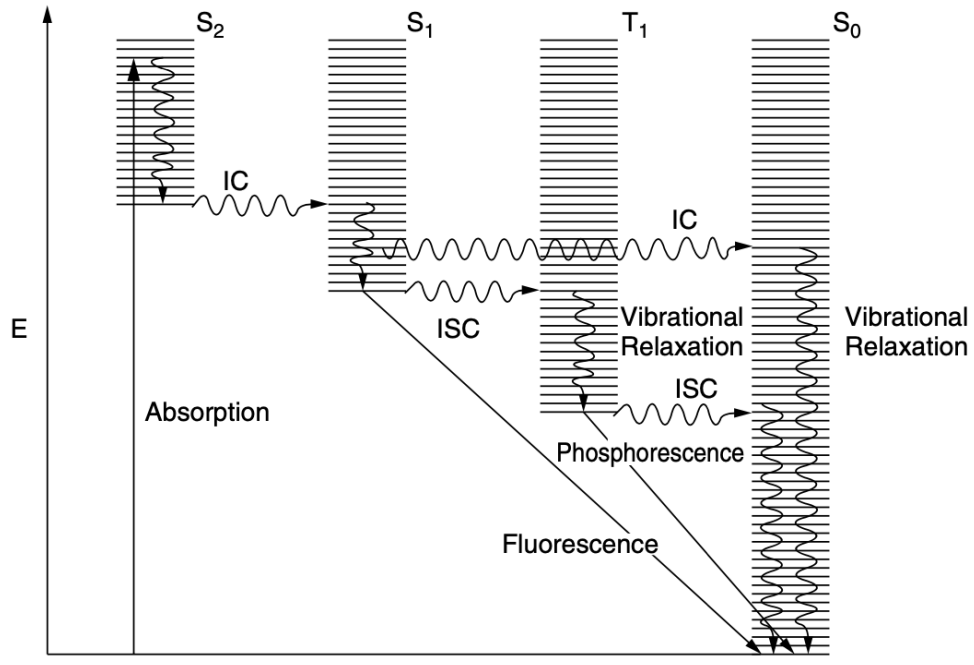


Figure 3.3 The Jablonski diagram describing the possible fates of excitation [42].

When light is absorbed by a material, the absorbing molecule is elevated to an excited state [42]. This is a temporary state and the molecule gets back to the ground state by the mechanisms depicted by the Jablonski diagram in Figure 3.3. These mechanisms can be categorised as radiative (fluorescence and phosphorescence), where a photon is emitted, and non-radiative (internal conversion, intersystem crossing, and vibrational relaxation), where no photon is emitted. Vibrational relaxation is the mechanism that generates heat within the tissue.

The Laser Parameters significant for photothermal interactions are wavelength, power, exposure duration, and mode of irradiation [3].

Wavelength: The wavelength, λ, of the laser light determines the tissue absorption and scattering coefficients, which are spectrally dependent parameters of materials. Hence, wavelength has a significant effect on the heat generation process, as well as the penetration depth of the laser irradiation.

Irradiation Power: Power, P, defined as the energy transferred per unit time, is one of the main parameters for controlling the energy delivered to the tissue affecting heat generation.

Exposure Duration: Exposure duration is defined as the duration of the laser application to the tissue. The duration of the laser irradiation determines the total optical energy delivered to the tissue leading to generation of heat and temperature buildup due to absorption and vibrational relaxation.

Mode of Laser Irradiation: The modes of laser irradiation can be generalized as continuous wave (CW) or pulsed. CW mode is the uninterrupted irradiation of the laser throughout the whole exposure duration, as its name implies. Pulsed mode is the intermittent irradiation of the laser showing a periodic square signal pattern. The parameters for controlling pulsed mode are the period and the duty cycle. In combination, these parameters determine the delivered optical energy, heat dissipation, and temperature buildup of the tissue. A lower duty cycle value allows more time for thermal relaxation processes, while reducing the delivered optical energy, and results in the reduction of the intensity of thermal effects.

Thermal Interactions: The absorbed laser energy is converted into heat, leading to an increase in tissue temperature as given by Eq. 3.6 [3]. This increase in temperature induces heat transport (thermal relaxation) processes, such as heat conduction, convection, and radiation, which distribute the heat within the tissue and may result in temperature gradients [44].

Heat Conduction: As the most prominent heat loss term, heat conduction is the dominant heat transfer mechanism for tissues [3]. The heat conduction is dependent on two parameters, the heat conductivity, k, of the tissue and the spatial temperature gradient, ∇T, within the tissue as given in Eq. 3.7.

Heat Convection: Tissue perfusion is the main contributor to heat convection in biological tissues. Heat convection may be neglected due to the low perfusivity of most tissues, generally [44]. However, during long exposure durations, tissue perfusion and heat convection play an important role in the distribution of the heat and thermal relaxation process [3].

Heat Radiation: Stefan-Boltzmann law describes the heat radiation as a function of temperature as given in Eq. 3.16. However, the amplitude of this radiation is rather negligible for tissue temperatures during photothermal interactions [3].

The absorbed photon energy is transformed to heat by vibrational relaxation of the excited molecules. The change in the tissue temperature with respect to the generated heat, Q, is given by

$$dQ = m\, c\, dT, \tag{3.6}$$

where m is the tissue mass, and c is the specific heat capacity of the tissue [3]. Consequently, the temperature difference induced within the tissue is inversely proportional to the mass and the specific heat capacity of the tissue. As these values increase, the induced temperature difference decreases.

The heat flow, j_Q, due to conduction is directly proportional to the temperature

gradient, ∇T, within the tissue given by

$$j_Q = -k\,\nabla T, \tag{3.7}$$

where k is the heat conductivity specific to the tissue [3]. The heat flow, which is the heat dissipation to the surrounding tissues, increases as the heat conductivity and the spatial temperature gradient increase.

Considering that any amount of heat transferred to the surrounding tissues as described by Eq. 3.7 is going to change the temperature gradient locally as described by Eq. 3.6 which will in turn affect the heat flow. Therefore, heat transfer is a dynamic process affected by the specific heat capacity and the heat conductivity of the tissue. These two parameters are combined into a single parameter called as the temperature conductivity or thermal diffusivity, κ, defined by

$$\kappa = \frac{k}{\rho\, c}, \tag{3.8}$$

where ρ is the density of the tissue [3,44]. This coefficient becomes useful in determining the spatial extent of the heat transfer as described by the time-dependent thermal penetration depth

$$z_{\text{therm}}(t) = \sqrt{4\,\kappa\, t}. \tag{3.9}$$

Considering that the thermal penetration depth is time-dependent, the optical penetration depth and the duration of the laser pulse have important effects in the temperature buildup of the irradiated tissue [3]. In order to minimize the thermal damage to the surrounding tissues, it is important to have a laser pulse duration that will allow thermal relaxation. If we equate the optical penetration depth, L, in Eq. 3.5 to the thermal penetration depth, z_{therm}, we end up with

$$L = \sqrt{4\,\kappa\,\tau_{\text{therm}}} \tag{3.10}$$

where the temperature term τ_{therm} becomes the thermal relaxation time. τ_{therm} is dependent on the wavelength of the laser, optical absorption and scattering coefficients, and thermal diffusivity of the tissue. For laser pulse durations $\tau < \tau_{\text{therm}}$, heat diffuses locally within the optical penetration depth leading to negligible thermal damage to the adjacent tissues. However, for pulse durations $\tau > \tau_{\text{therm}}$, heat diffuses further away than the optical penetration depth potentially leading to collateral damage to the adjacent tissues.

3.2 Thermo-Physiological Effects

As a simple rule, we can assume heat generation when tissues are irradiated using laser power densities $\geq$10 W cm^{-2} for durations longer than 1 µs leading to the thermal effects provided in Table 3.1. As tissue temperature rises during laser exposure, first, mitochondrial enzymes are denaturated and cellular membrane is destroyed, which results in the demise of the cell. At higher temperatures, intracellular and extracellular structural proteins coagulate; and cellular shrinking, collagen hyalinisation, and changes in collagen and muscle bi-refringence occurs along with tissue whitening.

Table 3.1
Thermal effects of laser irradiation [3, 45].

Temperature	Biological Effect
37 °C	Normal
45 °C	Hyperthermia
50 °C	Reduction in Enzyme Activity, Cell Immobility
60 °C	Denaturation of Proteins and Collagen, Coagulation
80 °C	Permeabilization of Membranes
>100 °C	Heat Fixation, Vaporization, Carbonization Decomposition/Thermal-ablation
>300 °C	Melting

As the temperature reaches 100 °C, intracellular water vaporises to form steam vacuoles that expand and explode resulting in the fragmentation and desiccation of the cell, consequently. When the pressure dependent boiling temperature of tissue water is exceeded, tissue carbonization and ablation occurs [3, 45].

Since thermal damage of the biological tissues are described as the first order Arrhenius rate equation, the onset of necrosis is also dependent on the temporal duration of the tissue temperature as depicted in Figure 3.4 [3]. Arrhenius equation can be used to approximate the remaining active molecules or cells with respect to the temporal temperature effects:

$$\ln \frac{C(t)}{C_0} = -A_{\text{Arrhenius}} \int_0^t \exp(-\frac{\Delta E}{RT(t')})dt' \equiv -\Omega, \tag{3.11}$$

where C_0 is the initial concentration of molecules or cells, $C(t)$ is the concentration at a time t, $A_{\text{Arrhenius}}$ is Arrhenius' constant, R is the universal gas constant, and ΔE and Ω are specific tissue properties. Then, the local tissue damage degree can be approximated by the time integral in Eq. 3.11.

The damage degree, $D_{\text{d}}(t)$, is a function of time and it is defined by the fraction

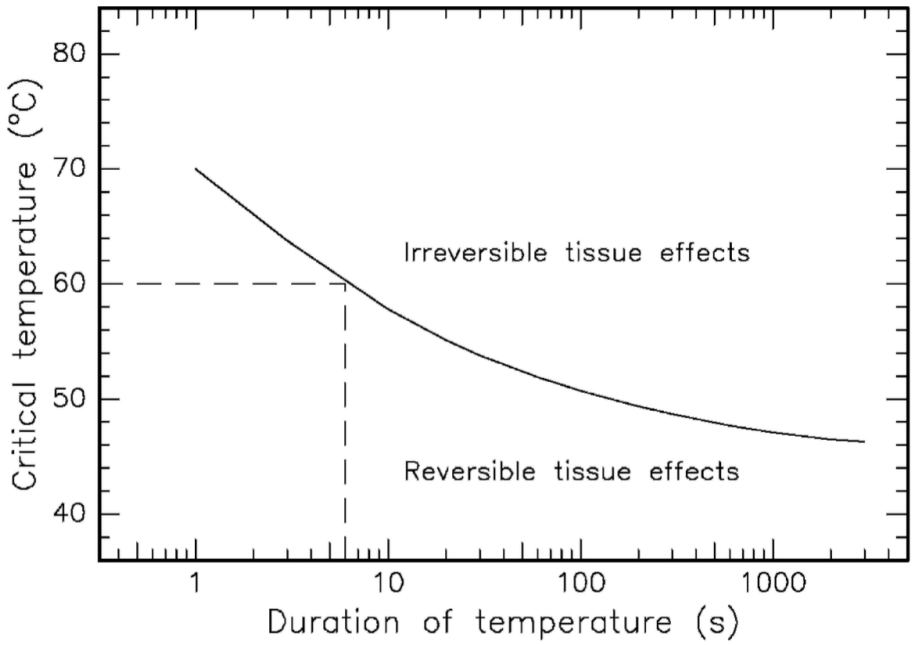


Figure 3.4 Critical temperatures for the occurrence of cell necrosis [3].

of deactivated molecules or cells and calculated by

$$D_{\mathrm{d}}(t) = \frac{C_0 - C(t)}{C_0} = 1 - \exp(-\Omega). \tag{3.12}$$

In most thermal laser applications, more than one thermal effect, listed in Table 3.1, occurs [3]. The general localisation of these thermal effects are illustrated in Figure 3.5. The spatial distribution of the laser power density and the delivered (absorbed) energy in combination with the exposure duration determine the location, degree, and extent of tissue thermal damage. Among these effects, vaporization, carbonization, and coagulation are strictly irreversible. However, hyperthermia can be can be reversible or irreversible depending on the aggregate time of the tissue temperature. Moreover, the absence of immediate necrosis does not mean that the induced damage will be reversible. It is still possible to trigger production of heat shock proteins which in turn cause cell death and apoptosis [19].

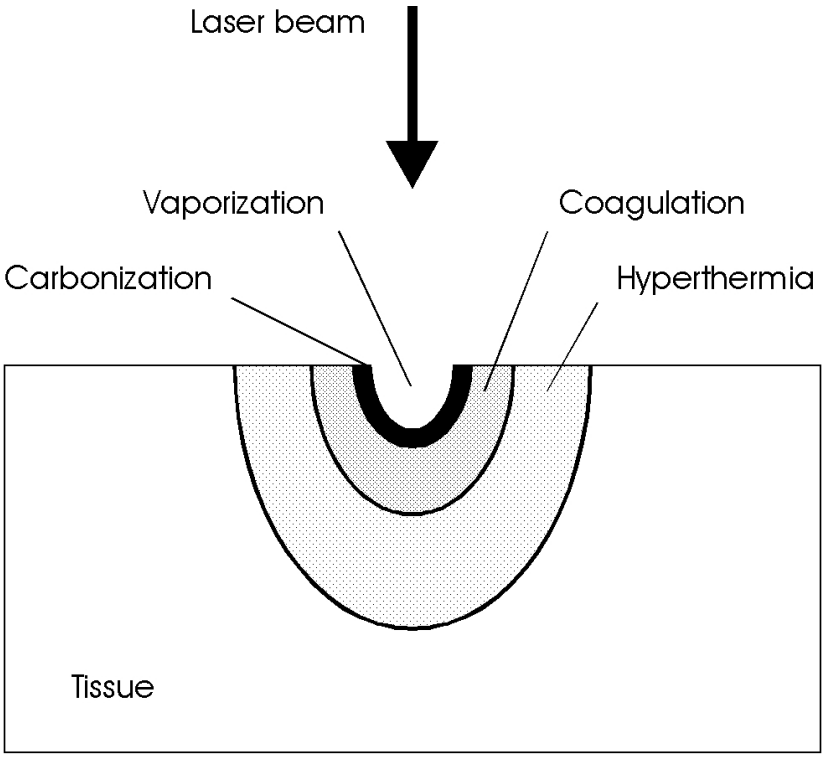


Figure 3.5 Location of thermal effects inside biological tissue [3].

Photothermal Medical Laser Applications

Some examples of the photothermal medical laser applications exploiting the above elaborated thermo-physiological effects are provided below.

Laser Surgery: Laser energy is used to cut, vaporize, or coagulate tissue, with minimal bleeding and scarring [21–23].

Laser Thermal-ablation: Laser energy is used to remove or ablate tissue, such as in the treatment of tumors or abnormal growths [15, 16].

Photothermal Therapy: Laser energy is used to selectively heat and destroy cancer cells or other abnormal cells (*e.g.* granulation tissue), while minimizing damage to surrounding healthy tissue [19]. One subset of this modality is nano-particle-assisted photothermal therapy, which has been a rising area of research after the advent of nanoparticle manufacturing capabilites, where the interaction between nanoparticles and irradiated photons is the main source of heat generation.

Laser Interstitial Thermal Therapy: Laser energy is used to selectively heat and destroy diseased soft tissue, such as in the treatment of liver, pancreas, prostate, and brain tumours [46–49].

Laser Tissue Welding: Laser energy is used to bond or seal tissues together, such as in the closure of wounds or surgical incisions [4–13].

Photocoagulation: Laser energy is used to coagulate or clot blood vessels, such as in the treatment of retinal or vascular disorders [14, 17, 18].

3.3 Temperature Dependence of Tissue Properties

The optical and thermal characteristics of tissues change with respect to their temperature and water content [10, 26, 28, 50–52]. As the tissue temperature increases due to laser irradiation, a multitude of phenomena occur simultaneously [53]. Coagulation and denaturation of proteins change the optical properties of the tissue [10, 28, 51].

Moreover, the absorption coefficient of water changes with increasing temperature [52]. The water content of the tissue may change due to evaporation induced dehydration.

As water content decreases, thermal conductivity of tissue reduces leading to drammatic increase in local temperatures during laser exposure [50, 54]. In contrast, the heat conductivity of tissues exhibit a small positive temperature coefficient at temperatures above freezing [44]. Additionally, at temperatures slightly higher than normal body temperature, the heat transport due to tissue perfusion may be increased because of the dilation of capillary blood vessels. However, at temperatures above coagulation and denaturation thresholds, the heat transport due to tissue perfusion may be reduced because of the coagulation of blood tissue and capillary vessels.

3.4 IR Radiometric Temperature Measurement

Infrared radiometry provides us with a versatile technique for non-contact measurement of surface temperatures. Comprehending the mechanism of radiometric temperature measurement requires understanding the laws governing this modality and knowledge about the concepts of blackbody radiation and emissivity.

Blackbody Radiation

A blackbody is an ideal physical body that has absolute absorption over the whole electromagnetic spectrum [55]. In other words, a blackbody absorbs all incident light regardless of its color (frequency). The angle of incidence does not modulate the absorptivity of the blackbody. The ideal absorption characteristic of this abstract object also renders it the best possible emitter of radiation [56]. The thermal radiation emitted from a body is therefore called a blackbody radiation. Blackbody radiation is incandescent in nature and has a characteristic and continuous spectrum. The temperature of the body determines the spectrum of emission defined by Planck's law.

Emissivity

In the real world, materials do not have the ideal emission and absorption

properties of a blackbody [56]. Therefore, real materials are considered graybodies [54]. The ability of a material's surface to mimic the ideal emission characteristics of a blackbody is defined as emissivity, ϵ. Emissivity is dimensionless (unitless), and its value ranges between 0 and 1 [57]. For blackbodies, ϵ is equal to 1.

Emissivity plays a significant role in the conversion of thermal radiation into accurate temperature measurements. Disregarding the emissivity of a material results in an erroneous measurement. The effect of emissivity is apparent in Stefan-Boltzmann law as stated in Eq. 3.16.

Emissivity has spectral and directional properties [57]. The dielectric constant, and subsequently the refractive index of the tissue determine its emissivity [56]. Therefore it is also wavelength dependent. Nevertheless, for the practical purpose of IR thermometry of biological tissues, ϵ can be considered constant and approaching to unity throughout the 2.5 µm to 15 µm spectral range [54]. Pigmentation of the tissues do not affect emissivity. Generally, we use the emissivity of water ($\epsilon_{\text{water}} = 0.96$ [56]) for soft organic tissues because of their high water content. In reality, the actual ϵ-values of tissues are occasionally accurately known, which introduces an unknown amount of error for temperature measurements. Additionally, the hydration level of tissues may change due to dynamic nature of physiological conditions or heating induced desiccation, leading to a change in emissivity, ϵ, and resulting in measurement errors. However, it is important to note that, according to Stefan-Boltzmann law, there is a linear relationship between the measured temperature and the fourth root of $1/\epsilon$ (inverse of emissivity), which corresponds to negligible measurement errors unless the change in emissivity is dramatic.

Planck's Law

Planck's law defines the relationship between the emissive power at a specific wavelength and the absolute temperature of a blackbody,

$$W_\lambda(T) = \frac{2\,\pi\,h\,c^2}{\lambda^5}\frac{1}{\exp(h\,c_{\text{light}}/\lambda\,k_{\text{B}}\,T) - 1} \quad [\text{W m}^{-3}], \tag{3.13}$$

where $h = 6.626 \times 10^{-34}\,\mathrm{W\,s^2}$ is Planck's constant, $c = 299\,792\,458\,\mathrm{m\,s^{-1}}$ is speed of light in vacuum, $k_\mathrm{B} = 1.381 \times 10^{-23}\,\mathrm{J\,K^{-1}}$ is Boltzmann's constant, λ [m] is the emission wavelength, and T [K] is the absolute temperature of the blackbody [54]. The evaluation of this equation over the whole emission spectrum results in the characteristic radiation spectrum at a specific absolute temperature as illustrated in Figure 3.6.

Wien's Displacement Law

The characteristic emission curve has a peak value (global maxima) corresponding to a specific wavelength that is a function of the absolute temperature as illustrated in Figure 3.6. Wien's displacement law describes this relationship between absolute temperature, T [K], and wavelength of peak emission, λ_peak [m], given by

$$\lambda_\mathrm{peak} = \frac{b}{T}, \tag{3.14}$$

where $b = 2.897 \times 10^{-3}\,\mathrm{m\,K}$ is Wien's displacement constant [54]. Wien's displacement

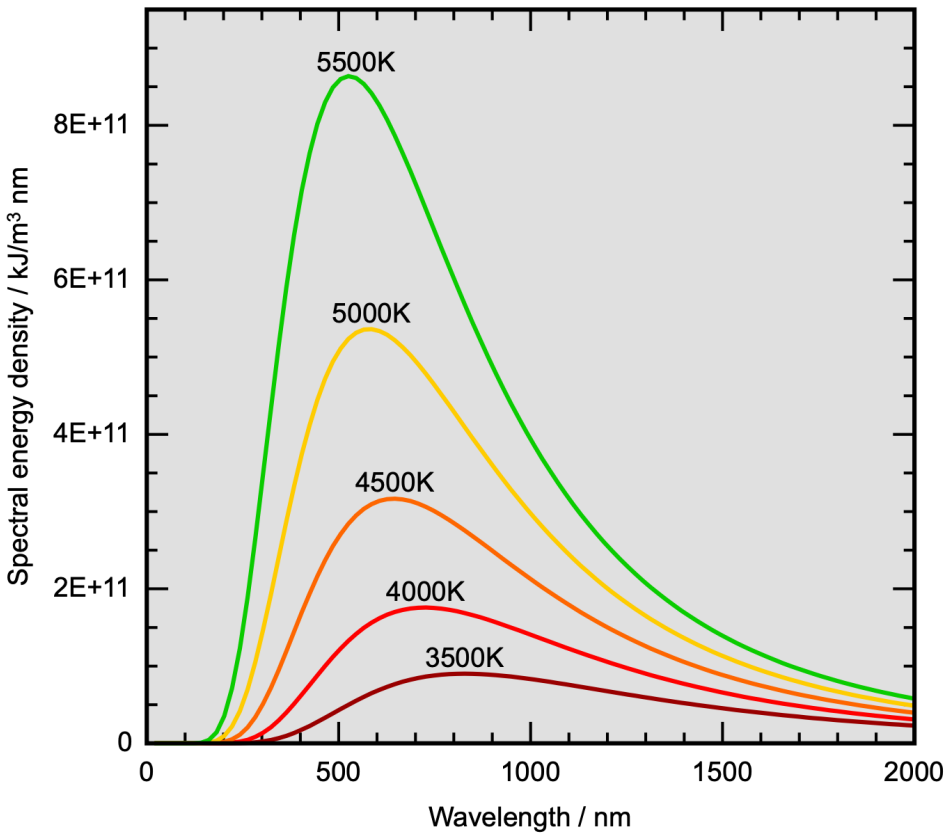


Figure 3.6 Characteristic emission spectrum for black bodies at various absolute temperatures. The wavelength of curve peak is described by Wien's displacement law [58].

law is mathematically derived from Planck's law. This relationship is useful when determining the detector type to be used in a measurement system for the temperatures of interest.

Stefan-Boltzmann Law

Integrating the monochromatic emissive power given in Eq. 3.13 over the wavelength (emission spectrum) provides the radiant emittance of a blackbody also known as the Stefan-Boltzmann law

$$W(T) = \int_{\lambda} W_{\lambda}(T)\, d\lambda = \frac{2\,\pi^5\, k_{\mathrm{B}}^4}{15\, c^2\, h^3}\, T^4 = \sigma\, T^4 \quad [\mathrm{W\,m^{-2}}], \tag{3.15}$$

where $\sigma = 5.670 \times 10^{-8}\,\mathrm{W\,m^{-2}\,K^{-4}}$ is the Stefan-Boltzmann constant [54]. Stefan-Boltzmann law defines the relationship between the emissivity, absolute surface temperature and emitted thermal radiation. IR thermometry exploits Stefan-Boltzmann law as presented in Eq. 3.15 to calculate the surface temperature of a material using the measured emissive radiation. However, Eq. 3.15 is valid for blackbodies. One should include the emissivity to this equation to find the relationship between measured radiant emittance and the surface temperature of graybodies like human tissue:

$$W'(T) = \int_{\lambda} \epsilon_{\lambda}(T)\, W_{\lambda}(T)\, d\lambda = \epsilon(T)\, \sigma\, T^4. \tag{3.16}$$

IR Radiometric Temperature Measurement Depth

Stefan-Boltzmann law defines the relationship between the total emitted thermal radiation for perfectly opaque materials throughout the emission spectrum. Consequently, given the opaqueness assumption of the material, the T value of Eq. 3.16 is dependent only on the surface temperature. However, biological tissues are not opaque throughout the IR spectrum. As a result, when conducting IR radiometric temperature measurements of biological tissues, we are registering IR emissions emanating from subsurface tissue, as well. Naturally, subsurface emissions are attenuated due to the optical absorption (and scattering) of the tissue along the optical path between the emission source and the tissue surface. Depending on the value of the subsurface

tissue temperature and the depth of the emission source, it is possible to observe the effect of the subsurface emissions. There are recent techniques utilising hyper-spectral IR cameras and this phenomena to compute the depth temperature profile of materials. [59]

Nevertheless, at the physiologically relevant PTT temperature range the emission depth remains only superficial. We can observe the thermal emissions between the surface and up to a depth of 25 µm–30 µm. It is a good practice to consider the temperature measurement depth in combination with the laser penetration depth when radiometrically measuring the tissue temperature during laser applications. The penetration depth of the laser wavelength will determine how deep within the tissue the heat is generated. In this Ph.D. thesis study, we used $\lambda = 1071\,\text{nm}$ because it is a commonly used wavelength for PTT and has a medium penetration depth ($\lambda = 1064\,\text{nm}$ has a penetration depth of 2 mm to 6 mm).

IR Sensor Types

We can categorize IR sensors into two general types: photon detectors or thermal detectors [56]. Each type has different capabilities regarding their spectral sensitivity, response time and operational requirements [57]. A summary of IR sensor types and characteristics is available in Table 3.2.

Table 3.2
IR sensor types, examples and characteristics [56, 57].

Sensor Category	Photon (Quantum)	Thermal
Sensor Type	Photodiode	Bolometer
	Phototransistor	IR Thermocouple / Thermopile
	Photoresistor	Pyroelectric Detector
Characteristics	High Detectivity	Low Detectivity
	Fast Response Time	Slow Response Time
	Cooling Required	No Cooling Required
	Narrow Spectral Bandwidth	Wide Spectral Bandwidth

Photon Detectors

Photon detectors operate on the principle of photoelectric effect first described by Albert Einstein [56]. There are several sub-classifications of photon detectors exploiting different phenomena of the photoelectric effect: photovoltaic devices with semiconductor p-n junction structures (photodiodes and phototransistors), photoconductive devices (photoresistors), and photoemissive devices with photocathodes (photomultiplier tubes, micro channel plates) [56, 57]. The photoelectric interaction is determined by the band gap of the sensor material and the energy of the incident photon [57]. If the photon energy is less than the band gap of the material, the photon is not absorbed, and it is either reflected or transmitted. On the other hand, a photon with sufficient energy would elevate an electron from the valence band to the conduction band. Therefore, the response of photon detectors is a function of wavelength and quantum efficiency. Hence, their response spectrum is generally narrow and never flat. Nevertheless, since a signal can be generated even with a small number of photons, these type of detectors are generally faster and more sensitive [56].

The blackbody radiation of cooler temperatures are composed of low energy photons that require sensor made of low band gap materials for the photoelectric effect to manifest [56]. For instance, HgCdTe or SiGa photon detectors have this characteristic. They have a very short response time (in the order of nanoseconds); and their temperature acquisition is very fast [22, 32]. However, these materials also exhibit very high intrinsic noise when operated at room temperatures, leading to low SNR values and erroneous temperature readings ($\pm 15\,^{\circ}\mathrm{C}$) [15, 56]. Therefore, they are bound to be used with cryogenic cooling systems, which are quite costly.

There are also photon sensors that do not require an external cooling system. These sensors are made of semiconductor materials like PbS, PbSe, and InGaAs [4, 7–9, 22–24, 31, 33, 34, 60]. These type of sensors exhibit low SNR values and do not respond to DC (constant) signals. Thus, it is mandatory to operate them alongside an optical chopper and lock-in amplifier assembly. The measurement accuracy and the time constant of the lock-in amplifier are inversely related, such that one has to sacrifice accuracy in order to achieve fast measurement, and vice versa.

As elaborated above, photon detectors all lack in one aspect or the other (SNR, response-time) to satisfy clinical requirements. They also require costly apparatus (cryogenic cooling or optical modulators and lock-in amplifiers). Besides the cost, they also complicate the operation of the system and increase the bulk size rendering it impractical for clinical environments.

Thermal Detectors

Thermal detectors operate on the basis of two processes: *i*) absorption of the incident optical radiation causes rise of the detector surface temperature and *ii*) the temperature gradient induces a physical effect which is measured [57]. Thermal detectors are less sensitive than photon detectors because the first process requires significantly higher photon counts [56]. Thermal detectors are wavelength independent. Since the first process (i) is related to Eq. 3.4, having a detector surface material with an absorption coefficient close to 1 is preferred for good performance. Additionally, Eq. 3.6 implies that detectors with small mass and specific heat capacity would have a faster response. There are several mechanisms for the second process (ii), the conversion of the induced temperature change into other phenomena generating electrical signals [57]. Thermoelectric detectors like thermocouples or thermopiles operate based on the thermoelectric effect, a combination of Seebeck effect and Peltier effect, in which the temperature difference induces a voltage difference. Thermoresistive detectors like bolometers utilise materials with high temperature coefficient of resistance and measure the temperature change induced electrical resistance variations. Pyroelectric detectors exploit the pyroelectric effect in which a transient temperature change generates a change in surface charges. Optomechanical detectors like the Golay cell or the Crooke radiometer make use of the thermal expansion of solids or gases and indirectly induce an electric signal.

Infrared Thermocouple

In this Ph.D. thesis study, I have used an IR thermo-couple (IRt/c) sensor. These type of sensors are comprised of an optical imaging system, a thermocouple (or a thermopile), and dedicated electronics. The optical imaging system focuses the temperature specific blackbody radiation of the target surface on the thermocouple. This results in a minuscule temperature change directly on the thermocouple which can be

accurately measured and then used for the computation of the target surface temperature. These type of sensors do not require a supplementary optical chopper and lock-in amplifier assembly for their ability to respond to DC signals and high SNR specifications. This property drastically decreases the system complexity, enabling easier set up and operations. Besides, as opposed to other type of non-contact temperature sensors, decreasing the sensor size (thermocouple size) results in both better spatial resolution and faster response time, in IR thermocouples. This fact is very advantageous considering the requirements of the proposed system. This type of temperature measurement systems were also successfully used in laboratory environments to control laser exposure for medical applications [5,6,22]. System specifications of this type of temperature measurement assemblies were reported as *c.a.* 0.4 mm spatial resolution, 1 °C accuracy, 0.2 °C sensitivity, and 50 ms response time. Considering all these specifications, this method of temperature measurement prevails for surgical laser applications. Today, IR thermocouple systems have evolved into integrated MEMS chips available from several producers (*e.g.* Texas Instruments, Dexter, Melexis), as foreseen several decades ago [61]. These products have a system-on-a-chip characteristic, including the IR thermocouple sensor, signal conditioning, A/D conversion, and dedicated signal processing and communication electronics on the same *c.a.* 2 mm × 2 mm chip.

4. MATERIALS & METHODS: DESIGN & DEVELOPMENT OF THE TEMPERATURE CONTROLLED MEDICAL LASER SYSTEM

The temperature controlled surgical laser system embodies three subsystems, each of which is indispensable and essential to the successful operation of the whole system. The general schematic of this system is depicted in Figure 4.1. The temperature measurement system elaborated in Section 4.1 is the most important constituent of this thesis project. It is used to measure the surface temperature of the tissue in a non-contact fashion. The laser system is used to deliver the laser irradiation required to achieve photothermal treatments. The selection criteria and operation of this laser system is provided in Section 4.2. A microcontroller board operates both the temperature measurement system and the laser system. The microcontroller creates the backbone of the temperature controlled medical laser system by combining both subsystems as described in Section 4.3.

Table 4.1
User requirements and related general specifications.

	User Requirements	General Specifications
temperature measurement range	from room temperature to above PTT relevant temperatures	20 °C–150 °C
operation distance	should provide line of sight	>2 cm
response time	significantly faster than human reflexes	«250 ms
laser wavelength	suitable for PTT application	near infrared
user experience	low complexity & easy to use	small number of components
cost	low	$1000

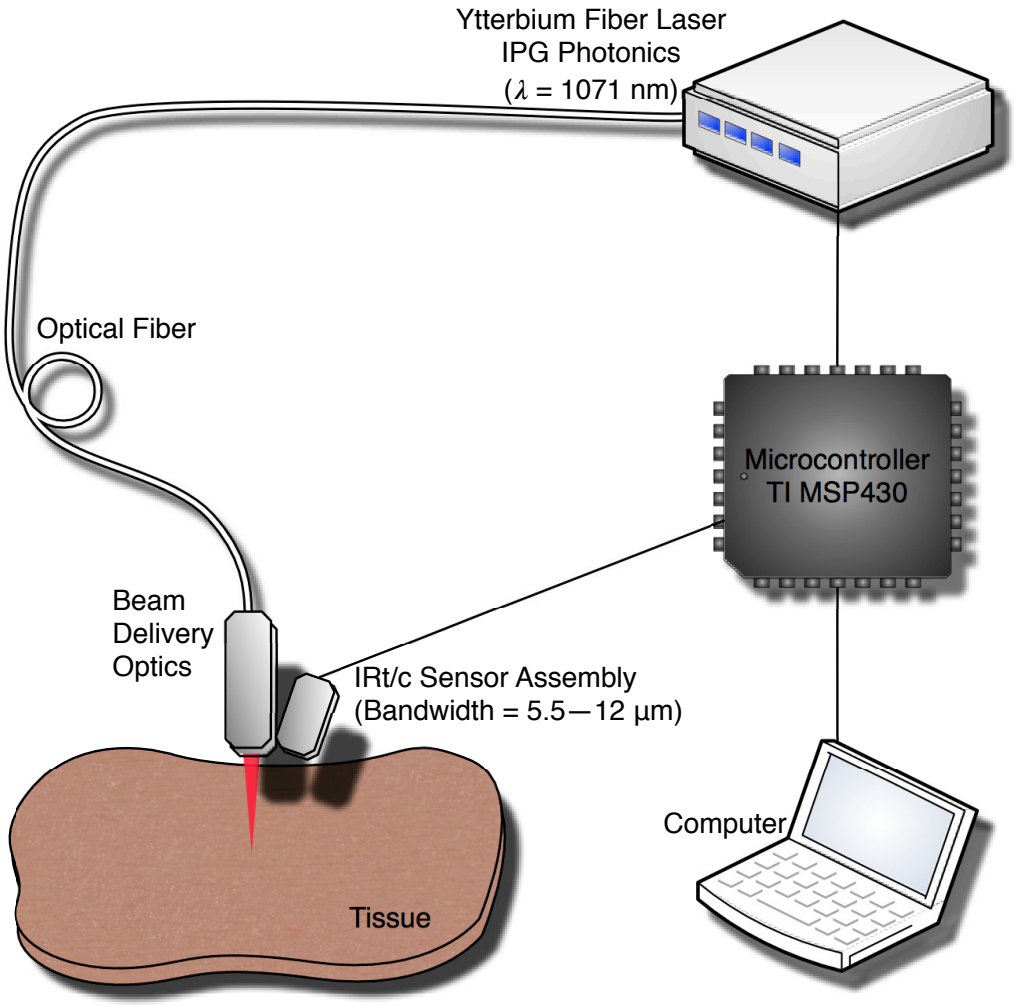


Figure 4.1 Schematic of the Temperature Controlled Medical Laser System.

The initial concept design of the beam delivery optics in combination with the temperature measurement optics is illustrated in Figure 4.2. This initial concept was designed before researching the available sensor technologies in detail and learning their optical, mechanical, and electronic limitations. As the iterative design process progressed, this temperature measurement assembly of this concept was found to be infeasible to realize due to optical and mechanical limitations.

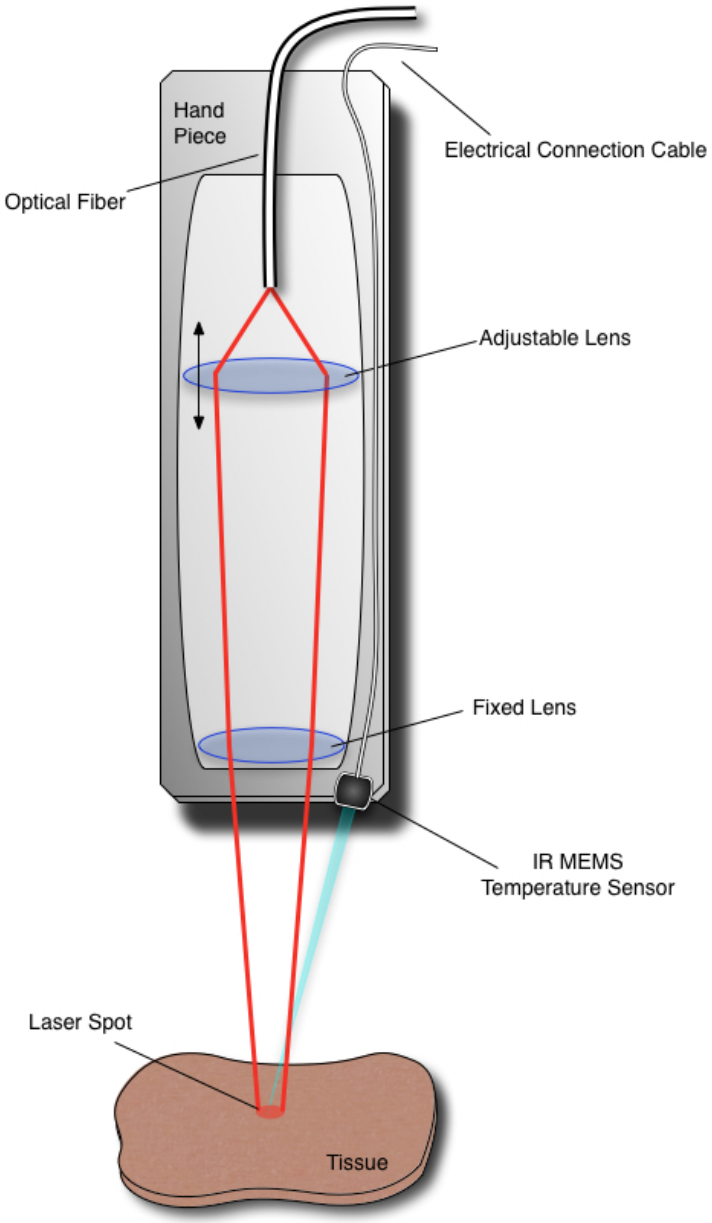


Figure 4.2 Initial design of the beam delivery optics.

4.1 Temperature Measurement System

The non-contact temperature measurement system is composed of an IRt/c temperature sensor (Section 4.1.1), a readout circuit (Section 4.1.2), and an opto-mechanical assembly (Section 4.1.3). The opto-mechanical assembly focuses the thermal radiation from the tissue surface onto the sensor, as well as providing a housing for the sensor.

The design and manufacturing of any opto-electro-mechanical system is an extremely iterative and recursive process. The specifications of the optical, electrical, and mechanical components are discrete. Each component of a certain domain has a nonlinear effect on the other two domains. Therefore, the design process cannot be conducted orthogonally in a single pass and multiple iterations are necessary. As a result, most of the time, the user requirements cannot be translated into exact technical specifications at the initial phases of the design process in these interdisciplinary domains.

For instance, the field of view (FOV) of the sensor affects the lens size and refractive power, which in turn affect the size of the opto-mechanic components. In several instances throughout this thesis study, we had to design custom parts and manufacture them using a lathe or 3D printer. The operating bandwidth (optical wavelength) of the sensor also affects the lens material selection and the suitable laser sources. The response time of the temperature sensor determines the viable temperature control methods. The available sensor technologies was the most limiting aspect within this design. Therefore, it was optimal to start with the surveying, short listing, and selection of the temperature sensor. I have decided on using an infrared thermocouple (IRt/c) sensor for the reasons elaborated in Section 4.1.1.

4.1.1 IRt/c Sensor

I chose infrared thermocouple (IRt/c) technology for the temperature sensor. The IRt/c sensor operates depending on the blackbody radiation phenomenon. The thermal radiation from the tissue surface heats a thermocouple/thermopile within the sensor generating a potential difference. The surface temperature is then deduced using the thermopile output voltage. Because the actual sensor is a thermopile, decreasing its size results in both faster readout times and better spatial resolution, which is very advantageous for this kind of application. Besides, the thermal capacity and the mass of the thermopile has a *low-pass* characteristic, increasing the noise performance of this system.

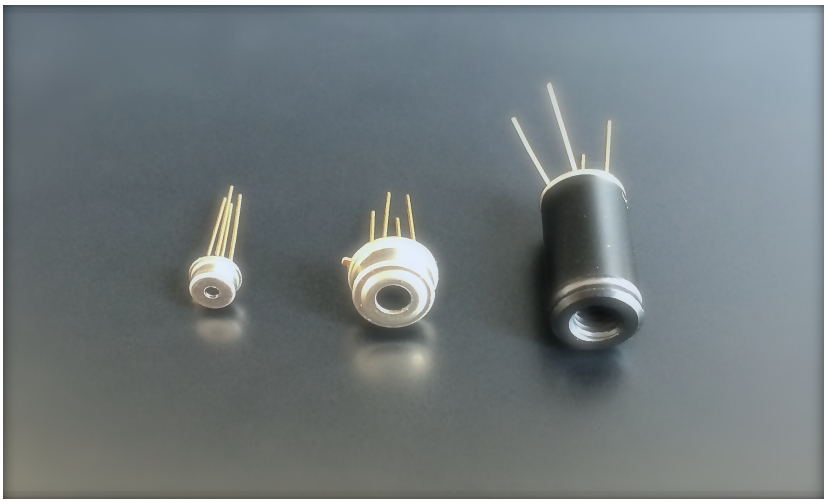


Figure 4.3 Melexis IRt/c Sensor Chips in Mini TO-46 & TO-39 Housing.

Recent advancements in the MOEMS technology enabled the production of embedded IRt/c sensor systems as presented in Figure 4.3. Currently, various IRt/c sensor systems are commercially available from several manufacturers (*e.g.*, Texas Instruments, Melexis, Dexter Research Center, Omega). These IRt/c sensor systems can embody the thermocouple sensor and readout electronics within the same minuscule (*ca.* 2 mm × 2 mm) embedded chip. Thus, the chip contains all necessary components for signal conditioning, analog-to-digital (A/D) conversion, digital signal processing, and communication protocols as depicted in Figure 4.4. The embedded nature of these sensors simplifies the design process and reduces the system cost dramatically. A microcontroller with the suitable communication peripheral is then sufficient to digitally acquire temperature data.

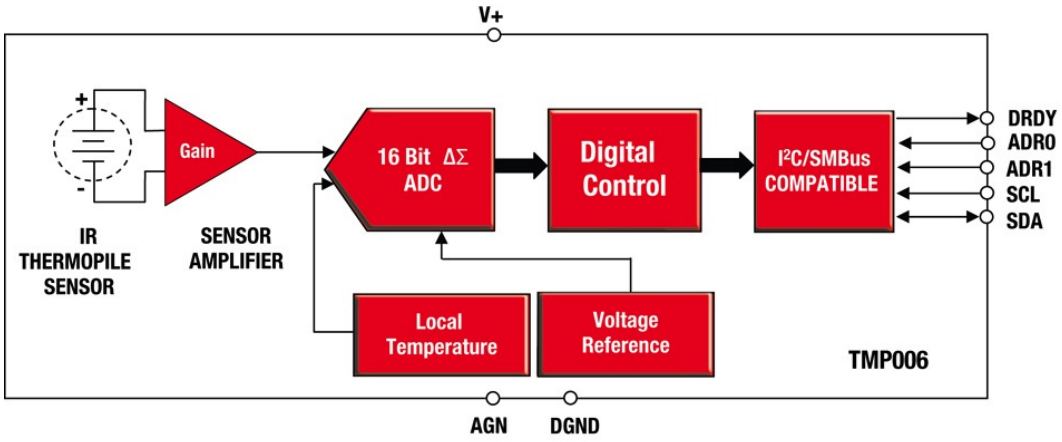


Figure 4.4 Block Diagram of Texas Instruments TMP006 IR MEMS Sensor.



Figure 4.5 Melexis IRt/c Sensor MLX90614ESF-BCC.

After surveying various alternatives, I have selected MLX90614ESF-BCC produced by Melexis as the temperature sensor to be used for this system, as depicted in Figure 4.5. It contains an IRt/c sensor, signal conditioning, A/D conversion, dedicated signal processing and communication circuits on the same 2 mm × 2 mm chip packaged hermetically in a TO can. The block diagram of this sensor is illustrated in Figure 4.6. The digital temperature data can be acquired using the SMBus protocol (a subset of I^2C protocol). The spectral bandwidth of the sensor (5.5 µm–12 µm) is suitable for the desired temperature measurement range of 20 °C–150 °C (corresponding to a maximum emission bandwidth of 6.9 µm–10 µm). It is important to note that this sensor cannot be used with lasers operating within its spectral bandwidth (*e.g.*, CO_2 laser) in order to avoid interference with the measurement.

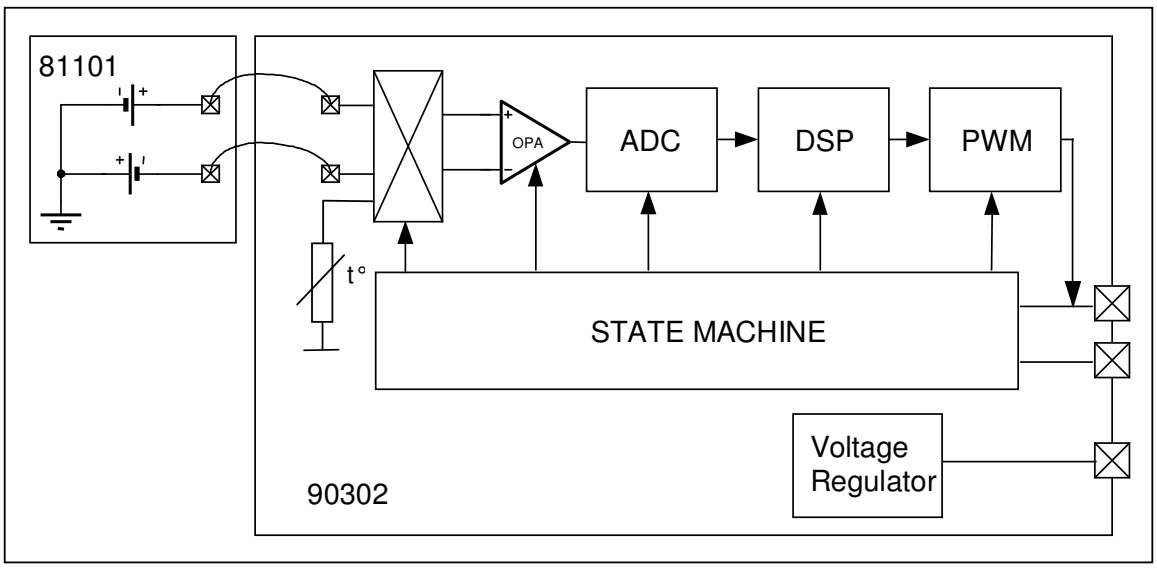


Figure 4.6 Block Diagram of the Melexis IRt/c Sensor Chips [62].

Accuracy & Resolution

The accuracy of the IRt/c sensors are ambient temperature and object temperature dependent as illustrated in Figure 4.7. In room temperature, the MLX90614 sensors have measurement error of ±0.5 °C, ±1 °C, and ±2 °C over the 0 °C to 60 °C, 60 °C to 120 °C, and 120 °C to 180 °C ranges, respectively. Considering that the major object temperature range of interest is 20 °C to 120 °C, I can conclude that the accuracy of the MLX90614 sensors are sufficient for PTT applications.

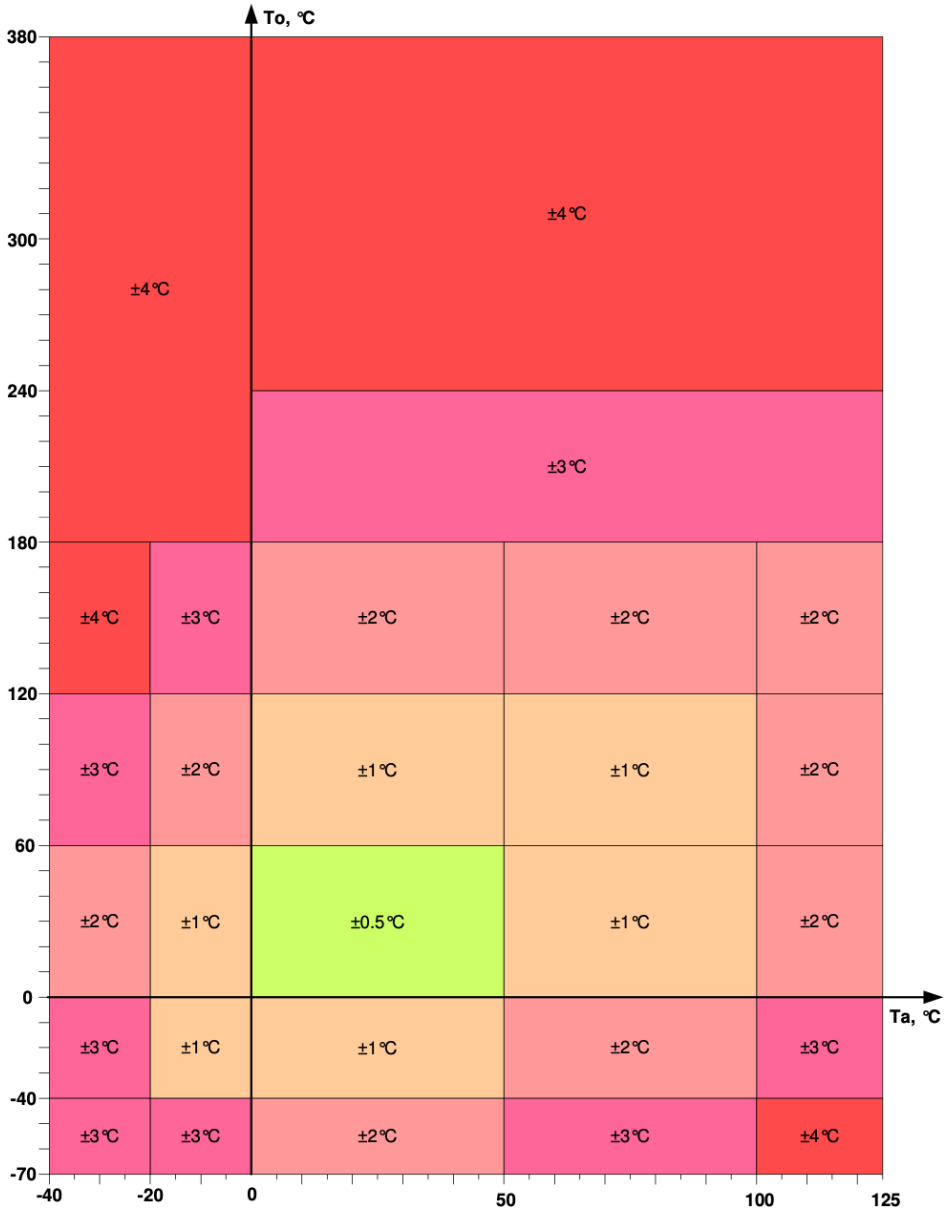


Figure 4.7 Accuracy of MLX90614 except for xCK type (Ta: ambient temperature, To: object temperature) [62].

The resolution of the MLX90614 sensors depend on the operation mode of the sensor. It is possible to have 10 bit resolution for an configurable range of temperatures using PWM mode. However, in the SMBus and two-wire modes, the temperature range is fixed and the readout is conducted by reading the RAM cells dedicated for this purpose resulting in a 0.02 °C resolution. The resolution for the SMBus mode is sufficient for our application.

Field of View

The field of view of the sensor has provides another significant optical design limitation to be considered during the iterative design process. Because the optical design is actually an imaging system, the measurement spot is actually the image of the sensor active surface. The FOV of the sensor determines the focal length of the focusing lens we are going to use for designing a high-spatial-resolution temperature measurement system. Thus, the spot size depended on the magnification factor of the imaging system. This required a lens placement further away from the sensor to achieve a small measurement spot size resulting in an increase of the required lens diameter. We need to select a lens with a sufficient diameter to ensure no or minimal clipping occurs to avoid affecting the accuracy of the sensor. The field of view (35°) of this sensor, as illustrated in Figure 4.8, is feasible for achieving the desired optical system.

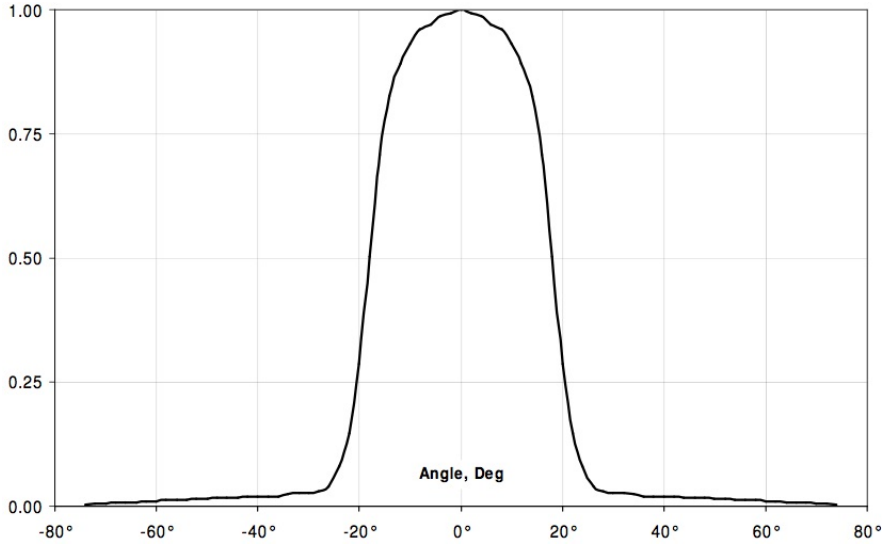


Figure 4.8 Field of View of MLX90614ESF-BCC [62].

IIR setting	FIR setting	Settling time (s) 90614xAx	Settling time (s) 90614xBx, 90614xCx	Spike limit
xxx	000…011	Not recommended		
100	100	0.04	0.06	100.00%
100	101	0.05	0.07	100.00%
100	110	0.06	0.10	100.00%
100	111	0.10	0.14	100.00%
101	100	0.12	0.20	80.00%
101	101	0.16	0.24	80.00%
101	110	0.22	0.34	80.00%
101	111	0.35	0.54	80.00%
110	100	0.24	0.38	66.70%
110	101	0.30	0.48	66.70%
110	110	0.43	0.67	66.70%
110	111	0.70	1.10	66.70%
111	100	0.26	0.42	57.00%
111	101	0.34	0.53	57.00%
111	110	0.48	0.75	57.00%
111	111	0.78	1.20	57.00%
000	100	0.30	0.47	50.00%
000	101	0.37	0.60	50.00%
000	110	0.54	0.84	50.00%
000	111	0.86	1.33	50.00%
001	100	0.70	1.10	25.00%
001	101	0.88	1.40	25.00%
001	110	1.30	2.00	25.00%
001	111	2.00	3.20	25.00%
010	100	1.10	1.80	16.70%
010	101	1.40	2.20	16.70%
010	110	2.00	3.20	16.70%
010	111	3.30	5.00	16.70%
011	100	1.50	2.40	12.50%
011	101	1.90	3.00	12.50%
011	110	2.80	4.30	12.50%
011	111	4.50	7.00	12.50%

Figure 4.9 IIR & FIR Filter Settings and Corresponding Settling Times for MLX90614 Series Sensors [62].

Response Time & Adjusting Sensor Settings

The response time of these sensors depend on the IIR and FIR filter coefficients as recited in Figure 4.9. It is possible to change the settling time of the sensor by adjusting the filter settings using the SMBus communication protocol. The MLX90614 series sensors (Figure 4.3, center and right) can be adjusted to have response times around 50 ms. Appendix A contains instructions for changing the sensor settings.

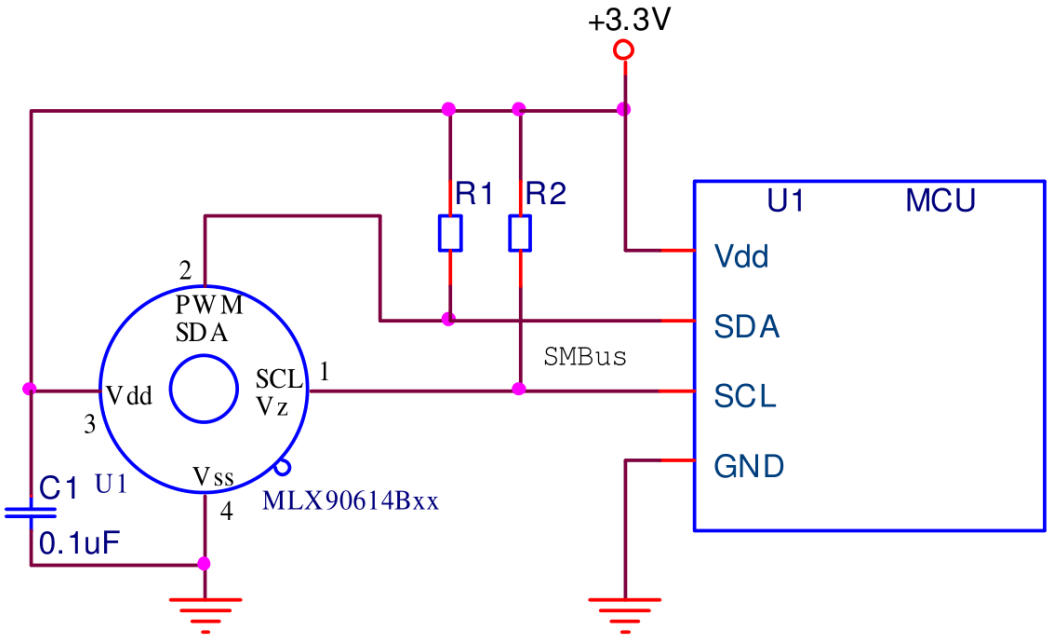


Figure 4.10 Electronic Circuit for SMBus communication of MLX90614ESF-BCC [62].

4.1.2 Electronic Design

In order to realize successful SMBus communication with the IRt/c sensor, it is necessary to construct a simple electronic circuit as illustrated in Figure 4.10 for interfacing the sensor to a microprocessor. The R1 and R2 are typically 1 kΩ to 10 kΩ resistors used for pull-up. We have realized this electronic circuit using a breadboard. The microcontroller development board provided the 5 V voltage source and the electrical ground. We connected the sensor to the microcontroller using long jumper cables.

4.1.3 Optical & Mechanical Design

We designed the optical system to image a small area of the target (tissue) surface onto the sensor surface using an IR lens. The distance between the optical system exit pupil and the measurement surface was a limiting factor for ensuring a small measurement spot diameter due to the magnification of the imaging system. The system was designed to realize a balanced compromise between operating distance and measurement spot size. The designed optical system was analyzed using an open source ray tracing software (Beam4, Stellar Software Inc., CA, USA).

IR Lens Selection

In this project, IR lenses will be used within the temperature measurement system, as well as within the beam delivery optics. In both cases, the bandwidth and transmission characteristics of these optics play an important role in the accuracy and efficacy of these systems. The temperature measurement system calculates the surface temperature by measuring its blackbody radiation. Any attenuation of this IR signal by the focusing optics results in a reduced measured temperature than the actual temperature. Therefore it is vital for the accuracy of the temperature measurement system to use highly transmissive optics throughout the measurement bandwidth of the sensor. A preliminary survey revealed the bandwidth and transmission percentages of several IR transparent materials as listed in Table 4.2. These materials are suitable for use in the production of windows, lenses or anti-reflection coatings.

The lenses available at the laboratory were not compatible with the sensor bandwidth, FOV and measurement spot size requirements. A larger diameter lens with a longer focal distance had to be chosen that also satisfied the transmission spectrum requirements. For this purpose, we conducted a further survey to figure out the transmission spectra of some of the IR lens materials that are commercially available. The

Table 4.2
IR Transmissive Materials [63, 64].

Material	Bandwidth	Peak T	Average T
Sapphire	0.1 µm to 7.0 µm	90%	85%
BaF_2	0.2 µm to 17.5 µm	91%	91%
KBr	0.2 µm to 20.0 µm	90%	90%
ZnSe	0.58 µm to 22.0 µm	70%	68%
CaF_2	0.2 µm to 12.5 µm	91%	91%
MgF_2	0.2 µm to 7.0 µm	95%	92%
Si (AR coated)	1.1 µm to 20.0 µm	92%	70%
Si (Uncoated)	1.1 µm to 9.0 µm	92%	70%
	9.0 µm to 300 µm	20%	10%
Ge (AR coated)	2.0 µm to 22.0 µm	92%	69%
Ge (Uncoated)	1.8 µm to 30.0 µm	45%	45%

result of this survey is presented in Figure 4.11. The corresponding temperature-wavelength couples for maximum emission with respect to the Wien's Displacement Law were marked in cyan at the bottom of this figure. The bandwidth of the sensor is marked on the graph with the colour light violet. The colour violet marks the bandwidth of interest in our device. The bandwidth of highest importance is marked with the colour purple. Considering the data presented in this figure, ZnSe material with an anti-reflection (AR) coating was determined to be the best candidate for the IR lens.

Through meticulous surveying of commercial catalogs and analyses a commercial ZnSe lens (ZnSe10Lens10, $f = 10\,\text{mm}$, $\varnothing = 10\,\text{mm}$, Crystran Ltd., UK) shown in Figure 4.12 was chosen to be used in the temperature measurement system. It is AR coated and has a 99% transmission over 3 µm to 11 µm range, which is suitable for use in our system.

Imaging System for Small Spot Measurement & Ray Tracing Analysis

In order satisfy the user requirements, the imaging system of the temperature measurement assembly is supposed to have a small spot size for high spatial resolution and provide a comfortable working distance to avoid blocking the line of sight of the operator. Thus, we designed various sensor and lens combinations and analysed them using the BEAM4 ray tracing software from Stellar Software Inc. Some of the sensor and lens combinations are depicted in Figures 4.14 to 4.16. The values in these plots are all in mm. The distance values on the right-hand-side of the plots are measured from exit pupil of the imaging lens (the second surface of the lens).

Clipping means that some of the measured infrared radiation is not coming from the object. Hence, clipping is a significant factor in the accuracy of the temperature measurement system. Clipping depends on the design of imaging system and the limitations introduced by the available optical elements. The extent of the error introduced by clipping is a function of the FOV of the sensor, as illustrated in Figure 4.8, and the non-clipping angle of the imaging system.

Eventually, we have chosen the sensor lens combination to be 90614ESF-BCC

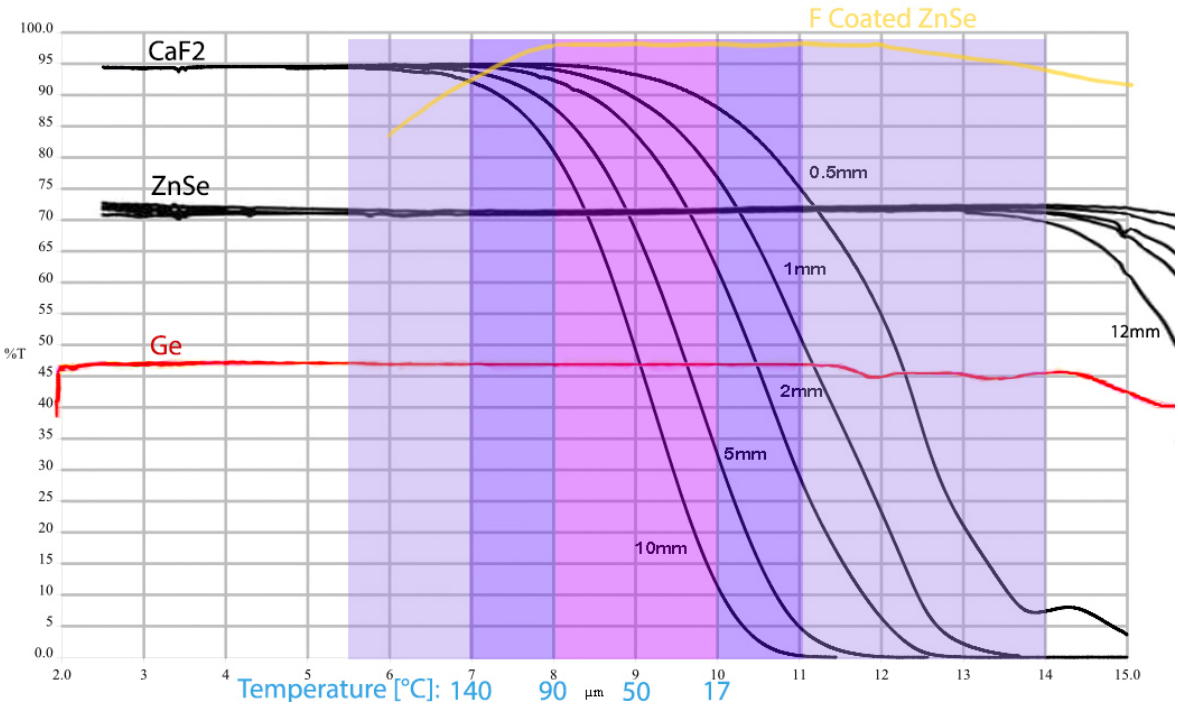


Figure 4.11 Transmission Spectra of Various Materials and Corresponding Temperatures.

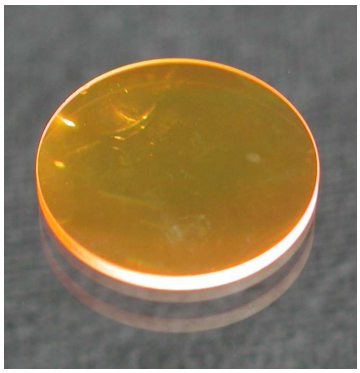


Figure 4.12 Crystran 3 µm to 11 µm AR Coated ZnSe Lens.

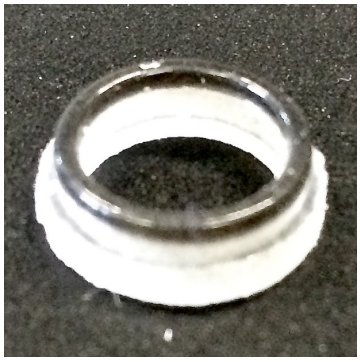


Figure 4.13 SM05–10 mm Lens Adapter.

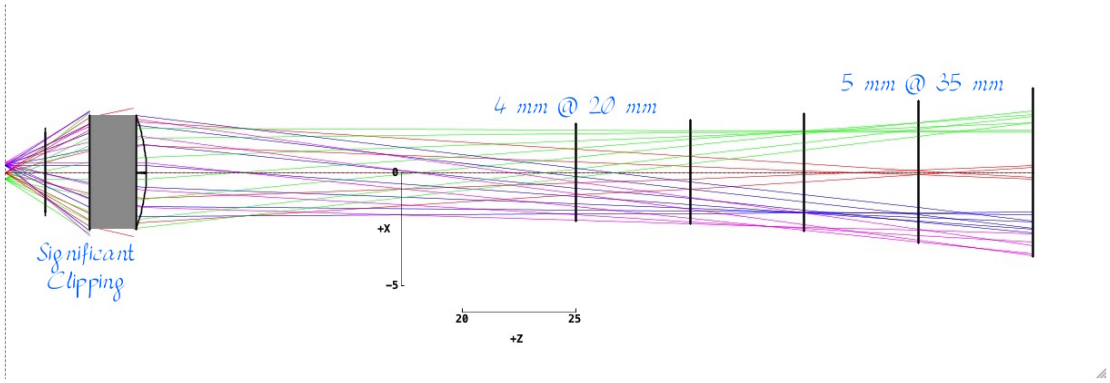


Figure 4.14 Ray Tracing Analysis of Melexis 90614ESF-BAA IRt/c Sensor & Thorlabs C036TME-F IR Lens Combination.

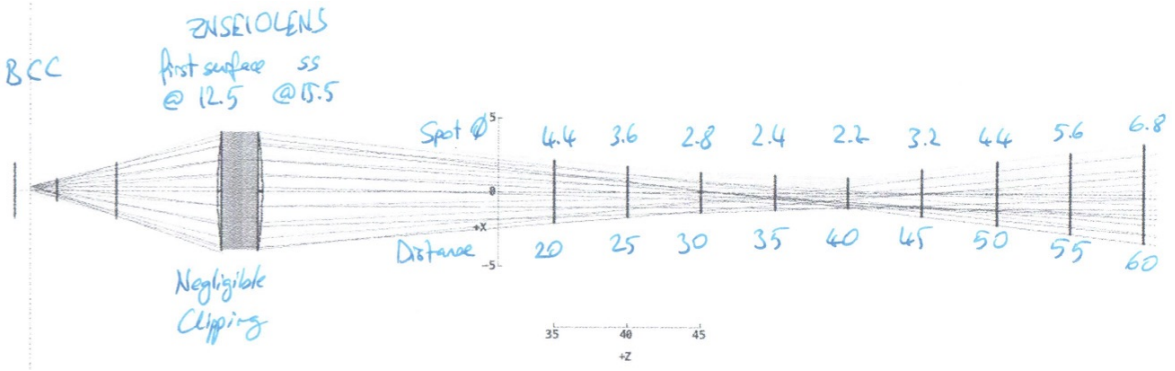


Figure 4.15 Ray Tracing Analysis of Melexis 90614ESF-BCC IRt/c Sensor & Crystran ZnSe10 IR Lens Combination 1.

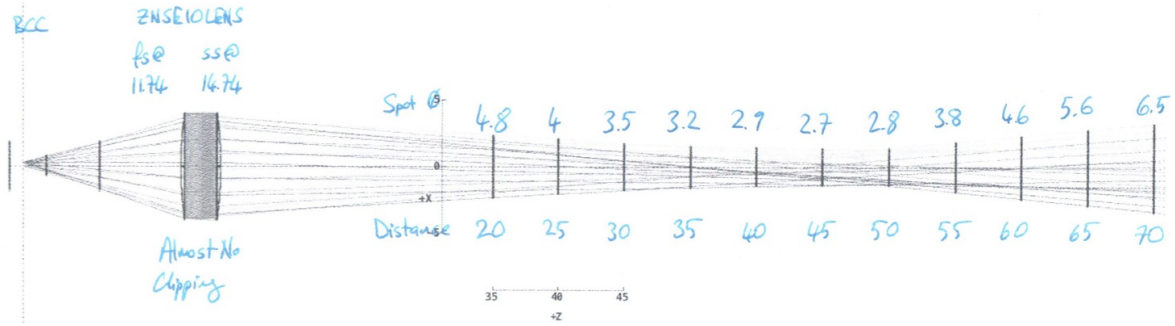


Figure 4.16 Ray Tracing Analysis of Melexis 90614ESF-BCC IRt/c Sensor & Crystran ZnSe10 IR Lens Combination 2.



Figure 4.17 Thorlabs SM05 Lens Tubes and A Retaining Ring ($\varnothing = 12.7\,\text{mm}$) [64].

sensor and Crystran ZnSe10Lens10 ($f = 10\,\text{mm}$, $\varnothing = 10\,\text{mm}$). Two of the suitable design options are provided in Figures 4.15 and 4.16. The sensor and lens selection processes were explained in detail in 4.1.1 and 4.1.3, respectively.

Lens Tube System

Lens tubes (Figure 4.17) are used for building lens arrays using mounted or unmounted optics without dealing with optical alignment issues. It is possible to use them as the main component of the hand probe due to their suitable shape. Lens tube system has various accessories such as standard-size lens adapters, fiber optic connector attachments, and retaining rings. SM05 lens tubes accept optical and mechanical components with a diameter of 0.5 inches (12.7 mm). For this project, we selected and purchased several SM05 lens tubes of various lengths, which are diameter-wise ergonomical.

Lens Adapter, Spacer & Sensor Holder

The Crystran ZnSe10Lens10 lens is not compatible with SM05 Lens Tube without an adapter. Unfortunately, 10 mm lens adapter was available commercially. Therefore, it was necessary to design a custom adapter and manufacture it using a high-resolution 3D printer after the acquisition of this lens to incorporate it into the temperature measurement system.

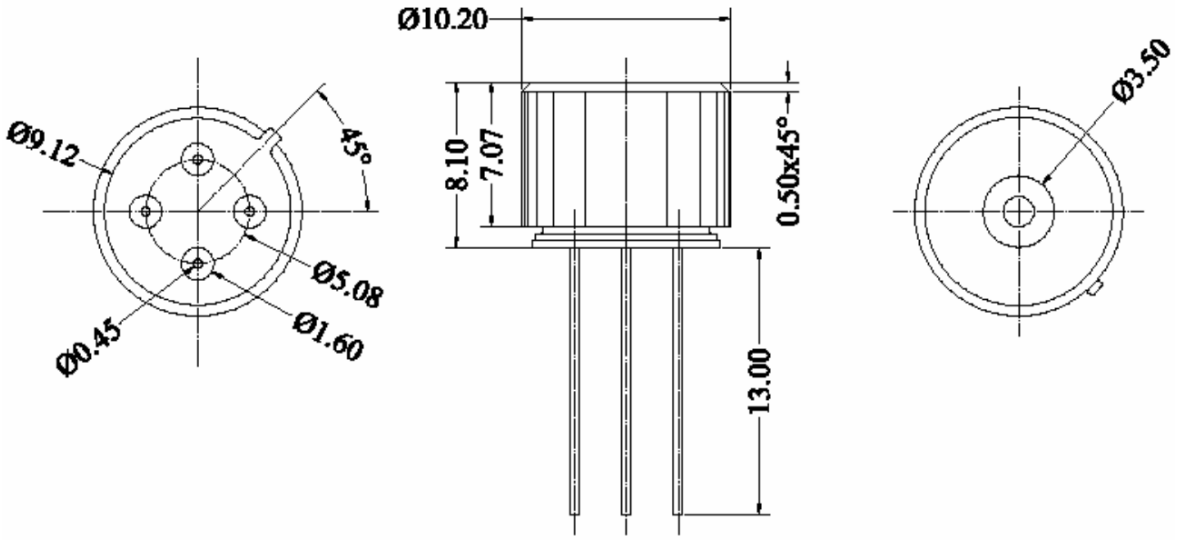


Figure 4.18 Technical Drawing of the MLX90614XCC package (all dimensions in mm) [62].

The distance between the lens and the sensor has an important effect on the measurement spot size and clipping as explained previously in this subsection and clearly illustrated in Figures 4.15 and 4.16. In order to precisely control this distance, we designed cylindrical tubes as spacer elements and manufactured them using a high-resolution 3D printer.

The diameter of the sensor (10.2 mm), as illustrated in Figure 4.18 was not compatible with the SM05 lens tubes. Additionally, there were no commercially available adapters capable of holding the sensor centred and aligned to the optical axis of the lens tube system, as well. Therefore, we had to design a custom sensor holder and manufacture it using a high-resolution 3D printer. We stacked the lens, the spacer, the sensor holder and the sensor within the lens tube and fixed them using the retaining rings depicted in Figure 4.17. The final temperature measurement assembly is provided in Figure 7.1.

4.2 Laser System

4.2.1 Laser Source

The laser system used in this study is an ytterbium fiber laser (YLM-20SC, IPG Photonics, MA, USA) operating at $\lambda = 1071\,\text{nm}$. This wavelength does not interfere with the temperature measurement because the spectral bandwidth of the sensor is 5.5 µm–12 µm. The maximum output of this laser source is 20 W. It is possible to run this laser in CW and pulse (modulated) modes, 1 ms being the shortest pulse width. The laser irradiation can be controlled using a TTL signal fed to a BNC connector on the backside of the laser enclosure. The output is collimated requiring an additional opto-mechanical assembly for coupling the output to an optical fiber.

4.2.2 Laser Irradiation Control Methods

In order to achieve temperature controlled laser application, it is necessary to come up with a closed-loop feedback system and an interface to set system parameters. The code developed in this environment will acquire the tissue temperature from the IR MEMS thermopile sensor, display it on the screen and modify the laser output depending on this temperature and user defined parameters. The system parameters that can be defined using the user interface are listed below:

Laser Parameters: operation mode (CW, pulsed), power, duty cycle, pulse period, exposure time

Feedback Parameters: target temperature, maximum temperature, control mode (feedback algorithm) and mode specific parameters

There are various feedback control methods reported in the literature that can be used for controlling the laser irradiation. The relevant control interface may contain the

following methods:

Exposure Modulation (On-Off Control): This is the most fundamental control method that ceases the laser exposure once the measured surface temperature reaches or exceeds the set target temperature. It is also possible to use this method to maintain a certain temperature by turning the laser exposure on and off by comparing the measurement temperature and the target temperature. It is applicable to CW and pulsed laser modes.

Duty Cycle Modulation: As its name suggests, this method can only be used during pulsed laser applications. It limits the laser energy delivered to the tissue per unit time by changing the duty cycle of the laser exposure. It is possible to use this method with *proportional*, *proportional-derivative*, and *proportional-integral-derivative* algorithms.

Laser Power Modulation: This method enables the temperature control by directly changing the laser power thus limiting the energy delivered per unit time. It is also possible to use this method with *proportional*, *proportional-derivative*, and *proportional-integral-derivative* algorithms. This method is applicable to both, CW and pulsed laser modes.

The realization of laser irradiation control in this study was achieved using a microcontroller and its associated embedded software as described in Sections 4.3.1 and 4.3.5.

4.2.3 Beam Delivery Optics

The beam delivery optics is composed of two main components: the laser source to fiber coupler assembly and the hand-held optical assembly for irradiating the target area. The output of the laser source we have used is collimated requiring an additional opto-mechanical assembly for coupling the output to an optical fiber for enabling practical positioning of the beam delivery optics. This optical fiber is then connected to

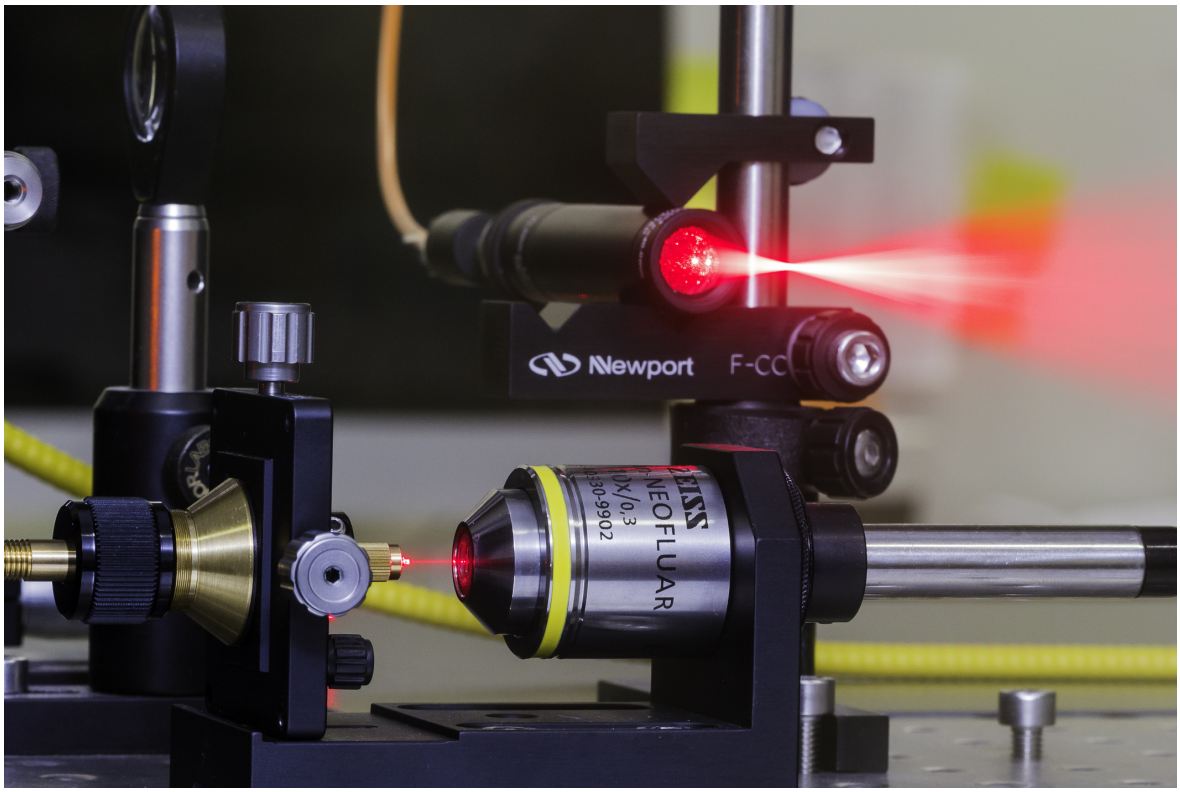


Figure 4.19 Bare Singlemode Fiber Coupler (F-91-C1, Newport Corp., USA) & Focusing Objective (Plan-Neofluar 10x/0.30 M27, Zeiss, Germany).

a hand-held optical assembly is used for delivering the laser beam to the application area, which enables the adjustment of the laser spot size. This assembly will also accommodate the temperature sensor in an off-axis placement to facilitate temperature controlled laser application. The design requirements for this assembly are to be ergonomic and robust, to provide a direct line of sight to the application area, and to ensure proper laser and temperature measurement spot registration for reliable control. The initial concept design of this optical assembly is illustrated in Figure 4.2.



Figure 4.20 Thorlabs Bare Fiber Terminator [64].

We have initially coupled the output from the laser source using a multi-axis fiber coupler depicted in Figure 4.19. We have used bare fiber terminators presented in Figure 4.20 for connecting the optical fibers to the lens tubes used during the system research and development phase. Nevertheless, we have realized that the multi-element focusing objective was reducing the transmission efficiency of the whole system. Later on we decided not to use the high-precision fiber coupler with the focusing objective and used a simpler optical assembly composed of a lens tube, an SM05 compatible centering optics holder, and an N-BK7 lens with higher optical transmission characteristics for coupling the beam into the fiber as depicted in Figure 6.1 and elaborated in Section 6.1.1.

We designed a simple optical system as the hand-held optical assembly and realized this system using lens tubes (SM05, Thorlabs) as illustrated in Figure 6.1. The input of this probe consists of a SMA connector. The design of this system contains a single uncoated spherical plano-convex lens (N-BK7 glass, Thorlabs) that is transmissive up to 2 µm. The reason for using only a single lens was to maintain high transmission efficiency enabling a wider range of optical powers for PTT applications.

4.3 Temperature Controlled Medical Laser System

The developed temperature measurement system consists of an IRt/c sensor within an optical imaging assembly that can be used off-axially in combination with a laser delivery optical assembly. It is necessary to setup the IRt/c sensor parameters prior to laser applications in order to ensure appropriate operation. The setup of the IRt/c sensor is detailed in Appendix A. The readout of the temperature sensor is processed using a microcontroller board that also regulates the modulation of the laser system, as explained in this Section. The schematic of the experimental setup is given in Figure 4.1.

4.3.1 Microcontroller Development

We have used a microcontroller as the central processing unit connecting all components of this system. The developed embedded codes for this thesis work are presented in Appendix B.

Development Board

A microcontroller development board (MSP-EXP430F5529LP, Texas Instruments, TX, USA) operating at 24 MHz was used as a central processing and control unit of this system: interfacing with the IRt/c sensor for temperature acquisition, processing the temperature information for laser control, and interfacing with a PC for user input and data output. The launchpad development board (Figure 4.21) provides the necessary circuitry in order to stably run the micro-controller, pins for interfacing, on-board switches and LEDs, as well as a flash programmer and a USB connection.

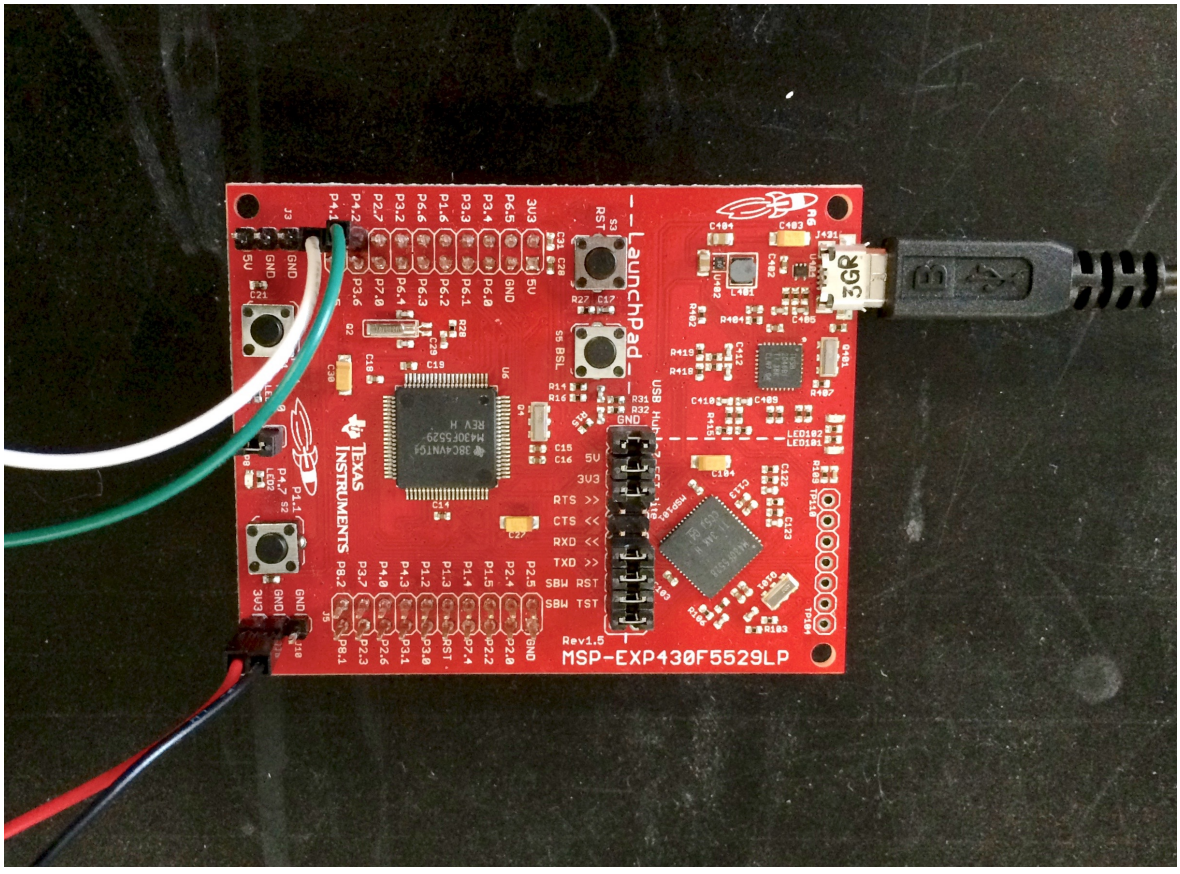


Figure 4.21 MSP430 F5529 Launchpad Microcontroller.

This micro-controller supports I^2C and UART communication protocols with dedicated hardware peripherals. It is possible to modify the I^2C peripheral in software to emulate SMBus protocol. Several hardware timer modules sourced by two reliable clock sources enable independent triggering of events as well as PWM output for modulated laser control.

Debouncing

MSP-EXP430F5529LP has two integrated push buttons that can be used for controlling the operation of the microprocessor. However, as all push buttons do, these push buttons bounce when pressed. This bouncing prevents straightforward operation of the microcontroller due to the multiple triggering of any interrupts connected to these buttons. It is possible to use a debouncing circuit in the form of a low pass filter to prevent bouncing. However, it is also possible to use a software debouncing method making use of a timer. In this study, we used a software debouncing algorithm using the Watchdog Timer of the MSP430F5529 as explained in Appendix B.1.

4.3.2 Communication

There are several hardware USCI peripherals available in MSP430F5529 to be used for communication protocols such as UART, USB, I^2C, SPI. In this study, we are making use of the UART protocol for the communication between the computer user interface and the microcontroller. We used a serial terminal program (*e.g.* RealTerm, CoolTerm) as the computer user interface. The UART communication is detailed in Appendix B.2. We are using the SMBus protocol for the communication between the IRt/c sensor and the microcontroller. The SMBus protocol is a subset of the I^2C protocol and therefore we can make use of one of the hardware USCIs for this communication, as well. Appendix B.4 provides the microcontroller codes necessary for IRt/s sensor readout using SMBus protocol.

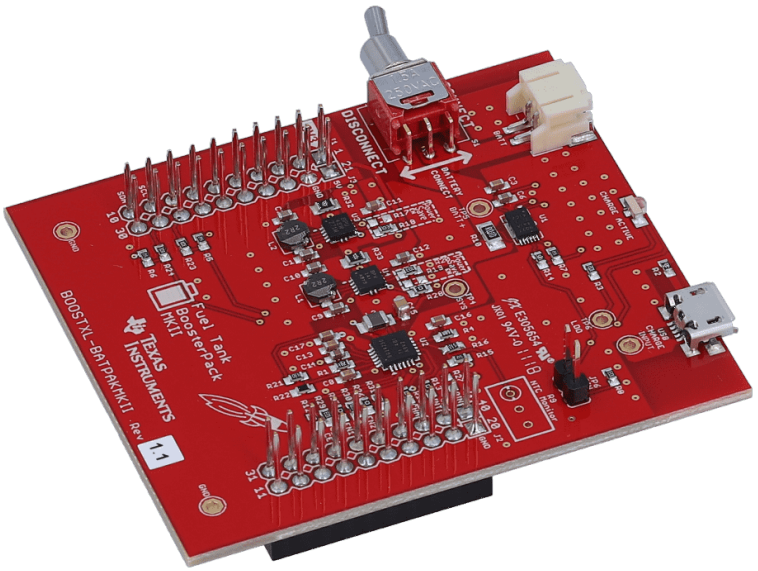


Figure 4.22 Fuel Tank, BOOSTXL-BATPAKMKII, Texas Instruments.

4.3.3 Noise, Power Source, and Bluetooth Connection

Initially, we have used an USB connector for both as the power source and the wired channel for the UART communication. However, during the operation of the system we have realized that this cable introduces a small but significant noise affecting the laser irradiation control decision making process even though the analog components of the sensor are shielded. Therefore, we decided to electrically isolate the microcontroller and temperature measurement system from the computer and the mains supply. For this purpose we stacked a battery expansion board as depicted in Figure 4.22 on the headers of the MSP430F5529 Launchpad development board. The Fuel Tank uses a LiPo battery as its power source.

Consequently, we had to come up with a different communication channel between the computer interface and the microcontroller. We have decided to use a Bluetooth SSP (Synchronous Serial Port) adapter (HC06) as illustrated in Figure 4.23. The bluetooth adapter registers as a standard serial port on the computer operating system. The HC06 acts as a repeater on the UART channel, sending serial data it receives to the other side of the channel in a duplex fashion.

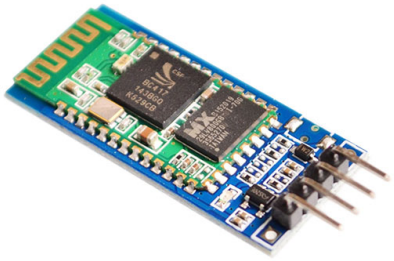


Figure 4.23 Bluetooth SSP (Standard Serial Port) Adapter, HC06, Generic.

4.3.4 IRt/c Sensor Readout

In order to ensure proper operation, the parameters of the IRt/c sensor should be set with respect to the requirements of the application. The Melexis IRt/c sensor setup was provided in detail in Appendix A. The raw temperature data acquired with the SMBus protocol is converted to a temperature value in the Celsius scale. The code for the temperature readout and conversion is provided in Appendix B.4.

"Divide & Conquer" (Bi-Linear Conversion) Method

The calibration of the temperature measurement system resulted in a conversion curve for maximum accuracy. Instead of using a lookup table, we have developed a new method for fast conversion of the raw data into temperature.

In this method, instead of a higher order formula (Figure 4.24) to be processed using high number of cycles

$$4 \times \text{multiplication}\,(13\,\text{cycles}) + 2 \times \text{addition}\,(6\,\text{cycles}) = 64\,\text{cycles},$$

we are making use of two separate linear conversion formulas (Figure 4.25) for different parts of the conversion curve: bi-linear conversion. This way, the conversion duration is reduced without sacrificing accuracy due to the combination of simpler operations

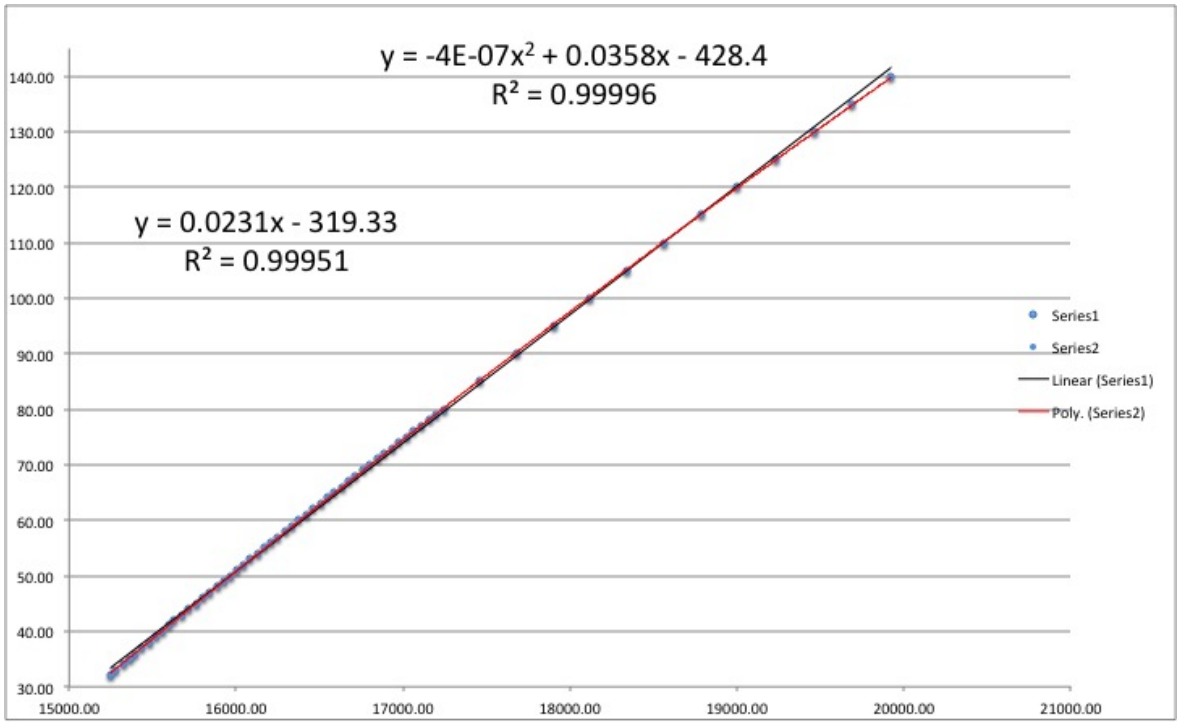


Figure 4.24 Calibration Data & Linear and 2^{nd} Order Polynomial Trendlines (x-axis: RAW data [int], y-axis: temperature [℃]).

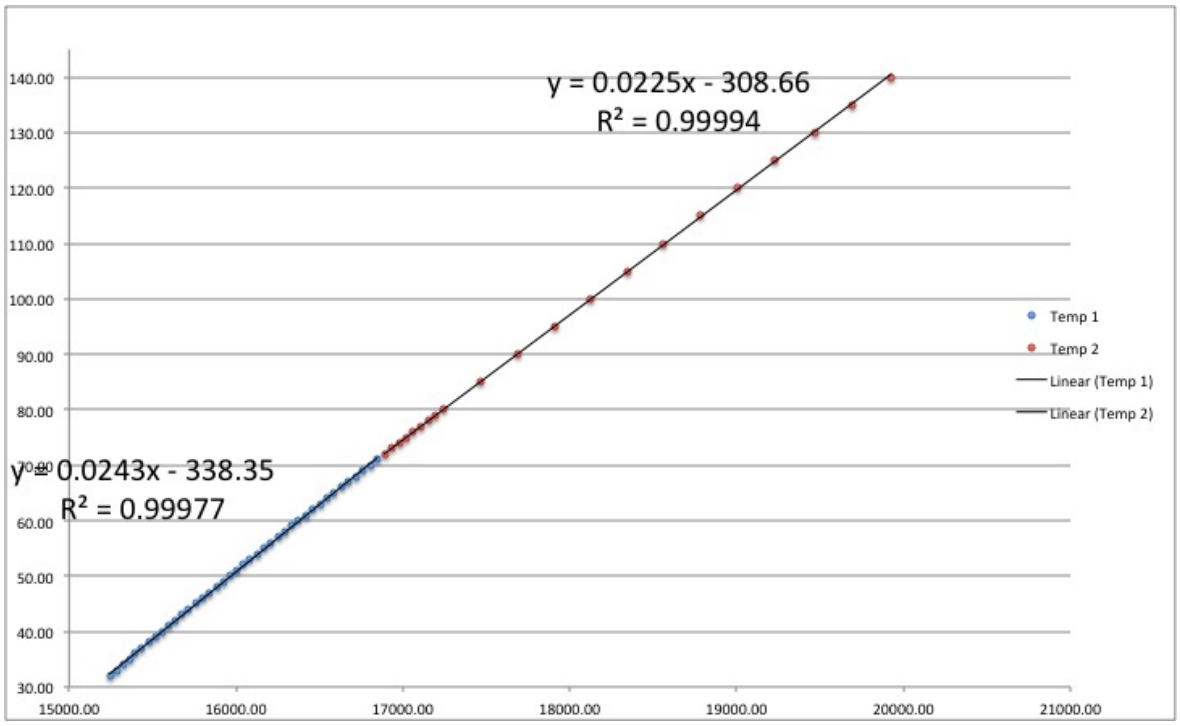


Figure 4.25 Calibration Data & Bi-Linear Trendlines (x-axis: RAW data [int], y-axis: temperature [℃]).

requiring significantly fewer cycles to complete:

$$1\times\text{comparison}\,(6\,\text{cycles})+1\times\text{multiplication}\,(13\,\text{cycles})+1\times\text{addition}\,(6\,\text{cycles}) = 25\,\text{cycles}.$$

The "divide & conquer" method improves the responsivity of the control system by reducing the temperature conversion duration. We have tested several values for switching from one linear conversion formula to the other one in order to optimize the error represented as R^2. We found the RAW data point corresponding to 70 °C optimal comparison value for switching formulas. The code for this method is provided in Appendix B.4.3.

Periodic Temperature Readout

The surface temperature feedback controlled laser operation requires periodic readout of the IRt/c sensor. The code for the periodic IRt/c readout is provided in Appendix B.6.

4.3.5 Control of Laser Irradiation

The irradiation control was achieved by sending a TTL signal generated by the microcontroller using a coaxial cable connected to the BNC port of the laser source controller. The MSP430F5529 code required for TTL laser irradiation control is provided in Appendix B.7.

In this dissertation study, we used the simplest control method, namely exposure modulation (on-off control), for controlling the irradiation of the laser. In this method, the laser irradiation is turned on while the measured temperature is below the target temperature, and vice versa. We have developed different versions of the embedded code as provided in Appendices B.8 to B.10 used for different experiments throughout this thesis work.

5. STUDY 1: MEASUREMENT OF SYSTEM SPECIFICATIONS

The performance of the developed temperature measurement system is of paramount importance for the control of irradiation during medical laser applications. Therefore, it is obligatory to measure the system specifications to evaluate whether it satisfies the requirements. The results of the conducted system specification tests were presented in Optical Interactions with Tissue and Cells XXVII conference during SPIE Photonics West 2016 (Appendix C). The manuscript of this presentation as published in Proceedings of SPIE, Vol. 9706 is available in Appendix D.

5.1 Materials & Methods

5.1.1 Microcontroller Techniques

I developed simple programs as part of the microcontroller code to assist us in the measurement of our systems technical specifications. These snippets are presented in Appendix B.

Hardware Stopwatch

I developed two functions (*i.e.*, `tic()` and `toc()`) for controlling one of the timer modules of the microcontroller as a hardware stopwatch to measure individual processes with a 10 µs precision. The stopwatch function operates independent of other processes because the timer module is an independent hardware peripheral. The codes for these functions are provided in Appendix B.3.

Moving Window Average Temperature Acquisition

A moving average function for temperature acquisitions were developed for the spatial resolution measurement procedure. The window size of this function was

dynamically adjustable (2, 4, 8, 16, 32, and 64 points) by pressing a pushbutton. This acts as a adjustable low-pass filter decreasing measurement noise while increasing response time. The codes for this function are provided in Appendix B.5.

5.1.2 Calibration & Accuracy

The temperature measurement system was calibrated using a blackbody calibrator (BB702, Omega Engineering, CT, USA) presented in Figure 5.1. The accuracy and the stability values of this device provided by the manufacturer are 0.5 °C and 0.1 °C, respectively. The blackbody calibrator was set to a temperature value and the measurement system was directed at the calibration target. The raw temperature data was recorded for 60 s after the calibrator reached steady-state. The recorded data was averaged, and this process was repeated for the temperature range of 30 °C to 150 °C. The resulting raw data – real temperature value pairs were used to calculate a mathematical formula for temperature conversion. Using this calibration technique, the average measurement error of the system was defined by the accuracies of the sensor and calibrator.

Our initial observation was that the temperature measurement suffers from noise to a small extent. This results in a transient measurement error which can be characterized by the standard deviation over a period of time. We calculated the standard deviation of the temperature measurement data over (*i.e.*, 60 s) as a measure of the transient error. We repeated this measurement when the calibrator was set to temperatures of physiological importance given in Table 6.1.

5.1.3 Spatial Resolution

The measurement of the spatial resolution was conducted using the knife-edge test as depicted in Figure 5.1. For this purpose, the blackbody calibrator was set to a temperature value higher than the ambient temperature. In this case we used 100 °C.

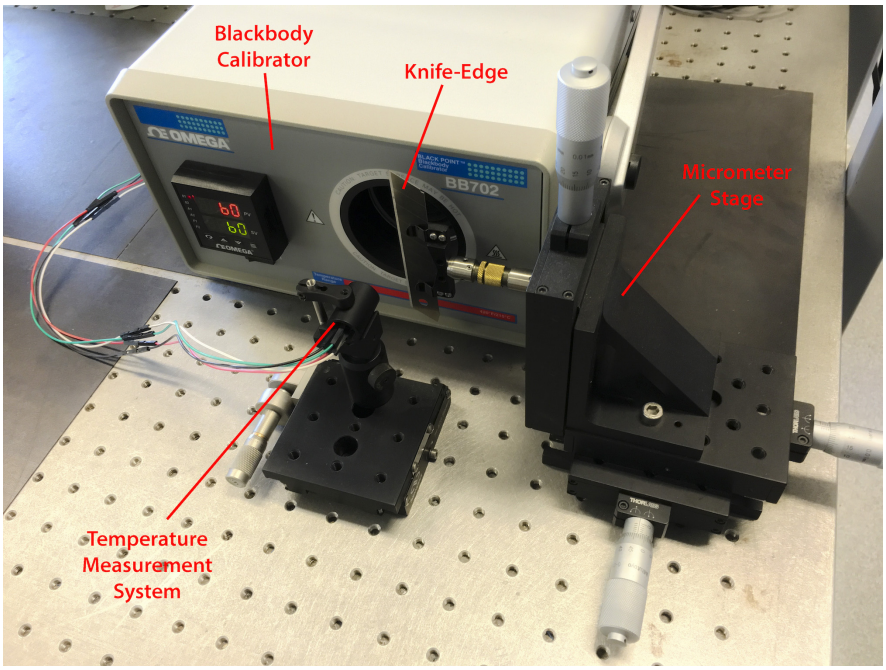


Figure 5.1 The blackbody calibrator and the knife-edge test setup.

The temperature measurement system was set to operate in 64-point moving average window mode to elude the effects of transient noise. The IRt/c sensor assembly was pointed to the calibrator target; and a razor blade attached to a micrometer stage was scanned between them. The average temperature value for each increment of the micrometer stage was recorded after the measurement data reached steady-state. The acquired data was analyzed to reveal 20/80 and 10/90 knife-edge diameter of the measurement spot.

5.1.4 Temporal Response

The procedure for measuring the response time of such a system requires a mechanical shutter and a target with known temperature value (*i.e.*, blackbody calibrator). The sensor is directed to the blackbody calibrator which is set to a high temperature value. The mechanical shutter at room temperature is positioned to block the line of sight of the sensor. When the shutter is opened, the time it takes for the measurement system to reach the blackbody target temperature value determines the time constant of the system. This measurement is conducted relatively easily using an

analog sensor that provides continuous output.

Nevertheless, our digital sensor provides periodic readout via SMBus (I^2C) communication protocol. In this case, one should sweep the readout interval from a small value to large value and acquire a series of measurements to determine the response time of the sensor. Luckily, the settling time of the sensor was provided by the manufacturer. Therefore, the temporal response of our system was not measured using conventional methods. I used the settling time to determine the readout interval of the system. The readout interval was set at a value slightly longer than the settling time to ensure proper operation. Even though the temperature readout is fast, it requires some time. The readout duration, defined as the time required for completing the SMBus (I^2C) communication with the sensor for temperature acquisition and conversion of the acquired data, is partly a function of the microprocessor speed. This duration was measured using the `tic()` and `toc()` functions of the developed microcontroller code. This duration is important because it affects the response time of the laser control signal.

5.2 Results & Discussion

5.2.1 Accuracy

The average accuracy of the system is expected to be $\pm 1\,^{\circ}C$, considering the sensor and calibrator accuracy values. The transient error of the system, defined as the standard deviation of the 60 s temperature recording, is given in Table 5.1. The standard deviation is observed as approximately $0.5\,^{\circ}C$ over a wide range of temperatures. Even though the noise present in the measurement system may result in momentary excessive or insufficient laser exposure, the thermal characteristics of the tissue can compensate for this error. Therefore, the average and transient accuracy values are sufficient for the reliable operation of the temperature measurement and laser control system.

5.2.2 Spatial Resolution

The 20/80 and 10/90 knife-edge diameters of the temperature measurement spot were found out as 2.5 mm and 3.6 mm, respectively. These values correspond with the measurement spot diameter values computed using the ray tracing software. Even though a smaller measurement spot diameter is preferable, the spatial resolution of the system is sufficient for many medical laser applications such as laser tissue welding, cartilage reshaping, photocoagulation, photodenaturation and treatment of granulation tissues.

5.2.3 Temporal Response

The durations of individual processes of the system provided in Table 5.2 accounted for a response time of less than 57 ms. The temperature acquisition, data conversion and processing processes take a total of 0.87 ms. The response time of the system is satisfactory for preventing thermal damage in most medical laser treatments.

Table 5.1
Transient error (measurement noise) for thermo-physiologically important temperatures.

T [°C]	σ [°C]
45	0.504
50	0.488
60	0.500
65	0.483
80	0.435

Table 5.2
Individual process durations of the temperature measurement system.

Process	t [ms]
Sensor Settling	55.516
Readout Interval	56
Temperature Acquisition, Data Conversion and Processing	0.87
Response Time	< 57

6. STUDY 2: TEMPERATURE CONTROLLED IRRADIATION ON WISTAR ALBINO RAT SKIN

We evaluated the practical performance of our temperature controlled medical laser system using Wistar albino rat skin tissue. This study revealed that our system is successful in controlling and maintaining tissue temperature at various physiologically important values over a long period of time (60 s). The results of this performance test were presented in Optical Interactions with Tissue and Cells XXVII conference during SPIE Photonics West 2016 (Appendix C). The manuscript of this presentation as published in Proceedings of SPIE, Vol. 9706 is available in Appendix D.

6.1 Study 2 Materials & Methods

6.1.1 Non-contact Temperature Controlled Medical Laser System

The temperature controlled medical laser system is basically the combination of the non-contact temperature measurement system and a laser system. A single microcontroller (MSP430F5529, Texas Instruments, USA) operates both systems.

The temperature measurement system is composed of a commercially available IRt/c sensor (MLX90614ESF-BCC, Melexis, Belgium) enclosed in an optical assembly



Figure 6.1 Fiber coupling (top) and laser beam delivery (bottom) assemblies.

and a microcontroller. The IRt/c sensor has a spectral bandwidth of 5.5 µm–12 µm. The optical assembly ensures that the diverging field-of-view (FOV) of the sensor is converted to a converging FOV, practically taking surface temperature measurements from a small spot at its focal distance. The measurement system has a spot diameter of 3.6 mm (10/90 knife-edge) at the focal distance of 41 mm. The sensor is setup to operate at 55.5 ms settling time. The microcontroller is operated with a 56 ms readout interval. The total response time of the system is *c.a.* 57 ms. Temperature measurement system has 1 °C accuracy and 0.02 °C resolution.

The laser system used in this study is an ytterbium fiber laser (YLM-20SC, IPG Photonics, MA, USA) operating at $\lambda = 1071$ nm. This wavelength does not interfere with the temperature measurement. The collimated output of the laser is coupled to a low-OH optical fiber patch cable ($\varnothing = 1000$ µm, $NA = 0.39$, M35L01, Thorlabs Inc., NJ, USA) using a lens tube assembly and a plano-convex N-BK7 lens (Thorlabs) as depicted in Figure 6.1. The other end of the patch cable was connected to another lens tube assembly sporting another plano-convex N-BK7 lens which functioned as the beam delivery optics. This beam delivery optical assembly was positioned perpendicularly above the target region to achieve a rather large laser spot diameter of *ca.* 7 mm for the sake of easy alignment. The laser spot had a Gaussian intensity profile due to the fiber coupling. The attenuation introduced by the optical assembly rendered the maximum achievable output power to a value of 8.3 W. This power value was used for the performance evaluation of our system.

The temperature measurement system was situated carefully above the target area with an oblique angle (off-axis placement with respect to beam delivery axis). This off-axis placement enabled coinciding the center of the laser spot with the measurement spot without blocking the laser beam. The experiment setup is exhibited in Figure 6.2.

The operation of the laser was modulated via a TTL signal generated by the microcontroller. An on-off control system was used for the temperature controlled laser irradiation.

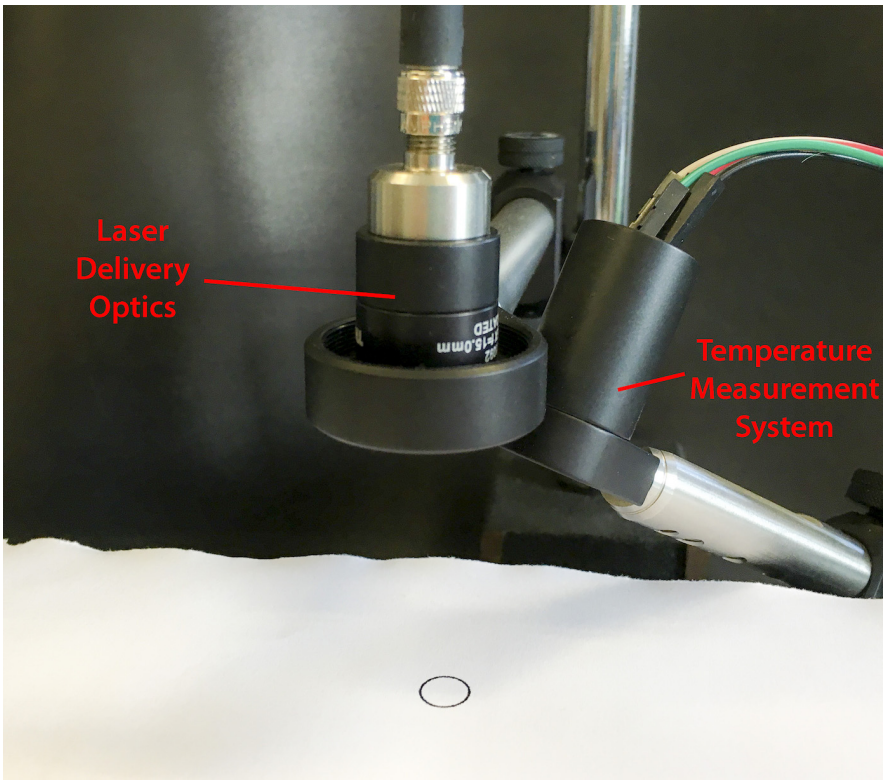


Figure 6.2 Temperature controlled laser irradiation setup.

Table 6.1
Temperature values used for the performance evaluation of the system.

Group T_{target}	Physiological Effect Laser Treatment
45 °C	Hyperthermia, Treatment of Granulation Tissue
50 °C	Reduction in Enzyme Activity, Cellular Immobilization Thermal Treatment of Malignant Tissues
60 °C	Denaturation of Proteins and Collagen, Coagulation, Surgical Hemostasis
65 °C	Ideal Temperature for Laser Tissue Welding
80 °C	Permeabilization of Membranes

6.1.2 Temperature Controlled Laser Irradiation Procedure

The preliminary practical performance criteria for this system was determined as its ability to maintain the tissue temperature at a set value by controlling the laser exposure. Five target temperature values were chosen to emulate significant thermo-physiological effects on tissues given in Table 6.1.

Full thickness skin tissue of a single Wistar albino rat ($n = 1$) recently sacrificed in course of another research project was harvested in flap form. The samples were placed on a lab jack epidermal side (fur side) down. The laser exposure was initiated while the temperature measurement and laser control system was operational. The system was kept active for at least 60 s after the set target temperature value has been reached. The temperature data and laser control signal was recorded for analysis. This procedure has been repeated for all five target temperature values.

The average temperature value was calculated for 60 s after the target temperature was reached (during temperature maintenance interval). The difference between the target and average temperature values provides a quantitative measure for the performance of the system for the set laser parameters and target temperature. The standard deviation of the same temperature data was also calculated for assessing the dynamic variation of the tissue temperature.

6.2 Study 2 Results & Discussion

The temperature data of the skin tissues undergoing controlled laser irradiation with various target temperatures are represented with different colors in Figure 6.3. The target temperatures are marked with horizontal lines in the same graph for convenience. The 60 s average temperatures and standard deviation values after reaching the target temperatures are provided in Table 6.2.

The small differences between the target and average tissue temperatures reveal

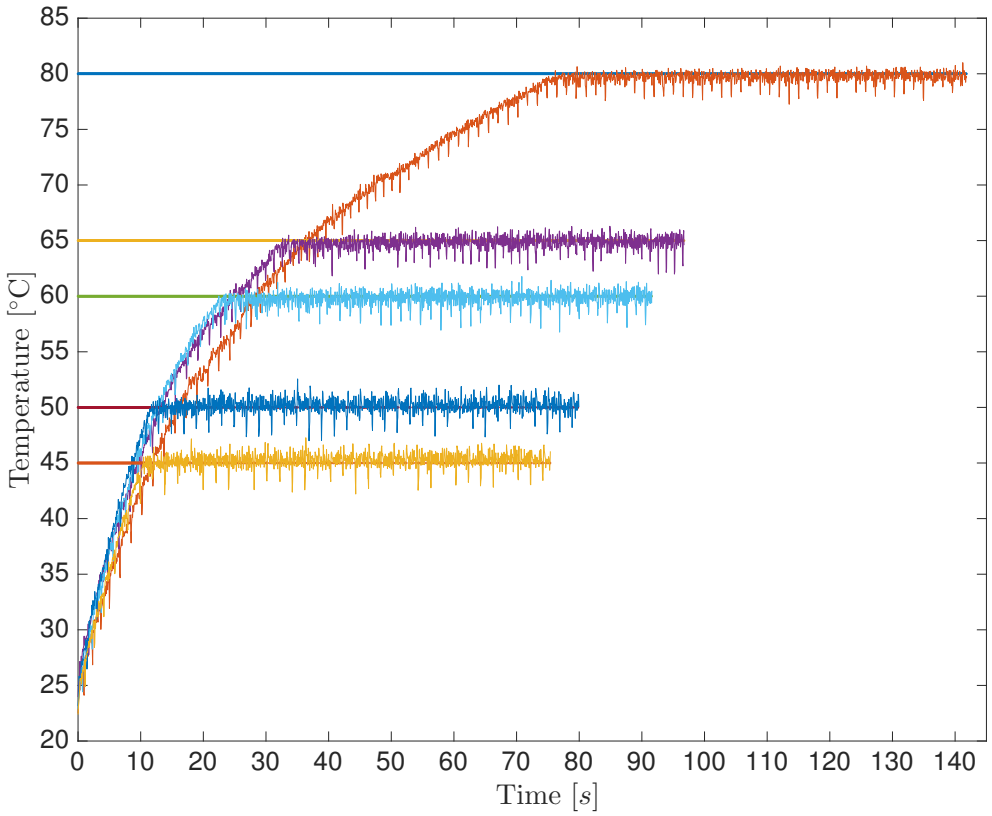


Figure 6.3 Temperature controlled laser irradiation.

that our system is capable of maintaining the tissue temperature by controlling laser irradiation. The on-off control system is satisfactory. The comparison of the standard deviation values given in Tables 5.1 and 6.2 reveal that the variation of the temperature after reaching the target value is significantly due to measurement noise. The noise certainly affected the laser exposure undesirably. Nevertheless, the thermal inertia of the tissue conveniently corrected for these momentary errors acting as a low pass filter.

The fact that temperature increase curves do not overlap in Figure 6.3 support the phenomena of non-homogenous optical/thermal characteristics even for the tissues of the same individual. This is a proof of the requirement for a temperature controlled medical laser system.

Table 6.2
Performance characteristics for thermo-physiologically important temperatures.
(μ: mean value, σ: standard deviation).

T_{target} [°C]	T_{tissue} ($\mu \pm \sigma$) [°C]
45	45.273 ± 0.704
50	50.158 ± 0.742
60	59.819 ± 0.698
65	64.855 ± 0.673
80	79.693 ± 0.524

7. STUDY 3: CONTROLLED THERMAL DENATURATION ON BOVINE LIVER TISSUE

Building on our previous study elaborated in Chapter 6, this study evaluates the practical performance of our system (*i.e.*, regulating thermal denaturation zone while preventing excessive thermal damage and ensuring target temperature is reached) using higher power densities. In addition, we use a non-homogenous and non-uniform large (statistically meaningful) sample population, *i.e. ex vivo* bovine liver. These *ex vivo* samples acquired from a slaughterhouse are considered as a phantom that is as close as possible to *in vivo* tissues in terms of thermal and optical characteristics. Furthermore, the variations among these samples are a better representative of clinical conditions which cannot be created using uniform laboratory animals. We used three laser powers (10.2 W, 6.8 W and 3.4 W corresponding to *c.a.* 106 W cm^{-2}, 71 W cm^{-2} and 35 W cm^{-2}) and three target temperatures (75 °C, 65 °C and 55 °C) in a total of nine groups ($n = 16$). We also compared our results with a fixed-dose application conducted as a control experiment composed of the same three laser power groups and corresponding three average energy groups (per laser power group) to reach the same target temperatures. Our results prove that our temperature-controlled system is capable of preventing excessive temperatures using different laser power and target temperature combinations. Additionally, using target temperature as a controlled variable, our system can control the denaturation diameter better than it can control the thermal denaturation depth. Besides, our system can also reduce the effect of laser power on the diameter and depth of the thermal denaturation zone in contrast to fixed-dose applications. Moreover, fixed-dose application resulted in a final temperature range of more than 26 °C at the end of the exposure duration in ⅓ of groups. Furthermore, we present the temperature-time response data in a unique style (superimposition of all measurements within the same group) facilitating qualitative and quantitative interpretation and comparison. This representation style enabled us to instantly recognize that optical and thermal properties of tissues dominate the temperature-time response when using low laser powers leading to wider ranges of final temperatures and exposure

durations (to reach target temperature) in the fixed-dose and temperature-controlled applications, respectively.

7.1 Study 3 Materials & Methods

We used bovine liver as tissue sample for several reasons. Bovine liver is easy to acquire and conforms with other soft tissues regarding water content. Besides, its thermal denaturation is easy to determine when macroscopically observed. Furthermore, using *ex vivo* tissue samples acquired from a slaughterhouse on different days enabled us to match clinical conditions (widely varying optical and thermal characteristics among subjects) in contrast to the more uniform properties among laboratory animals. Near-IR, and specifically Nd:YAG ($\lambda = 1064\,\text{nm}$) lasers are commonly used for thermal denaturation of liver tissue due to their ideally balanced tissue penetration and absorption characteristics [46, 65]. For this purpose, we used a near-IR laser with a similar center wavelength ($\lambda = 1071\,\text{nm}$).

7.1.1 Non-contact Temperature Controlled Medical Laser System

The experimental setup is identical to the one we used in our previous study (Chapter 6 and Appendix D) [66]. We only made slight modifications on that system. It is composed of a laser ($\lambda = 1071\,\text{nm}$, Ytterbium Fiber Laser, YLM-20SC, IPG Photonics, MA, USA), laser delivery optics designed for a converging beam with a Gaussian profile, providing a spot diameter of 3.5 mm ($1/e^2$) at the application distance (40 mm), and an IRt/c temperature measurement and laser control system (5.5 µm–12 µm spectral bandwidth) as illustrated in Figure 4.1. We used a commercially available IRt/c sensor (MLX90614ESF-BCC, Melexis, Belgium) in our temperature measurement system. The control system takes measurements from a 3.6 mm diameter spot at 41 mm focal distance. It operates at 57 ms refresh time with 1 °C accuracy and 0.02 °C resolution. The IRt/c sensor assembly is attached to the side of the laser delivery optics at an oblique angle to perfectly coincide laser and temperature measurement spots

without interfering with the laser beam as depicted in Figure 7.1. We have used an ON-OFF feedback control mechanism for ensuring fast response of the system. The laser exposure is modulated using a TTL signal generated by the microcontroller. It also feeds real-time temperature data and the laser control signal to a computer via USB cable using UART protocol to display and store for further processing.

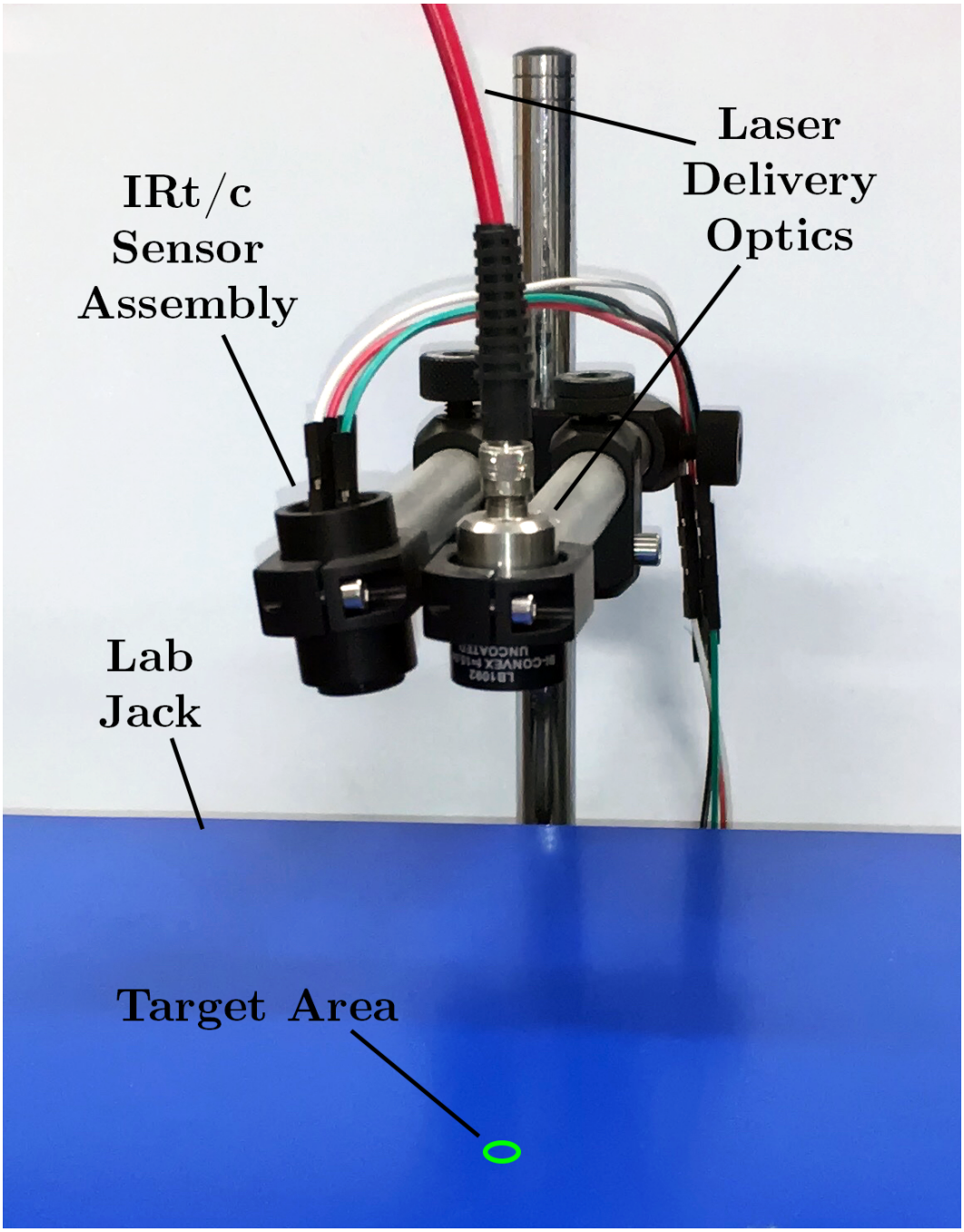


Figure 7.1 Experiment setup: The laser delivery optics ($\varnothing_{\text{laser}} = 3.5\,\text{mm}$ @ $\text{d} = 40\,\text{mm}$, Gaussian) and the temperature measurement system ($\varnothing_{\text{measurement}} = 3.6\,\text{mm}$ @ $\text{f} = 41\,\text{mm}$) are in an off-axis alignment configuration.

7.1.2 Thermal Denaturation of Bovine Liver Tissue

Groups

We used three different laser powers and three different target temperatures in the temperature controlled application enabling us to evaluate their effect on the extent of thermal denaturation diameter and depth. We also conducted a fixed-dose application as a control experiment which, additionally, enabled us to show the difference between tissue temperatures reached at the end of the exposure within the same group. We used the same three power levels in the fixed-dose application. The fixed-dose of each group in the control experiment was determined from the temperature controlled application data by computing the average delivered dose (energy) in its corresponding group. The power levels 3.4 W, 6.8 W and 10.2 W correspond to average power densities of 35 W cm^{-2}, 71 W cm^{-2} and 106 W cm^{-2}, respectively, for the 3.5 mm ($1/e^2$) diameter Gaussian profile laser spot. The maximum power density values can reach to twice these values for the most central part of the beam due to the Gaussian profile. The target temperatures and fixed-dose values of groups ($n = 16$) are provided in Table 7.1.

Sample Preparation

Fresh bovine livers were acquired from the abbatoir as soon as possible after the slaughtering of the animal and stored at 4 °C. Then, the liver of each animal was dissected to end up with 9 or 18 samples of *ca.* 3 cm × 3 cm × 1.5 cm. This size was sufficient for providing a smooth and even surface for the target area, away from fascia

Table 7.1
Average dose delivered in the temperature controlled (experiment) groups and their equivalent exposure duration for the given power setting in fixed-dose (control) groups.

	55 °C	65 °C	75 °C
3.4 W	83.4 J (24.54 s)	142.5 J (41.91 s)	215.1 J (63.26 s)
6.8 W	53.5 J (7.87 s)	74.3 J (10.93 s)	104.0 J (15.29 s)
10.2 W	41.7 J (4.09 s)	64.5 J (6.32 s)	79.8 J (7.82 s)

and veins. The samples were packaged in aluminum foil for preventing desiccation and assigned randomly to groups. After reaching room temperature (*ca.* 23 °C), they were placed on a lab jack for irradiation.

The temperature controlled and fixed-dose applications were conducted at different time intervals and durations. Hence, there was an unintended and unavoidable difference in the variation of acquired samples between both experiments. The samples used in the fixed-dose application were more uniform in color and texture, and that may lead to smaller standard deviation values for final tissue temperature ranges (at the end of exposure) and thermal denaturation zones.

Irradiation Procedure

The lab jack height was adjusted for aligning the top surface of the tissue sample with the laser spot and temperature measurement spot (Figure 7.1). The sample was positioned with the help of a visible guide beam to target an ideal locus. Laser irradiation procedure was initiated from the computer by first starting the temperature data recording and then turning CW laser exposure on. In the temperature controlled application, once the tissue temperature reached the target value, the microcontroller modulated the laser exposure to maintain the target temperature for 5 s and then ceased the irradiation. In the fixed-dose application, the irradiation was ceased after the corresponding fixed exposure duration passed.

7.1.3 Evaluation of Thermal Denaturation Area & Statistical Analysis

Ideally, thermal damage is evaluated histologically with the help of staining techniques. Hematoxylin and eosin (H&E) or trichrome stains are used to visualize thermally denatured collagen in tissues, which is a surrogate marker for thermal damage [67]. Collagen can also be utilized in polarization microscopy by observing loss of its birefringence due to thermal denaturation [68,69]. A recent trend for the evaluation of thermally treated tissues is viability staining methods. Tetrazolium based stains [*e.g.*, triphenyltetrazolium chloride (TTC) and nitroblue tetrazolium chloride (NBT)]

interact with active cellular enzymes and mitochondrial cofactors to demarcate viable tissues [67, 69]. Denaturation of these enzymes and disruption of mitochondrial processes due to thermal damage (non-viable tissues) will result in unstained (native colored) tissues.

Unfortunately, none of the above mentioned techniques are suitable for the evaluation of our samples. Liver tissues contain very little amounts of collagen ruling out H&E and trichrome staining as well as polarization microscopy techniques. Actually, we also conducted a histological evaluation using H$E staining in combination with bright-field, dark-field and polarization microscopy techniques. However, we were not able to distinguish thermally denatured areas from intact areas. Abattoir regulations in our country prevent acquisition of tissues at early stages of the process and render the tissues incompatible with viability staining methods (due to immediate cooling and prolonged acquisition time) as per the procedure described by Beatty *et al.* (2015). Therefore, we evaluated the thermal denaturation in our samples by macroscopical inspection of color change and opacification (whitening).

The thermal denaturation diameter and depth of the irradiated samples were photographed using cross-polarization imaging technique to eliminate reflections that can complicate the evaluation process [70]. A camera fitted with a prime macro lens and a circular polarizer (linear polarizer and quarter-wave plate combination) was placed perpendicularly at a fixed distance above the sample. The light source (flash) fitted with a linear polarizer was placed at an oblique angle (45°) to further avoid surface reflections. The thermal denaturation depth images were taken after dissecting the sample along the center of the thermal denaturation zone. All photographs were taken with fixed magnification, shutter speed, f-number, ISO, and flash intensity. A scale was aligned to the sample surface as a reference. A MATLAB code was composed to facilitate the blinded acquisition of manual measurements by three evaluators by marking the perceived thermal denaturation boundary. The three measurements for each sample were averaged.

We performed one-way analysis of variance (ANOVA) of thermal denaturation

zone measurements for each set of three groups with a common parameter (three laser powers & three target temperatures for temperature controlled application and three laser powers & three $E_{T_{target}}$ for fixed-dose application). Scheffe's procedure was used to determine statistical differences between groups in the *post hoc* multiple comparison test after the one-way ANOVA conducted in MATLAB. Two-way ANOVA was performed to evaluate the interaction between laser power and target temperature in the temperature controlled application (laser power and $E_{T_{target}}$ in the fixed-dose application) on thermal denaturation zone. Significance level was set at $p < .05$ for all statistical tests.

7.2 Study 3 Results & Discussion

7.2.1 Temperature-Time Response

Figures 7.2 and 7.3 reveal the raw (unfiltered) temperature measurement data of all samples superimposed according to their groups in the temperature-controlled and the fixed-dose applications, respectively. The same axis ranges were used for time and temperature axes within each figure to facilitate comparison among groups. Presentation of temperature data in this style provides meaningful insight into the thermal response of tissue. Further descriptive quantitative thermal data is provided in Tables 7.2 and 7.3, for the temperature-controlled and the fixed-dose experiments, respectively.

Temperature-time responses of samples vary significantly within the same application group as depicted in Figures 7.2 and 7.3. These results confirm our initial assumptions regarding the non-uniformity of optical and thermal characteristics among subjects and prove that temperature control is necessary for photothermal medical laser applications. As illustrated in Figure 7.2, our system can successfully control the tissue temperature during laser exposure. Mean tissue temperatures during the 5 s temperature-controlled period do not deviate from the target value more than 0.6 °C on average. The maximum and minimum temperatures observed during this period also

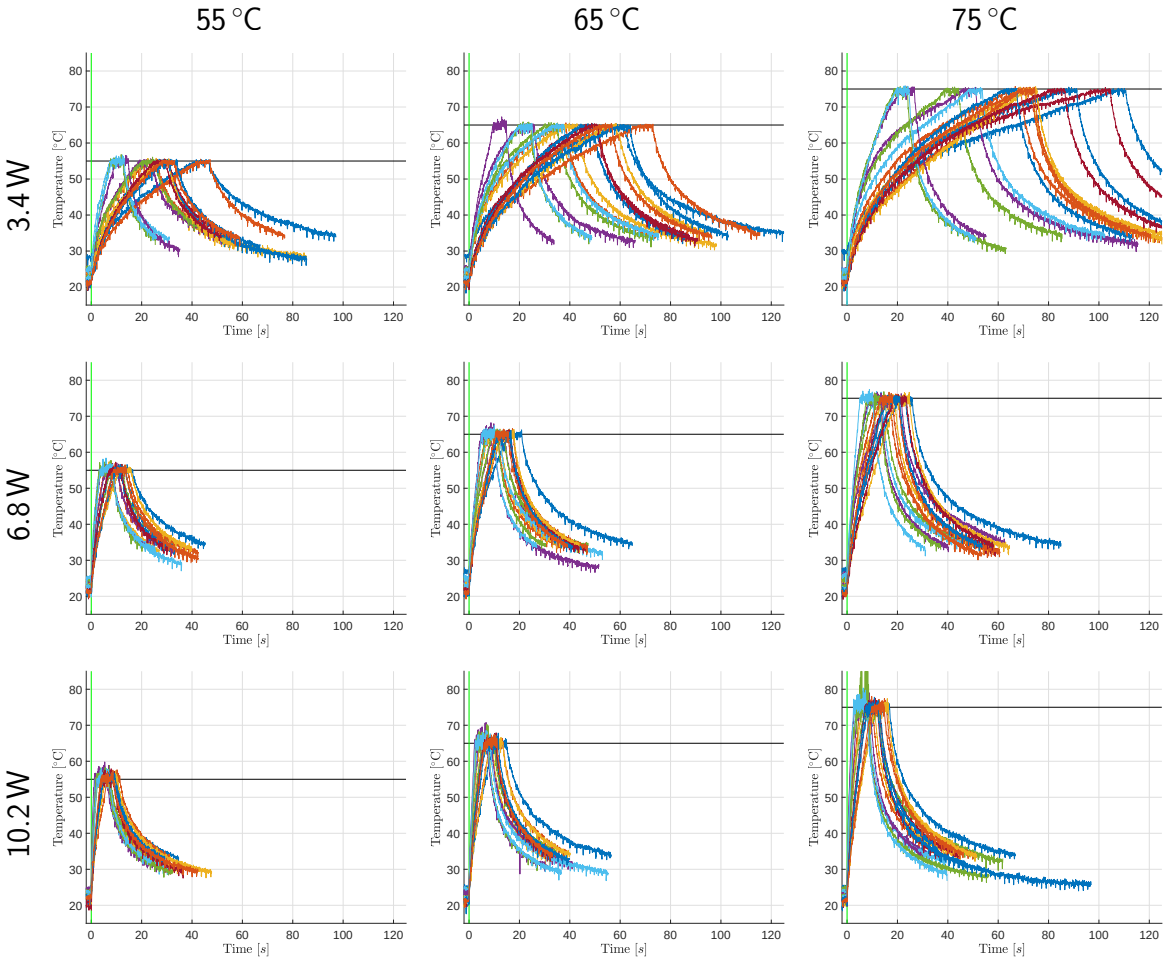


Figure 7.2 Temperature monitorization data of the temperature controlled application. The temperature-time response graphs within each group are superimposed. The horizontal black lines and the vertical green lines represent the target temperature values and the laser emission commencement marks, respectively.

remain within a narrow range (4.1 °C on average) demonstrating the temperature stability our system can provide. This finding is also supported by the small magnitudes of all standard deviation values in Table 7.2.

On the other hand, fixed-dose application results display increasing tissue temperatures until the end of the procedure (cessation of irradiation), as shown in Figure 7.3, resulting in a wide range of final temperatures within each group, as presented in Figure 7.4. The large standard deviation values (5.6 °C on average) and range (19.8 °C on average) of final temperature is provided in Table 7.3. Considering that the sample population of the fixed-dose application was more uniform in tissue color

Table 7.2
Descriptive temperature values for the surface temperature controlled application: The mean (μ) and standard deviation (σ) values of maximum (T_{max}), minimum (T_{min}), mean (μ_T) and standard deviation (σ_T) values of the tissue surface temperature during the 5 s-period at the target value.

P_{laser}	T_{target}	$\mu_{T_{5\,s}}(\mu\pm\sigma)$[°C]	$\sigma_{T_{5\,s}}(\mu\pm\sigma)$[°C]	$T_{max}(\mu\pm\sigma)$[°C]	$T_{min}(\mu\pm\sigma)$[°C]
	55 °C	54.6 ± 0.1	0.6 ± 0.1	55.8 ± 0.5	52.8 ± 0.4
3.4 W	65 °C	64.5 ± 0.1	0.5 ± 0.1	65.6 ± 0.5	62.8 ± 0.4
	75 °C	74.4 ± 0.1	0.6 ± 0.1	75.5 ± 0.2	72.6 ± 0.7
	55 °C	55.0 ± 0.2	0.7 ± 0.1	57.0 ± 0.6	52.9 ± 0.5
6.8 W	65 °C	64.8 ± 0.2	0.8 ± 0.2	66.6 ± 0.6	62.6 ± 0.6
	75 °C	74.6 ± 0.1	0.8 ± 0.1	76.4 ± 0.5	72.4 ± 0.5
	55 °C	55.3 ± 0.2	1.0 ± 0.2	57.8 ± 0.9	52.8 ± 0.5
10.2 W	65 °C	65.1 ± 0.3	1.1 ± 0.3	67.8 ± 1.2	62.3 ± 0.7
	75 °C	74.9 ± 0.8	1.3 ± 0.8	77.5 ± 1.1	71.8 ± 1.3

Table 7.3
Descriptive temperature values for the fixed-dose application: The mean (μ), standard deviation (σ), maximum (max) and minimum (min) values of the achieved tissue temperature at the end of laser exposure (T_{final}).

P_{laser}	$t_{exposure}$	E	$T_{final}(\mu\pm\sigma)$[°C]	$T_{final\,(max)}$[°C]	$T_{final\,(min)}$[°C]
	24.54 s	83.4 J	56.5 ± 3.2	64.3	53.8
3.4 W	41.91 s	142.5 J	69.5 ± 7.5	91.2	61.6
	63.26 s	215.1 J	77.5 ± 8.7	97.4	66.2
	7.87 s	53.5 J	59.0 ± 4.6	70.1	53.1
6.8 W	10.93 s	74.3 J	67.8 ± 4.3	74.5	60.2
	15.29 s	104.0 J	81.0 ± 7.9	96.6	70.0
	4.09 s	41.7 J	57.5 ± 2.9	61.4	52.2
10.2 W	6.32 s	64.5 J	70.9 ± 5.5	85.1	63.0
	7.82 s	79.8 J	79.3 ± 6.1	89.4	71.0

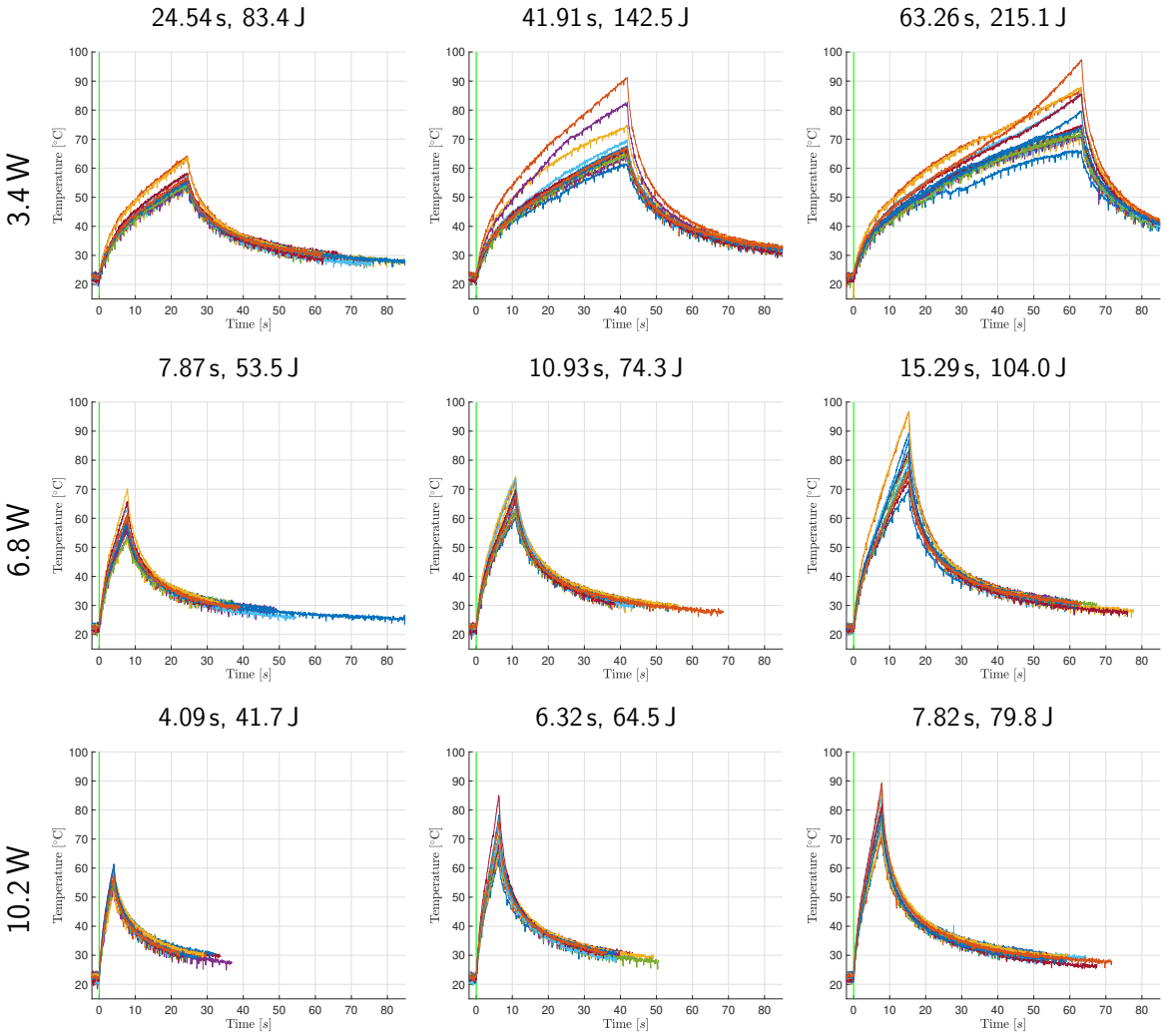


Figure 7.3 Temperature monitorization data of the fixed-dose application. The temperature-time response graphs within each group are superimposed. The vertical green lines represent the laser emission commencement marks.

and texture than the sample population of the temperature-controlled application, a wider range of final temperatures than we report in this study is more probable for fixed-dose applications. Nevertheless, these results prove that a fixed-dose cannot be relied upon to ensure treatment success (reaching desired temperature) while preventing excessive thermal damage in the clinical conditions due to the high temperature sensitivity of physiological effects generated in PTT.

Arrhenius integral suggests that the progression of thermal damage is linear for constant tissue temperatures and exponential for linearly increasing tissue temperatures [10]. Consequently, swiftly reaching a target value (depending on the desired

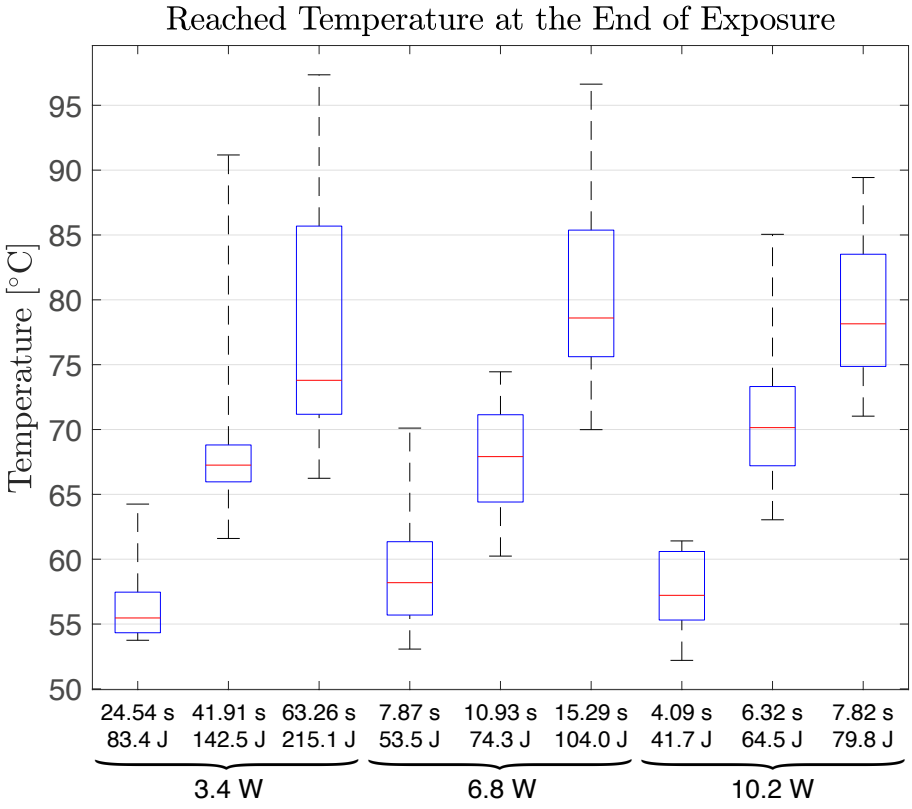


Figure 7.4 Box and whiskers plot of the tissue temperature reached at the end of exposure in the fixed-dose application. The red horizontal lines are the group medians. The blue boxes mark the interquartile ranges. The whiskers indicate the whole data range.

physiological effect) and maintaining the tissue temperature at that value renders the progression of thermal damage a linear function of time. Evidently, fixed-dose applications can neither provide linear progression of thermal damage (due to the constant change in tissue temperature), nor ensure that the desired physiological effect is generated while preventing others (due to the wide range of final temperatures). In contrast, our system can be used to constrain tissue temperature during laser exposure to control progression of thermal damage while guaranteeing induction of desired physiological effects and preventing undesirable outcomes (*e.g.*, carbonization, heat fixation, coagulative necrosis).

Among a total of 144 samples, only two samples of group C ($P_{laser} = 10.2\,W$, $T_{target} = 75\,°C$) in the temperature controlled application displayed anomalies indicating limitations of the system. Upon further investigation, we found that one sample contained fascia tissue underneath the target area, and temperature increase caused

it to contract, moving the laser irradiated surface away from the measurement spot. The fact that ours is a confocal *but* not a coaxial optical system caused measurement errors due to the alteration of the target surface distance to the probe. Off-axis alignment requires a precise and constant application distance. Use of a mechanical spacer or another technology (*e.g.*, a distance sensor) to ensure the required target to probe distance is necessary for handheld operation. The other sample experienced a high rate of temperature change ($>20\,^{\circ}\mathrm{C\,s^{-1}}$) and has undergone partial carbonization following desiccation, even though the highest measured temperature was below 90 °C. In the fixed-dose application, one sample in group 3.4 W & 63.26 s (215.1 J) and one sample in group 6.8 W & 15.29 s (104.0 J) have undergone partial carbonization at the center of the denaturation area. Considering the Gaussian laser beam generates higher temperatures at the center of the spot, partial carbonization at that location is natural.

In both samples, the measured tissue temperature was below 100 °C. The reason for not detecting these local high temperature values (causing carbonization) may be the averaging of the blackbody radiation over the whole measurement spot of the IRt/c system. This phenomenon acts as a spatial low pass filter and averages out local thermal maxima and minima preventing detection of localized high temperatures. Even though the IRt/c system has a centrally weighted measurement spot, it has a wider distribution profile than a Gaussian beam, which also would have negatively influenced the averaging effect. Another consideration may be the vulnerability of the measurement system to changes in tissue emissivity, which in this case would be due to local desiccation. The accuracy and thus the performance of this system relies on the assumption of constant tissue emissivity that is equal to the emissivity of water. Yet, there is a linear relationship between the measured temperature and the fourth root of $1/\epsilon$ (inverse of emissivity), which corresponds to negligible measurement errors unless the change in emissivity is dramatic.

In the temperature-controlled application, we observed a positive correlation between the average rate of temperature increase ($^{\Delta T}/_{\Delta T}$) and the temperature variation at the target value, where ΔT is the CW exposure time necessary for reaching target temperature and ΔT is the difference between initial and target temperatures. The

Spearman ($r = .90$, $p < .001$) and Pearson ($r = .87$, $p < .001$) coefficients were computed for the correlation between $\Delta T/\Delta T$ at the temperature increase phase and the standard deviation of temperature measurements during the 5 s period at the target value. The temperature measurement data of all samples ($n = 143$) were used for this analysis but one, which was an exception that showed signs of desiccation and carbonization. This correlation is probably due to the synergistic effect of the measurement noise and the 57 ms refresh rate of our control system. As in the scenario illustrated in Figure 7.5, measurement noise may delay the detection of threshold (T_{target}) crossing (from t_1 to t_2, or from t_3 to t_4). Meanwhile, the actual tissue temperature continues to rise above or fall below the target temperature, leading to higher variation. Thus, a measurement system with a faster refresh rate or smaller measurement noise would result in less variation at the target temperature. Nonetheless, the contribution of high dT/dt values for the temperature variation at target value is expected to diminish *in vivo*, where active perfusion of tissues will decrease the rate of temperature increase [26].

As the tissue is exposed to laser light, its temperature increases and a multitude of phenomena occur simultaneously [53]. Coagulation and denaturation of proteins

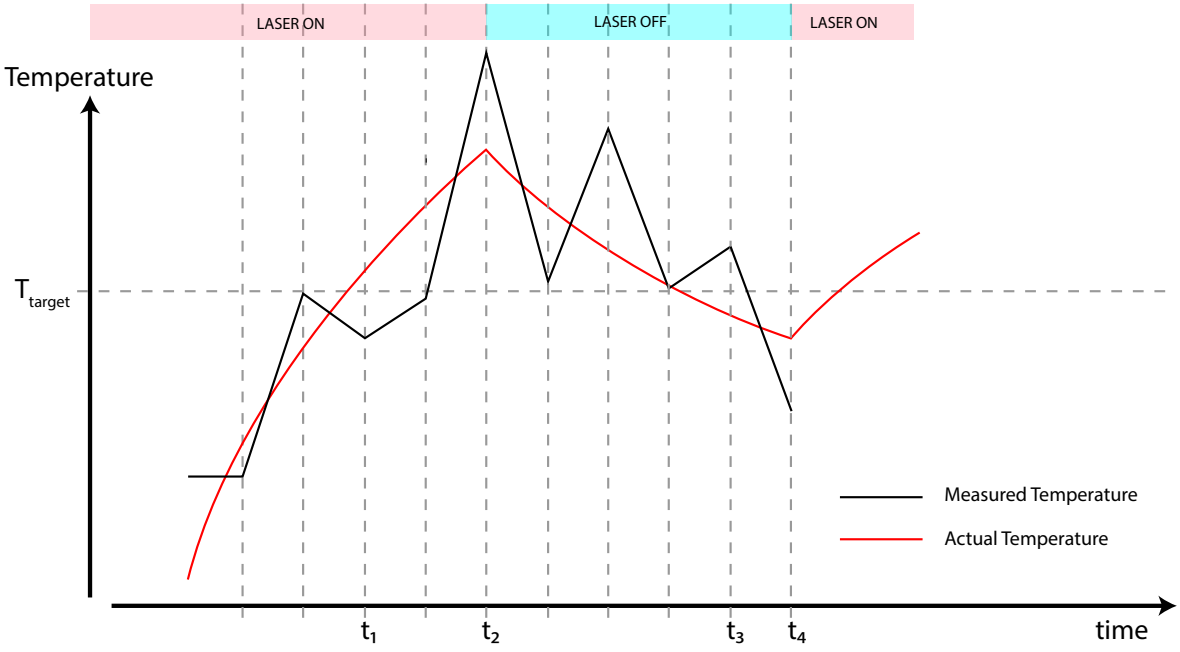


Figure 7.5 Synergistic effect of measurement noise and discrete refresh time on temperature variation at target value.

change the optical properties of the tissue [10, 28, 51]. Moreover, the absorption coefficient of water at the ytterbium fiber laser wavelength ($\lambda_{\text{center}} \approx 1070\,\text{nm}$) decreases with increasing temperature [52]. The water content of the tissue may change due to evaporation induced dehydration (in conditions with very high temperatures or extended exposure durations). As water content decreases, thermal conductivity of tissue reduces [50]. Optical and thermal properties of the tissue dynamically change with its temperature and hydration level during laser irradiation [10, 26, 28].

In the temperature-controlled application, the lower power groups display a higher variation in their temperature increase curves. It seems that optical and thermal differences of samples dominate the temperature-time response of tissue when laser power is low. Besides, low power groups require longer to reach the target temperature. Thus, the tissue has more time to undergo optical and thermal property changes elaborated above. The same observation and deduction are also valid, albeit to a lesser extent, for higher target temperature groups corresponding to longer exposure durations. Low power and longer duration groups (3.4 W & 41.91 s and 3.4 W & 63.26 s) in the fixed-dose application also display a higher variation in their temperature-time response curves. This resulted in higher final temperature ranges as presented in Table 7.3.

Generally, the temperature-time response of our samples showed a logarithmic characteristic. We observed regions with a more abrupt change of curvature in some of the low power groups (especially groups 3.4 W & 65 °C and 3.4 W & 75 °C, corresponding to longer exposure times) leading to slight deviations from the logarithmic model. We were not able to generalize the characteristics of these changes. The change of temperature-time response curves may be due to the modifications of optical and thermal characteristics the tissues experience at these temperature values, which are also varying among subjects [50–52]. Another reason for these deviations in the temperature increase curves may be dehydration-induced emissivity reduction. Nevertheless, we did not observe extreme desiccation in our samples that may lead to dramatic reductions in emissivity except the three partially carbonized samples. Additionally, under normal circumstances, we do not expect significant dehydration at the temperatures and

the exposure durations we encounter in our study. Moreover, a significant reduction of tissue emissivity affecting a large percentage of the measurement spot would have manifested itself as a higher reduction of $^{dT}/_{dt}$ at high temperatures (>80 °C) which is not apparent in our data. Hence, we assume that the desiccation induced measurement errors are negligible.

7.2.2 Thermal Denaturation

The representative thermal denaturation area photographs are depicted in Figure 7.6. Box and whiskers plots of the measured thermal denaturation diameters and depths for the temperature-controlled and fixed-dose applications are provided in Figures 7.7 and 7.8, respectively. Tables 7.4 and 7.5 exhibit the mean and standard deviation values of the thermal denaturation diameters and depths in temperature-controlled and fixed-dose applications, respectively. The thermal denaturation size clearly increases with rising target temperature values and corresponding doses for all power groups. There is also a trend for an increase in thermal denaturation size with decreasing laser power for all target temperature and corresponding dose groups.

One-way ANOVA results provided in Tables 7.6 and 7.7 indicate that both laser power and dose statistically significantly affect denaturation diameter and depth in the fixed-dose application. In the temperature controlled- application, target temperature has a statistically significant effect on denaturation diameter and depth. But, there is no statistically significant effect of laser power on denaturation diameter in 75 °C target temperature groups and on denaturation depth in any of the target temperature groups. Tables 7.8 and 7.9 contain the *post hoc* tests conducted using Scheffe's procedure for denaturation diameter and depth values of the temperature-controlled and fixed-dose experiments, respectively. In these tables, the p-value of comparison between two groups are provided along the solid or dotted lines connecting them. A solid line and a bold p-value represents statistical significance ($p < .05$).

Post hoc Test Results for Thermal Denaturation Diameter

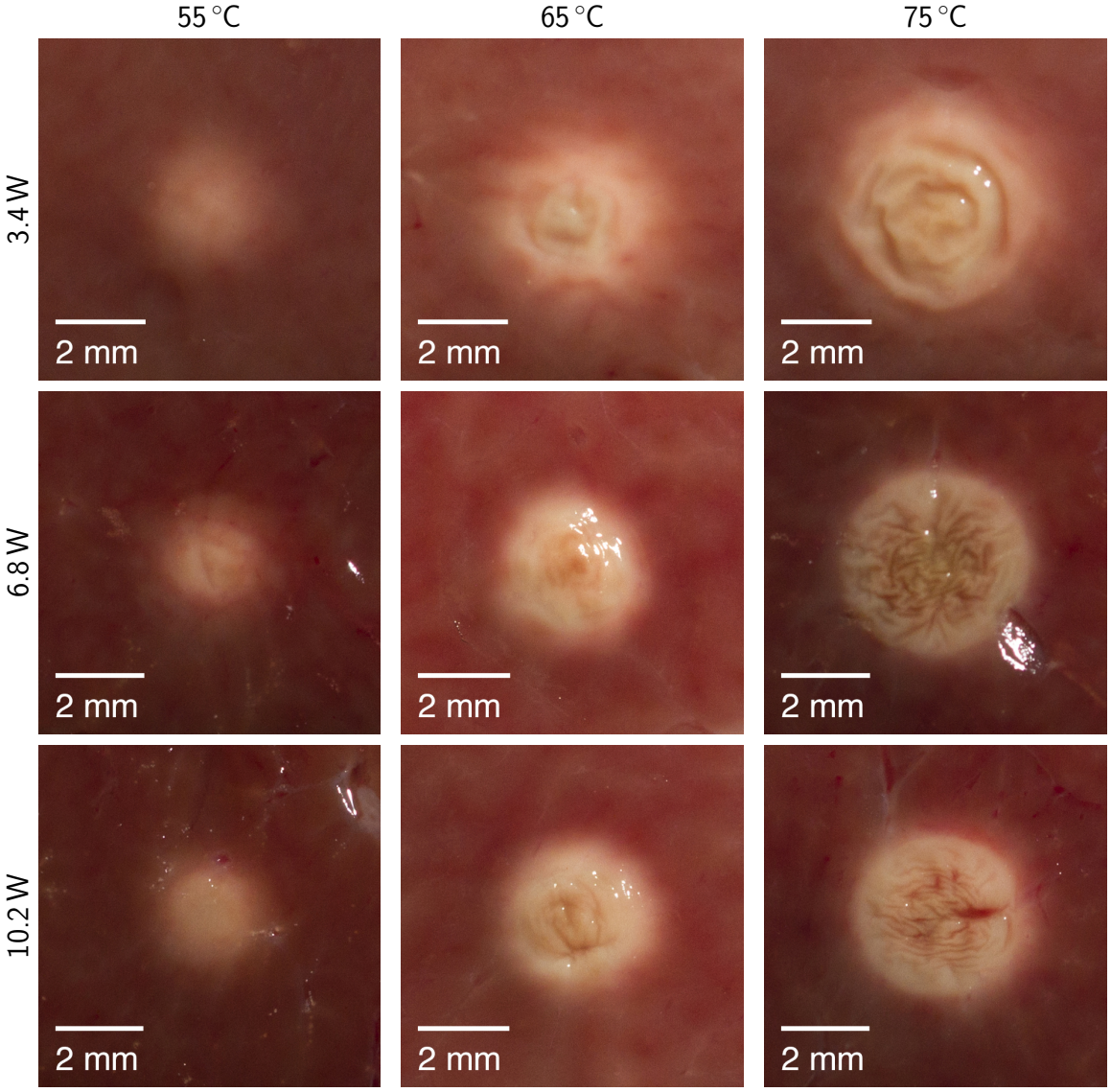


Figure 7.6 Exemplary bovine liver photothermal denaturation photographs for temperature controlled application groups.

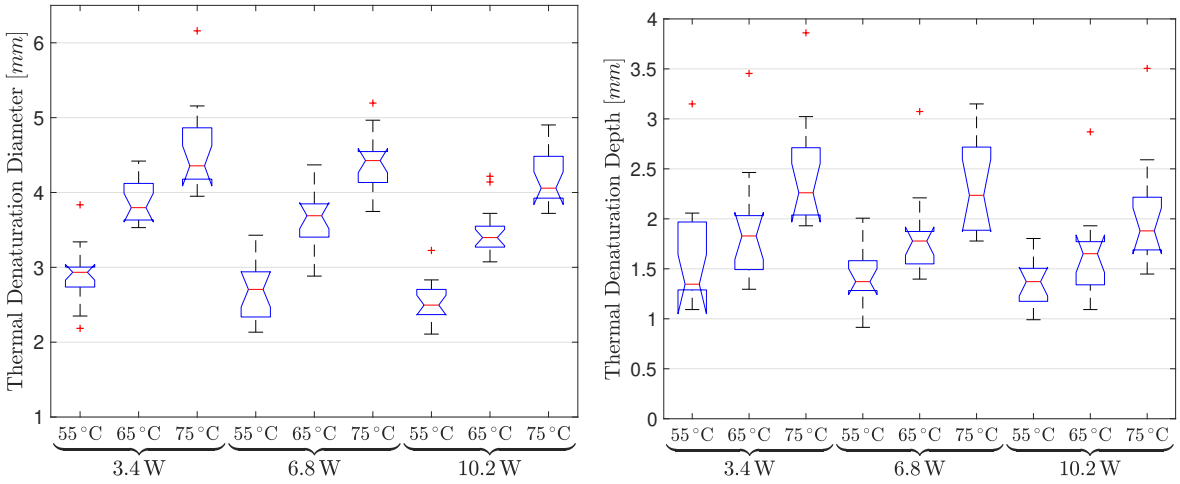


Figure 7.7 Box and whiskers plot of thermal denaturation diameters ($n = 16$) and depths ($n = 13$) of the temperature-controlled experiment.. The red horizontal lines are the group medians. The blue boxes mark the interquartile ranges. The red '+' signs represent the outliers. The whiskers indicate the most extreme data that is not an outlier.

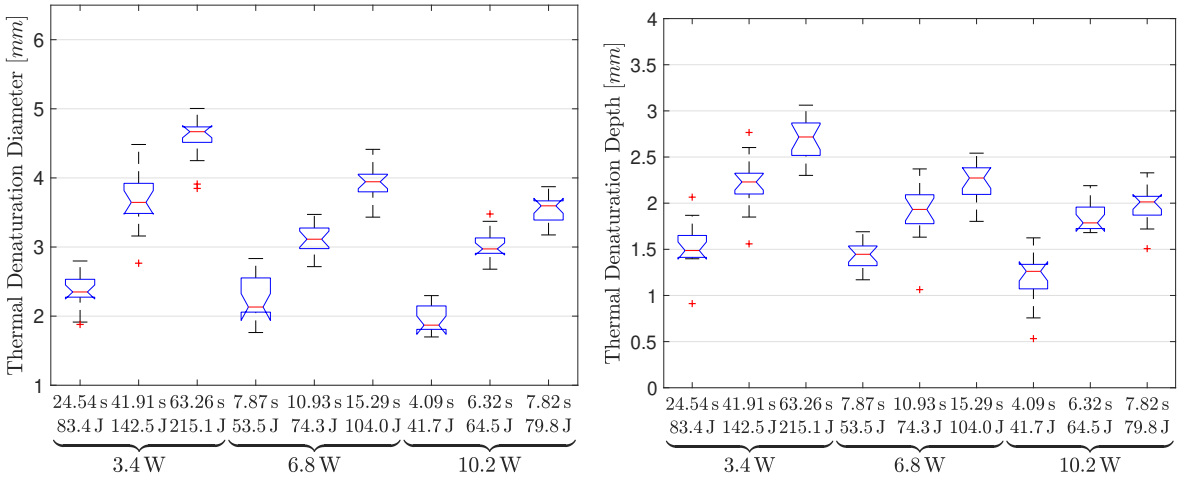


Figure 7.8 Box and whiskers plot of thermal denaturation diameters ($n = 16$) and depths ($n = 16$) of the fixed-dose application. The red horizontal lines are the group medians. The blue boxes mark the interquartile ranges. The red '+' signs represent the outliers. The whiskers indicate the most extreme data that is not an outlier.

Table 7.4
Temperature Controlled Application Results: The mean (μ) and standard deviation (σ) of thermal denaturation diameters ($n = 16$) and depths ($n = 13$).

P_{laser}	T_{target}	Diameter ($\mu \pm \sigma$) [mm]	Depth ($\mu \pm \sigma$) [mm]
	55 °C	2.90 ± 0.38	1.65 ± 0.56
3.4 W	65 °C	3.85 ± 0.28	1.93 ± 0.59
	75 °C	4.52 ± 0.56	2.47 ± 0.55
	55 °C	2.68 ± 0.39	1.44 ± 0.28
6.8 W	65 °C	3.64 ± 0.38	1.85 ± 0.44
	75 °C	4.37 ± 0.38	2.35 ± 0.48
	55 °C	2.53 ± 0.27	1.37 ± 0.23
10.2 W	65 °C	3.47 ± 0.32	1.68 ± 0.44
	65 °C	4.18 ± 0.38	2.04 ± 0.55

Table 7.5
Fixed-Dose Application Results: The mean (μ) and standard deviation (σ) of thermal denaturation diameters ($n = 16$) and depths ($n = 16$).

P_{laser}	$t_{exposure}$	E	Diameter ($\mu \pm \sigma$) [mm]	Depth ($\mu \pm \sigma$) [mm]
	24.54 s	83.4 J	2.36 ± 0.26	1.53 ± 0.25
3.4 W	41.91 s	142.5 J	3.66 ± 0.41	2.21 ± 0.29
	63.26 s	215.1 J	4.58 ± 0.32	2.70 ± 0.22
	7.87 s	53.5 J	2.27 ± 0.32	1.44 ± 0.14
6.8 W	10.93 s	74.3 J	3.10 ± 0.21	1.91 ± 0.31
	15.29 s	104.0 J	3.94 ± 0.23	2.25 ± 0.19
	4.09 s	41.7 J	1.96 ± 0.20	1.18 ± 0.27
10.2 W	6.32 s	64.5 J	3.03 ± 0.21	1.85 ± 0.15
	7.82 s	79.8 J	3.54 ± 0.21	1.97 ± 0.19

Table 7.6
One-way ANOVA of thermal denaturation diameter: First column represents the common parameter for each ANOVA test conducted with respect to the independent variables presented in the first row of top and bottom parts. The results of temperature-controlled and fixed-dose applications are on the left- and right-side, respectively. Statistical significance ($p < .05$) is marked with bold font.

	Target Temperature			Fixed-Dose		
	df	F	$Prob > F$	df	F	$Prob > F$
3.4 W	2, 45	58.990	$\mathbf{p < .001}$	2, 45	173.896	$\mathbf{p < .001}$
6.8 W	2, 45	77.804	$\mathbf{p < .001}$	2, 45	169.400	$\mathbf{p < .001}$
10.2 W	2, 45	102.840	$\mathbf{p < .001}$	2, 45	248.011	$\mathbf{p < .001}$

	Laser Power			Laser Power		
	df	F	$Prob > F$	df	F	$Prob > F$
55 °C & $E_{55\,°C}$	2, 45	4.591	$\mathbf{p = .015}$	2, 45	10.499	$\mathbf{p < .001}$
65 °C & $E_{65\,°C}$	2, 45	5.505	$\mathbf{p = .007}$	2, 45	22.580	$\mathbf{p < .001}$
75 °C & $E_{75\,°C}$	2, 45	2.304	$p = .112$	2, 45	65.782	$\mathbf{p < .001}$

Table 7.7
One-way ANOVA of thermal denaturation depth: First column represents the common parameter for each ANOVA test conducted with respect to the independent variables presented in the first row of top and bottom parts. The results of temperature-controlled and fixed-dose applications are on the left- and right-side, respectively. Statistical significance ($p < .05$) is marked with bold font.

	Target Temperature			Fixed-Dose		
	df	F	$Prob > F$	df	F	$Prob > F$
3.4 W	2, 36	7.011	$\mathbf{p = .003}$	2, 45	83.321	$\mathbf{p < .001}$
6.8 W	2, 36	16.180	$\mathbf{p < .001}$	2, 45	53.703	$\mathbf{p < .001}$
10.2 W	2, 36	8.118	$\mathbf{p = .001}$	2, 45	63.571	$\mathbf{p < .001}$

	Laser Power			Laser Power		
	df	F	$Prob > F$	df	F	$Prob > F$
55 °C & $E_{55\,°C}$	2, 36	1.900	$p = .164$	2, 45	9.946	$\mathbf{p < .001}$
65 °C & $E_{65\,°C}$	2, 36	0.860	$p = .432$	2, 45	8.974	$\mathbf{p < .001}$
75 °C & $E_{75\,°C}$	2, 36	2.279	$p = .117$	2, 45	52.998	$\mathbf{p < .001}$

Table 7.8

Results of post hoc tests using Scheffe's procedure after one-way ANOVA of thermal denaturation diameter ($n = 16$) and depth ($n = 13$) values in the temperature-controlled experiment. Each row represents multiple comparisons conducted for the common parameter provided in the first column. Solid lines connecting two groups represent a statistically significant difference ($p < .05$).

	Denaturation Diameter ($\mu \pm \sigma$) [mm]			Denaturation Depth ($\mu \pm \sigma$) [mm]		
	55 °C	65 °C	75 °C	55 °C	65 °C	75 °C
3.4 W	2.90 ± 0.38	3.85 ± 0.28	4.52 ± 0.56	1.65 ± 0.56	1.93 ± 0.59	2.47 ± 0.55
	$\boldsymbol{p < .001}$	$\boldsymbol{p < .001}$	$\boldsymbol{p < .001}$	$p = .474$	$p = .063$	$\boldsymbol{p = .003}$
6.8 W	2.68 ± 0.39	3.64 ± 0.38	4.37 ± 0.38	1.44 ± 0.28	1.85 ± 0.44	2.35 ± 0.48
	$\boldsymbol{p < .001}$	$\boldsymbol{p < .001}$	$\boldsymbol{p < .001}$	$p = .052$	$\boldsymbol{p = .013}$	$\boldsymbol{p < .001}$
10.2 W	2.53 ± 0.27	3.47 ± 0.32	4.18 ± 0.38	1.37 ± 0.23	1.68 ± 0.44	2.04 ± 0.55
	$\boldsymbol{p < .001}$	$\boldsymbol{p < .001}$	$\boldsymbol{p < .001}$	$p = .198$	$p = .107$	$\boldsymbol{p = .001}$

	3.4 W	6.8 W	10.2 W	3.4 W	6.8 W	10.2 W
55 °C	2.90 ± 0.38	2.68 ± 0.39	2.53 ± 0.27	1.65 ± 0.56	1.44 ± 0.28	1.37 ± 0.23
	$p = .228$	$p = .454$	$\boldsymbol{p = .016}$	$p = .383$	$p = .897$	$p = .188$
65 °C	3.85 ± 0.28	3.64 ± 0.38	3.47 ± 0.32	1.93 ± 0.59	1.85 ± 0.44	1.68 ± 0.44
	$p = .216$	$p = .317$	$\boldsymbol{p = .007}$	$p = .918$	$p = .688$	$p = .446$
75 °C	4.52 ± 0.56	4.37 ± 0.38	4.18 ± 0.38	2.47 ± 0.55	2.35 ± 0.48	2.04 ± 0.55
	$p = .667$	$p = .473$	$p = .113$	$p = .846$	$p = .341$	$p = .132$

Table 7.9

Results of post hoc tests using Scheffe's procedure after one-way ANOVA of thermal denaturation diameter ($n = 16$) and depth ($n = 13$) values in the fixed-dose experiment. Each row represents multiple comparisons conducted for the common parameter provided in the first column. Solid lines connecting two groups represent a statistically significant difference ($p < .05$).

	Denaturation Diameter ($\mu \pm \sigma$) [mm]			Denaturation Depth ($\mu \pm \sigma$) [mm]		
	$E_{55\,°C}$	$E_{65\,°C}$	$E_{75\,°C}$	$E_{55\,°C}$	$E_{65\,°C}$	$E_{75\,°C}$
3.4 W	2.36 ± 0.26	3.66 ± 0.41	4.58 ± 0.32	1.53 ± 0.25	2.21 ± 0.29	2.70 ± 0.22
	$\boldsymbol{p < .001}$	$\boldsymbol{p < .001}$		$\boldsymbol{p < .001}$	$\boldsymbol{p < .001}$	
		$\boldsymbol{p < .001}$			$\boldsymbol{p < .001}$	
6.8 W	2.27 ± 0.32	3.10 ± 0.21	3.94 ± 0.23	1.44 ± 0.14	1.91 ± 0.31	2.25 ± 0.19
	$\boldsymbol{p < .001}$	$\boldsymbol{p < .001}$		$\boldsymbol{p < .001}$	$\boldsymbol{p < .001}$	
		$\boldsymbol{p < .001}$			$\boldsymbol{p < .001}$	
10.2 W	1.96 ± 0.20	3.03 ± 0.21	3.54 ± 0.21	1.18 ± 0.27	1.85 ± 0.15	1.97 ± 0.19
	$\boldsymbol{p < .001}$	$\boldsymbol{p < .001}$		$\boldsymbol{p < .001}$	$p = .257$	
		$\boldsymbol{p < .001}$			$\boldsymbol{p < .001}$	

	3.4 W	6.8 W	10.2 W	3.4 W	6.8 W	10.2 W
$E_{55\,°C}$	2.36 ± 0.26	2.27 ± 0.32	1.96 ± 0.20	1.53 ± 0.25	1.44 ± 0.14	1.18 ± 0.27
	$p = .605$	$\boldsymbol{p = .006}$		$p = .494$	$\boldsymbol{p = .012}$	
		$\boldsymbol{p < .001}$			$\boldsymbol{p < .001}$	
$E_{65\,°C}$	3.66 ± 0.41	3.10 ± 0.21	3.03 ± 0.21	2.21 ± 0.29	1.91 ± 0.31	1.85 ± 0.15
	$\boldsymbol{p < .001}$	$p = .786$		$\boldsymbol{p = .008}$	$p = .795$	
		$\boldsymbol{p < .001}$			$\boldsymbol{p = .001}$	
$E_{75\,°C}$	4.58 ± 0.32	3.94 ± 0.23	3.54 ± 0.21	2.70 ± 0.22	2.25 ± 0.19	1.97 ± 0.19
	$\boldsymbol{p < .001}$	$\boldsymbol{p < .001}$		$\boldsymbol{p < .001}$	$\boldsymbol{p = .002}$	
		$\boldsymbol{p < .001}$			$\boldsymbol{p < .001}$	

In the temperature-controlled application, target temperature creates statistically significant differences in denaturation diameters between all groups for all laser powers. Yet, we only observe statistically significant differences in the denaturation diameters between lowest and highest laser power groups (3.4 W and 10.2 W) for target temperatures of 55 °C and 65 °C. There is no statistically significant difference between laser power groups for 75 °C target temperature in the temperature-controlled application.

In the fixed-dose application, corresponding dose ($E_{T_{target}}$) creates statistically significant differences in denaturation diameters between all groups for all laser powers. There are statistically significant differences in denaturation diameters between all laser power groups for each corresponding dose, except between 3.4 W and 6.8 W groups for $E_{55\,^{\circ}C}$, and 6.8 W and 10.2 W groups for $E_{65\,^{\circ}C}$.

Post hoc Test Results for Thermal Denaturation Depth

In the temperature-controlled application, there are statistically significant differences in denaturation depths between 55 °C and 75 °C target temperature groups for all laser powers. Additionally, there is a statistically significant difference between 65 °C and 75 °C target temperature groups for 6.8 W. There is no statistically significant difference in denaturation depths between any laser power groups for any target temperature groups.

In the fixed-dose application, there are statistically significant differences in denaturation depths between all $E_{T_{target}}$ groups for each laser power, except between $E_{65\,^{\circ}C}$ and $E_{75\,^{\circ}C}$ groups for 10.2 W. There are statistically significant differences in denaturation depths between all laser power groups for each corresponding dose, except between 3.4 W and 6.8 W groups for $E_{55\,^{\circ}C}$ and 6.8 W and 10.2 W groups for $E_{65\,^{\circ}C}$.

Interactions

Two-way ANOVA results for denaturation diameter and depth measurements are provided respectively in Tables 7.10 and 7.11 for the temperature-controlled application, and in Tables 7.12 and 7.13 for the fixed-dose application. The temperature-

Table 7.10
Temperature Controlled Application Results: Two-way ANOVA of thermal denaturation diameter.

Source	SS	df	MS	F	$Prob > F$
Target Temperature	66.030	2	33.015	228.581	$\mathbf{p < .001}$
Laser Power	3.232	2	1.616	11.188	$\mathbf{p < .001}$
Interaction	0.028	4	0.007	0.048	$p = .996$
Error	19.499	135	0.144		
Total	88.788	143			

Table 7.11
Temperature Controlled Application Results: Two-way ANOVA of thermal denaturation depth.

Source	SS	df	MS	F	$Prob > F$
Target Temperature	12.807	2	6.403	28.252	$\mathbf{p < .001}$
Laser Power	2.037	2	1.018	4.493	$\mathbf{p = .013}$
Interaction	0.244	4	0.061	0.270	$p = .897$
Error	24.479	108	0.227		
Total	39.567	116			

Table 7.12
Fixed-Dose Application Results: Two-way ANOVA of thermal denaturation diameter.

Source	SS	df	MS	F	$Prob > F$
$E_{T_{target}}$	80.452	2	40.226	544.298	$\mathbf{p < .001}$
Laser Power	11.778	2	5.889	79.682	$\mathbf{p < .001}$
Interaction	2.328	4	0.582	7.873	$\mathbf{p < .001}$
Error	9.977	135	0.074		
Total	104.534	143			

Table 7.13
Fixed-Dose Application Results: Two-way ANOVA of thermal denaturation depth.

Source	SS	df	MS	F	$Prob > F$
$E_{T_{target}}$	21.101	2	10.551	196.841	$\mathbf{p < .001}$
Laser Power	5.610	2	2.805	52.331	$\mathbf{p < .001}$
Interaction	0.985	4	0.246	4.593	$\mathbf{p = .002}$
Error	7.236	135	0.054		
Total	34.932	143			

controlled application results indicate no interaction between laser power and target temperature with respect to thermal denaturation diameter and depth. In contrast, the fixed-dose application results mark a statistically significant interaction between laser power and dose. This is expected considering the doses were determined using the results of temperature-controlled application for enabling comparison between both applications. As laser power decreases, a larger average dose (nonlinearly longer exposure duration) is required to reach target temperatures. Naturally, this phenomenon is mirrored in the fixed-dose application.

In light of these results, we can state that our temperature controlled medical laser system can successfully regulate thermal denaturation diameter (by creating significant differences between groups) using target temperature as a parameter, as well as a fixed-dose application. Target temperature was less effective in regulating the denaturation depth in comparison to fixed-dose application. The reason for this phenomenon may be the fact that our system measures and controls surface tissue temperature. Additionally, our system is capable of significantly decreasing the effects of laser power on denaturation diameter and depth, in contrast to fixed-dose applications.

The rate of temperature increase has a major role in controlling the resulting thermal effect successfully. Higher values of $^{dT}/_{dt}$ are associated with narrower gradients of thermal damage and provide more control over the denaturation area when using temperature feedback control [38, 45]. The representative thermal denaturation area photographs depicted in Figure 7.6 illustrate this phenomenon clearly. Higher laser power groups (corresponding to high $^{dT}/_{dt}$) exhibit a more defined thermal denaturation border than the lower laser power groups. A high $^{dT}/_{dt}$ also means reaching the target temperature faster, which enables us to minimize the exponential phase of the thermal damage progression. Conversely, a low $^{dT}/_{dt}$ allows the heat to diffuse into surrounding tissues for a longer duration (exponential phase), resulting in a less controlled thermal buildup due to the preponderate changes in optical and thermal characteristics. However, an extremely high $^{dT}/_{dt}$ value may prove hard to regulate thermally using a control system with limited response time. A momentary overshoot of tissue temperature may

cause excessive thermal damage, especially when the target temperature value is high. Therefore, the ideal $^{dT}/_{dt}$ value should be optimized depending on the response time of the temperature control system.

In the temperature-controlled application, tissues with different temperature increase curves receive different amounts of energy until the target temperature is reached. A difference in the delivered dose can lead to changes in the extent and size of thermal denaturation. The modulation of laser power to regulate the temperature-time response of tissue may be beneficial in controlling the thermal damage. Dosimetry studies may reinforce efficiency and effectiveness of temperature and temperature change rate controlled medical laser systems, by providing the feasible $^{dT}/_{dt}$ ranges and ideal initial laser power values specific to different tissues.

Study Limitations

Even though our IRt/c system is calibrated, one limitation of this study is the lack of a secondary temperature measurement system for confirming our results. We abstained from using a contact requiring temperature measurement method to avoid changing the thermal dissipation characteristics of the tissue and interfering with the laser exposure. Unfortunately, a high resolution thermal camera with a fast temperature response was not available at the time of the experiments.

Additionally, the off-axial design of the temperature measurement and beam delivery optics renders the system highly sensitive to operating distance variations. In several instances, we have observed that the irradiated tissue changed shape and moved slightly affecting the temperature measurement accuracy.

Another limitation of this experiment is the lack of *in vivo* testing, which prevented us from observing dynamic response of the perfused tissue and latent effects of the thermal damage. Additionally, we were not able to use viability staining methods for histological examination due to using *ex vivo* tissues, which would provide clear results about the extent of the thermal damage induced.

8. CONCLUSION

The non-contact tissue surface temperature controlled laser system presented in this dissertation is a feasible candidate for controlling laser exposure for photothermal medical laser applications. In Chapter 6, we have shown that the system is reliable for maintaining target tissue temperature within a narrow range even using the simplest laser control method (On-Off Exposure Modulation). In Chapter 7, we have demonstrated that the temperature controlled medical laser system developed in our laboratory is capable of ensuring the success and reproducibility of PTT modalities and patient safety while also regulating thermal denaturation size even when using a sample population representative of the wide optical and thermal property ranges encountered in clinical conditions. Moreover, in Chapter 7, our system successfully maintained tissue temperatures at required target values to induce desired thermophysiological effects and prevent excessive thermal damage even when using different (and higher) laser powers in comparison to Chapter 6. It can also reduce the effect of laser power on denaturation size.

Our system comprises relatively inexpensive components that perform efficiently even when using the simplest control method. The total cost of this system including the microcontroller board, optical, opto-electronical, and -mechanical components and excluding the laser source and driver is ca. 300 USD (single unit retail prices). It has an easy to operate, simple design that can be set up and used in the clinical environment in an appropriate enclosure without requiring complicated training.

This system is a promising candidate as an add-on for medical laser systems operating in UV, visible and near-IR region of the spectrum in order to ensure patient safety and treatment success during photothermal applications. Thus, it may accelerate and enable the translation of novel photothermal laser applications currently confined to the controlled and uniform conditions of the laboratory (*e.g.*, laser-tissue welding, PTT of granulation tissue, cartilage reshaping) into the clinic by rendering them more

successful, reproducible and safe even for a wide range of subjects which cannot be provided by manual dosimetry (surgeon's decision) or fixed-dosimetry. This system can also ensure the safety of photochemical (non-thermal) laser treatments like low level laser therapy (LLLT) and photodynamic therapy (PDT). Considering the low-cost advantage of this tissue surface temperature controlled laser system, it is possible to implement it in resource-limited environments democratising the access to safe PTT applications and PTT-related academic and clinical research. Researchers may use our system for investigating and developing new, and improving pre-existing, photothermal laser applications on various biological tissues by monitoring tissue temperature, controlling laser exposure, and facilitating gathering of information of related parameters (*i.e.* thermal characterization of tissues).

A significant scientific contribution of the work conducted for this thesis study was recognising that low laser power values accentuate the effect idiosyncratic differences of optical and thermal properties of tissues has on their temperature-time responses. This interaction between low laser power and idiosyncratic properties of tissues led to a wider range of exposure durations (required to reach target temperatures) and a wider range of final temperatures, in temperature-controlled and fixed-dose applications, respectively. Observing the superimposed representations of the temperature-time response curves measured during laser applications presented in Figures 7.2 and 7.3 enabled this discovery.

8.1 Future Research & Development Options

The system can be optically further improved by designing a coaxial temperature measurement system and beam delivery system that would be more immune to operating distance variations.

The temperature measurement system can be easily adapted for use with other laser sources so that different laser wavelengths, power densities, and tissues can be tested for various photothermal medical laser treatment techniques.

Regulating photothermal medical laser applications by tissue temperature feedback is currently the gold standard of the trade. Controlling the rate of temperature change ($^{dT}/_{dt}$) has an important effect on the duration of the exposure and the induced thermal damage. Further research on using $^{dT_{tissue}}/_{dt}$ as a controlled variable for modulating laser power or exposure may improve PTT results.

It is imperative that temperature-controlled and fixed-dose experiments should be repeated *in vivo* to observe the effect of the perfusion and evaluate immediate and latent thermal damage by using viability staining methods. Furthermore, the temperature measurements during these experiments should be confirmed using a calibrated high-resolution fast-response IR thermal camera.

Considering that tumour and cyst tissues have increased perfusion characteristic, it is expected that their thermal properties are different from healthy tissues. Investigating the feasibility of using our system for the non-destructive characterization of the thermal properties of the tissues to diagnose tumours and cysts would be another potential research subject.

APPENDIX A. ADJUSTING IRt/c SENSOR SETTINGS

Settling time, ms	Min FIR (100b)	FIR 101b	FIR 110b	Max FIR (111b)
IIR 100%	55.615	67.903	92.479	141.631
IIR 80%	193.303	242.455	340.759	537.367
IIR 67%	376.887	475.191	671.799	1065.015
IIR 57%	422.783	533.375	754.559	1196.927
IIR 50%	468.679	591.559	837.319	1328.839

Figure A.1 Settling Times of 90614-BCC Sensors for Various IIR & FIR Filter Settings.

The factory settings of the chosen sensor for settling time is not suitable for use in the surgical laser system. Moreover, the system specification measurements require different settling times as well. Therefore, it is necessary to change the settings according to the table provided in Figure A.1 using the SMBus protocol. This is accomplished by flashing certain registers within the sensor by sending device specific SMBus commands. Even though it is possible to use the microcontroller to do this chore, it is more convenient to use the I2C adaptor depicted in Figure A.2. This adaptor is used to send control sequences via a terminal software to set up the sensor to the desired settings.



Figure A.2 I2C2PC Device.

Table A.1
PC to I^{2}C Adaptor (I2C2PC) Terminal Settings.

Display	Ansi, Half Duplex, newLine mode
Port	57600, 8N1, RTS/CTS
Send	CR+LF (only for manual temperature readout, not necessary with the SMBus command routines provided in this appendix.)

A.1 PC to I^{2}C Adaptor (I2C2PC) Terminal Settings using Realterm

The PC to I^{2}C Adaptor requires the parameters provided in Table A.1 to be set for successful communication using a terminal program. We have used the open source software Realterm serial terminal for the experimental work in this study.

A.2 IRt/c Sensor Settings

It is important to note that when writing the settings to EEPROM, the least significant byte is transferred first. Thus, one must swap the byte order as in the expample given in Appendix A.2.1.

A.2.1 Read Settings

The following command prompts the Melexis sensor to return its current settling time configuration. When we used this command on an unmodified sensor we received this response:
F4 AF (This is the factory default settings, and it corresponds to AFF4 (MSB-LSB) –> 1010 1111 1111 0100 –>FIR:111 IIR:100 –> 141ms)

: S0025R02P\r\n

A.2.2 Original Settings

25-F4AF-87 –> FIR:111 IIR:100 –> 141.631ms

:S0025000083P\r\n L0005 :S0025F4AF87P\r\n L0005
:S00FFF3P\r\n O00FE O00FF O00FD L0010 O00FF
:SB425P\r\n L0300 :SB425R02P\r\n

A.2.3 Normal Operation & Response Time Measurement(Fast)

25-F4AC-8E –> FIR:100 IIR:100 –> 55.615ms

:S0025000083P\r\n L0005 :S0025F4AC8EP\r\n L0005
:S00FFF3P\r\n O00FE O00FF O00FD L0010 O00FF
:SB425P\r\n L0300 :SB425R02P\r\n

25-F4AD-89 –> FIR:101 IIR:100 –> 67.903ms

:S0025000083P\r\n L0005 :S0025F4AD89P\r\n L0005
:S00FFF3P\r\n O00FE O00FF O00FD L0010 O00FF
:SB425P\r\n L0300 :SB425R02P\r\n

A.2.4 Spot Size Measurement (Moderate)

25-F0AF-D3 –> FIR:111 IIR:000 –> 1.33s

:S0025000083P\r\n L0005 :S0025F0AFD3P\r\n L0005
:S00FFF3P\r\n O00FE O00FF O00FD L0010 O00FF
:SB425P\r\n L0300 :SB425R02P\r\n

A.2.5 Accuracy Measurement & Calibration (Slow)

25-F3AF-EC –> FIR:111 IIR:011 –> 7.00s

:S0025000083P\r\n L0005 :S0025F3AFECP\r\n L0005
:S00FFF3P\r\n O00FE O00FF O00FD L0010 O00FF
:SB425P\r\n L0300 :SB425R02P\r\n

A.2.6 Change IIR & FIR Settings

25-F4AC-8E –> FIR:100 IIR:100 –> 60ms

:S0025000083P\r\n L0005 :S0025F4AC8EP\r\n L0005
:S00FFF3P\r\n O00FE O00FF O00FD L0010 O00FF
:SB425P\r\n L0300 :SB425R02P\r\n

A.2.7 Change Sensor SMBus Address to B4 (5A in 7bit notation)

:S002E00006FP\r\n L0005 :S002E5A00E1P\r\n L0005
:S00FFF3P\r\n O00FE O00FF O00FD L0010 O00FF
:SB425P\r\n L0300 :SB42ER02P\r\n

APPENDIX B. MICROPROCESSOR CODES

MSP430F5529 specific code snippets/functions are provided in this appendix. In order to use these codes in other microcontrollers, the F5529 specific registers should be ported to match the new microcontroller registers. One should also note that the proper operation of most functions provided in this appendix are dependent on the specific clock frequencies used in this project.

MCLK $= 24\,\text{MHz}$

SMCLK $= 4\,\text{MHz}$

ACLK $= 32\,768\,\text{Hz}$

B.1 Watchdog Timer (WDT) Pushbutton Debouncing

Generally, pushbuttons tend to bounce and send a high signal several times within one push duration. This results in multiple consecutive triggering of related interrupts. Most commonly, this problem is addressed in the hardware by incorporating a lowpass RC filter. Unfortunately, it is not practical to incorporate components to the onboard pushbutton of the MSP430F5529 Launchpad. Therefore, we used a software debounce algorithm to disregard rapid consecutive pushbutton presses.

B.1.1 Initiate Watchdog Timer

This function is used in P1.1 or P2.1 interrupt service routines as the first command after disabling interrupts of that port. It clears the WDT flag, enables WDT interrupt, sets the WDT to trigger after a period of time, and activates WDT.

```
void WDTdebounce(void) {
```

```
    SFRIFG1 &= ~WDTIFG; // clear WDT flag
// Interval Counter, ACLK, 250 ms
    WDTCTL = WDTPW + WDTTMSEL + WDTSSEL_1 + WDTIS_5 + WDTCNTCL;
// Interval Counter, SMCLK, 131 ms
// WDTCTL = WDTPW + WDTTMSEL + WDTSSEL_0 + WDTIS_3 + WDTCNTCL;
    SFRIE1 |= WDTIE;   // enable WDT interrupt
}
```

B.2 UART

UART is the main peripheral used for communicating with the microcontroller during operation. This peripheral enables a serial terminal software to send commands to the microcontroller to set parameters and control the operation. Properly coded, the microcontroller code can also use this interface to respond to commands with ACK signals or register values.

In this study, the UART peripheral has been used for the real time data transfer of the laser control status and surface temperature measurements.

B.2.1 UART Baudrate Settings Registers

```
/*************************************************************
SET THESE CONSTANTS, TO CONFIGURE THE BACKCHANNEL UART LIBRARY

1) Set the SMCLK speed and desired baudrate.

   The baudrate is determined by the UCA1BR0, UCA1BR1, and
   UCA1MCTL registers.
   UCA1MCTL has three relevant fields:
   UCA1BRF, UCA1BRS, and UCOS16.
```

```
    The settings below are for:
    SMCLK = 4MHz
    baudrate = 115200

    If you change the SMCLK speed, or want a different baudrate,
    you need to change these values.  An easy way to determine
    them is the calculator at the MSP430 wiki page:

http://processors.wiki.ti.com/index.php/
USCI_UART_Baud_Rate_Gen_Mode_Selection

    (If the link is somehow broken, the wiki page name is "USCI
    UART Baud Rate Gen Mode Selection", or try web-searching
    "msp430 usci calculator". Ultimately, the final reference
    is the UCS chapter of the F5xx Family User's Guide.) */

// 1 = oversampling mode, 0 = low-freq mode
#define UCA1_OS    1

// Value of UCA1BR0 register
#define UCA1_BR0   2

// Value of UCA1BR1 register
#define UCA1_BR1   0

// Value of UCBRS field in UCA1MCTL register
#define UCA1_BRS   3

// Value of UCBRF field in UCA1MCTL register
#define UCA1_BRF   2
```

B.2.2 UART Buffer Settings and Variable Initializations

```
// The index within uartRxBuffer, where the next byte will
// be written.
unsigned int uartRxIndex = 0;
unsigned int rxSize = 0;
unsigned int rxIFG = 0;
unsigned int rxLen;

/*
2) If needed, re-configure the library's characteristics:

The size of the UART receive buffer.  Set smaller if RAM is
in short supply. Set larger if larger data chunks are to be
received, or if the application can't process incoming data
very often.
*/

#define BC_RXBUF_SIZE  (64)

/*
The threshold within bcUartRcvBuf at which main() will be
awakened.  Must be less than BC_RXBUF_SIZE.  A value of '1'
will alert main() whenever even a single byte is received.
If no wake is desired, set to BC_RXBUF_SIZE+1
*/

#define BC_RX_WAKE_THRESH  (1)

// Boolean flag indicating whether uartRxIndex has reached
// the threshold BC_RX_WAKE_THRESH.  0 = FALSE, 1 = TRUE
```

```
// Receive buffer for the UART.  Incoming bytes need a place
// to go immediately, otherwise there might be an overrun
// when the next comes in. The USCI ISR puts them here.
char uartRxBuffer[BC_RXBUF_SIZE];
```

B.2.3 USCI_A1 Interrupt Service Routine for UART

```
// The USCI_A1 receive interrupt service routine (ISR).
// Executes every time a byte is received on the
// back-channel UART.
#pragma vector=USCI_A1_VECTOR
__interrupt void bcUartISR(void)
{
   P1OUT ^= BIT0;   // Toggle Red LED

   if (UCA1RXBUF != 0x0A)
      // Fetch the byte, store it in the buffer.
      uartRxBuffer[uartRxIndex++] = UCA1RXBUF;
   else{
      rxSize = uartRxIndex;
      rxIFG = 1;
      // Move index back to the beginning of the buffer
      uartRxIndex = 0;
    }
    P1OUT ^= BIT0;        // Toggle Red LED
}
```

B.2.4 Watchdog Timer Interrupt Service Routine

This interrupt service routine activates after the debouncing period defined in the `WDTdebounce()` function expires. It disables WDT interrupt, stops WDT, and enables P1.1 and P2.1 interrupts, so that pushing any one of the buttons will trigger its interrupt service routine again.

```
#pragma vector=WDT_VECTOR
__interrupt void WDT_ISR(void) {
    SFRIE1 &= ~WDTIE;   //disable WDT interrupt
    WDTCTL = WDTPW + WDTHOLD;   //hold WDT to save energy

    // Restore P1.1
    P1IFG &= ~BIT1; //clear P1.1 flag
    P1IE |= BIT1; // enable interrupts on P1.1

    // Restore P2.1
    P2IFG &= ~BIT1; //
    P2IE |= BIT1; //enable interrupts on P2.1
}
```

B.3 Hardware Stopwatch

A hardware stopwatch is useful in determining the operating durations between code sequences within the embedded software. Using the MSP430F5529 microprocessor, we have utilized the TIMERA2 as a counter operating at 100 kHz for the hardware stopwatch. This operating frequency results in a 10 µs resolution. At this frequency the 16-bit counter can measure up to 655.35 ms. The stopwatch is set up using the code provided in Appendix B.3.1. `tic()` function starts the stopwatch and `toc()` function stops the stopwatch and displays the counted duration. The codes for these functions are provided in Appendices B.3.2 and B.3.3.

B.3.1 Initial TIMERA2 Setup

This function stops the timer for facilitating error free setup. Then it defines the necessary setting registers for selecting the clock source (SMCLK), clock divider ($5 \times 8 = 40$) and count mode (continuous up).

```
TA2CTL = MC_0 + TACLR; // stop timer, clear TA2R
TA2EX0 = TAIDEX_4; // divider extension 5
//SMCLK, divider 8, start timer (continuous up), clear counter
TA2CTL = TASSEL_2 + ID_3 + MC_2 + TACLR;
```

B.3.2 `tic()`

This function resets the timer counter and starts the timer.

```
void tic(void) {
    TA2CTL = TASSEL_2 + ID_3 + MC_2 + TACLR;
}
```

B.3.3 `toc()`

This function stops the timer, reads the counter value, converts it to duration in µs and displays the duration using UART.

```
void toc(void) {
    TA2CTL = MC_0; \\ Stop Timer
    unsigned int ticTocDuration = TA2R; \\ Readout counter value
    // Compute the duration value in us and print it to a string
    sprintf(dummy3, "%u us\r\n", ticTocDuration*10);
    txUart(dummy3, 11); // display duration using UART
}
```

B.4 Readout from MLX90614 Sensor

B.4.1 Initialize I²C for SMBus Operation

This function defines the USCI hardware peripheral registers for SMBus operation over I²C protocol. The MLX90614 sensor operates in slave mode using a 100 kHz SMBus protocol. Therefore, I set the USCI to operate in master mode at 100 kHz. The sensor slave address is also defined in this function.

```
void initI2C(void) {
    P4SEL |= BIT1 + BIT2; // Assign I2C pins to USCI_B1

    UCB1CTL1 |= UCSWRST; // Stop operation for set up
    UCB1CTL0 = UCMST + UCMODE_3 + UCSYNC; // master, I2C,...
    ... synchronous
    UCB1CTL1 = UCSSEL_3 + UCSWRST; // SMCLK, Stop operation
    UCB1BR0 = 40; // BRCLK = SMCLK/UCB1BR0 = 4 MHz / 40...
    ... = 100 kHz
    UCB1BR1 = 0;
    UCB1I2CSA = 0x5A; // Slave Address of MLX90614
    UCB1CTL1 &= ~UCSWRST; // Enable Operation
}
```

B.4.2 Raw Data Readout

Reads out raw temperature data with SMBus protocol using the I²C hardware peripheral. The readout sequence is specific to the MLX90614 sensor.

```
unsigned int getTRAW(void) {
    uint8_t tempLow = 0x00;
    uint8_t tempHigh = 0xFF;
    uint8_t PEC = 0x00;
```

```
unsigned int tempRAW = 0x0000;
static const unsigned int TIMEOUT = 12000;
unsigned int timeout = TIMEOUT;

UCB1CTL1 |= UCTR + UCTXSTT;
while (!(UCB1IFG & UCTXIFG) && --timeout);
if (timeout==0) {
    return 0;
}
timeout = TIMEOUT;
UCB1TXBUF = 0x07;   // Send Tobj1 RAM Address 0x07

while (UCB1CTL1 & UCTXSTT);
UCB1CTL1 &= ~UCTR;

UCB1CTL1 |= UCTXSTT;
while (!(UCB1IFG & UCRXIFG) && --timeout);
if (timeout==0) {
    return 0;
}
timeout = TIMEOUT;
tempLow=UCB1RXBUF;
while (!(UCB1IFG & UCRXIFG) && --timeout);
if (timeout==0) {
    return 0;
}
timeout = TIMEOUT;
tempHigh=UCB1RXBUF;
while (!(UCB1IFG & UCRXIFG) && --timeout);
if (timeout==0) {
    return 0;
```

```
    }
    timeout = TIMEOUT;
    UCB1CTL1 |= UCTXSTP;
    while (UCB1CTL1 & UCTXSTP);
    PEC=UCB1RXBUF;
    if (!(tempHigh == 0xFF)){
        tempRAW = tempLow | (tempHigh << 8);
    }
    return tempRAW;
}
```

B.4.3 "Divide & Conquer" Temperature Conversion

I divided the second-order conversion function of the modified and calibrated MLX90614 sensor into two linear functions in order to decrease computation time.

```
static const float tempFactor = 0.0243;   //0.2
static const float tempOffset = 338.35;   //275.25
static const float tempFactor2 = 0.0225;
static const float tempOffset2 = 308.66;

float convertRAW2Temp(unsigned long tempRaw) {
  float temperature;

  if (tempRaw < 16850) {
        temperature = ( (float) tempRaw * tempFactor )...
        ...- tempOffset;
  } else {
        temperature = ( (float) tempRaw * tempFactor2 )...
        ...- tempOffset2;
  }
```

```
  return temperature;
}
```

B.5 Moving Window Average

I developed a moving window average filter with variable window size to use during system calibration and characterization.

B.5.1 Variable Initializations

Initially, the moving window average function is set to operate with a 64-point long window, which is the largest window. The size of the window has to be a power of 2 because I am using a binary right shift operation for fast computation of the average value. The raw temperature register is permanently set to 64 points long to accommodate the largest window.

```
int iAvg = 0;
int movingAvgWindow = 64; // moving average window size
int movingAvgPower = 6; // sqrt(movingAvgWindow)
int tempRegisterRAW[64];
```

B.5.2 Averaging Function

This function acquires raw temperature data from the MLX90614 sensor and stores it into the moving window register. At each run the function stores the raw temperature value with an incremental index. The index is reset when it reaches the determined window size, n_w. At each run, the function also computes the average of first n_w points within the 64-point averaging register. This function returns average value of the raw temperature data. It also uses a pointer trick to return the converted

average temperature value. The pointer of a variable is defines as an input to this function, such that any value stored using that pointer within this function will also be accessible outside of this function as well.

```
unsigned long getMovingAvgTemp(float* tempMovingAvg) {
    unsigned long tempMovingAvgRAW=0;
    unsigned int i;
    *tempMovingAvg = 0;

    if (iAvg == movingAvgWindow) iAvg=0;
    tempRegisterRAW[iAvg] = getTRAW();
    iAvg++;
    for (i=0; i<movingAvgWindow; i++) {
        tempMovingAvgRAW += tempRegisterRAW[i];
    }
    tempMovingAvgRAW >>= movingAvgPower;
    *tempMovingAvg = convertRAW2Temp(tempMovingAvgRAW);

    return tempMovingAvgRAW;
}
```

B.5.3 Window Size Selection

This interrupt service routine allow us to change the window size using push-button P1 on the launchpad. The operating setting is displayed by blinking the green LED of the launchpad.

```
// Port 1 interrupt service routine
#pragma vector=PORT1_VECTOR
__interrupt void Port_1(void)
{
// float tempVal;
```

```
// unsigned int tempRAW;
    P1IFG &= ~BIT1; // P1.1 IFG cleared
    P1IE &= ~BIT1; //disable interrupts on P1.1
    WDTdebounce();

    port1Mode++;
    if (port1Mode == 6) port1Mode = 0;
    greenLED(0);
    pulseGreenLED(port1Mode);

    memset(tempRegisterRAW, 0, 64);
    iAvg=0;

    switch(port1Mode) {
        case 0: {
                    movingAvgWindow = 64;
                    movingAvgPower = 6;
                    break;
                }
        case 1: {
                    movingAvgWindow = 32;
                    movingAvgPower = 5;
                    break;
        }
        case 2: {
                    movingAvgWindow = 16;
                    movingAvgPower = 4;
                    break;
        }
              case 3: {
                    movingAvgWindow = 8;
```

```
                movingAvgPower = 3;
                break;
        }
            case 4: {
                movingAvgWindow = 4;
                movingAvgPower = 2;
                break;
            }
        case 5: {
                movingAvgWindow = 2;
                movingAvgPower = 1;
                break;
            }
    }
}
```

B.6 Periodic Sensor Readout

B.6.1 TIMERA0 Settings

This code defines the initial TIMERA0 settings registers. The counter limit register `TA0CCR0` is redefined later on.

```
TA0CCTL0 = CCIE;   // CCR0 interrupt enabled
TA0CCR0 = 65535; // Poll every 2s
// ACLK, up to CCR0, clear TA Counter
TA0CTL = TASSEL_1 + MC_1 + TACLR;
```

B.6.2 Readout Interval Selection

This code is the ISR of the P2 pushbutton. It is used to adjust the TIMERA0 counter limit register (CCR0) value by pressing the P2 pushbutton. The operating setting is displayed by blinking the green LED of the launchpad. `port2Mode = 5` is used for the bovine liver denaturation study elaborated in Chapter 7.

```
#pragma vector=PORT2_VECTOR
__interrupt void Port_2(void)
{
    P2IFG &= ~BIT1; // P2.1 IFG cleared
    P2IE &= ~BIT1; //disable interrupts on P2.1
    WDTdebounce();

    port2Mode++;
    if (port2Mode == 6) port2Mode = 0;
    redLED(0);
    pulseRedLED(port2Mode);

    switch(port2Mode) {
        case 0: {
// This is used for the Temperature Calibration Measurement.
// Timer Period with timerCoeff = 4
// 57350 * timerCoeff / 32768 = 7s
            TA0CCR0 = 57350;
            break;
        }
        case 1: {
// This mode is used for Spot Size Measurement.
            TA0CCR0 = 16348; // 2s Timer Period
            break;
        }
```

```
        case 2: {
            TA0CCR0 = 10977; // 1.34s Timer Period
            break;
        }
        case 3: {
            TA0CCR0 = 1200; // 146.484 ms Timer Period
//          TA0CCR0 = 1639; // 0.2s Timer Period
            break;
        }
        case 4: {
// This mode is used for normal operation.
            TA0CCR0 = 565; // 69ms Timer Period
            break;
        }
        case 5: {
// This mode is used for normal operation.
            TA0CCR0 = 466; // 56.6ms Timer Period
// Stopwatch timer for 5s laser application
            TIMERCOEFF2 = 352;
//          timerCoeff2 = 5*32768/466
            break;
        }
    }
}
```

B.7 Laser Control Signal (TTL)

The exposure of the 1071 nm ytterbium fiber laser (YLM-20-SC, IPG Photonics, MA, USA) can be controlled with a TTL signal delivered to a BNC connector at the back panel of the instrument. I manufactured a BNC-jumper conversion cable to

connect the MSP430 launchpad with the laser for on-off control.

```
P8DIR |= BIT2;   // Set P8.2 as digital output
P8OUT |= BIT2; // Turn off laser

void laser(int status) {
// 1070 nm laser is turned on when TTL signal is low
    if (status) {
        P8OUT &= ~BIT2;
    } else {
        P8OUT |= BIT2;
    }
}
```

B.8 Continuous Temperature Controlled Operation

B.8.1 TIMERA0 Interrupt Service Routine

This code is used for running the system perpetually. The laser is on as long as the tissue temperature is below the target temperature (`intInput`) value. Whenever the tissue temperature is above `intInput` value, the laser is turned off.

The `timerCoeff` is a handy trick to enable triggering at longer intervals. This code also shows how to use the hardware stopwatch functions (`tic()` and `toc()`).

```
#pragma vector=TIMER0_A0_VECTOR
__interrupt void TIMER0_A0_ISR(void) {
// txUart(("*** System OK ***\a\r\n"), 20);
    float tempVal;
    unsigned int tempRAW;

    timerCoeff++;
```

```
    if ( timerCoeff == 4 ) {
        timerCoeff = 0;
       tempRAW = getTempRAW(&tempVal);

    if (tempVal > (float) intInput) {
        laserStatus = 0;
    } else {
            laserStatus = 1;
    }
    laser(laserStatus);

    sprintf(str,"%.2f\t%u\t%u\r\n",tempVal,laserStatus...
    ...,tempRAW);
    txUart(str,16);
          }
}
```

B.9 5 s Temperature Controlled Operation

B.9.1 Main Code

This code is used for the temperature controlled laser applications conducted in the bovine liver denaturation study. It monitors a software interrupt flag (`rxIFG`) that is triggered whenever an UART message is received. The message is transmitted as a character array (string) from a computer using a serial terminal program via the RS2323-UART interface. The message should be composed of only the target temperature value. After the message is received, it is converted to integer and this value is stored in `intInput` value. Then `intInput` echoed back for confirmation.

```
while (1) {
```

```
    if (rxIFG) {
        rxLen = rxUart(dummy);
        txUart("\r\a", 3);
        intInput = atoi(dummy);
        memset(dummy, 0, rxLen); // Clear dummy string
        sprintf(str, "%i\r", intInput);
        txUart(str, 8);
    }
}
```

B.9.2 TIMERA0 Interrupt Service Routine

This code is used for the temperature controlled laser applications conducted in the bovine liver denaturation study. Timer ISR is the part of the code that controls the operation of the laser. Once a target temperature value above the tissue temperature value is transmitted via UART, the laser exposure is turned on. The ISR triggers every `TA0CCR0` counts corresponding to 14.2 ms and clears the 5 s counter `timerCoeff2` if the target temperature has not been reached (`tempFlag = 0`). The code takes temperature measurements every `(TA0CCR0 x TIMERCOEFF)` counts corresponding to 56.6 ms, raises `tempFlag` and starts on-off laser control to maintain tissue temperature at the target value. It also transmits the measured tissue temperature and laser control signal status to the computer via UART. Once the `tempFlag` is raised, the `timerCoeff2` is no longer cleared, and the code counts up to 5 s. After 5 s of target temperature maintenance, the `timeFlag` software interrupt is raised, which overrides the other laser control assignments with `laserStatus = 0` turning the laser off.

```
#pragma vector=TIMER0_A0_VECTOR
__interrupt void TIMER0_A0_ISR(void) {

    float tempVal;
    unsigned int tempRAW;
```

```
    timerCoeff++;
    timerCoeff2++;

    if (timerCoeff2 == TIMERCOEFF2) {
        timerCoeff2 = 0;
// once the TIMERCOEFF2 is reached (5s), timeFlag
// is raised to prevent laser emission
        timeFlag = 1;
        intInput = 0;
        laserStatus = 0;
        laser(laserStatus);
    }

    if ( timerCoeff == TIMERCOEFF ) {
        timerCoeff = 0;
        tempRAW = getTempRAW(&tempVal);

        if (tempVal > (float) intInput) {
            laserStatus = 0;
            if (intInput == 0) {
                tempFlag = 0;
            } else {
// once the temperature reaches the target value,
// tempFlag is raised and timerCoeff2 is not
// cleared anymore
                tempFlag = 1;
            }
        } else {
            laserStatus = 1;
        }
```

```
        if (timeFlag) {
            laserStatus = 0;
        }
        laser(laserStatus);

        sprintf(str,"%.2f\t%u\t%u\r\n",tempVal,laserStatus...
        ...,tempRAW);
        txUart(str, 16);
    }

//used for clearing timerCoeff2 if tempFlag = 0
    if (!tempFlag) {
        timerCoeff2 = 0;
    }
}
```

B.10 Temperature Monitored Fixed-Dose Operation

B.10.1 Main Code

This code is used for the fixed-duration/energy laser applications (control group) conducted in the bovine liver coagulation study. It runs continuously to see if the software interrupt flag (`rxIFG`) is raised by the transmission of the exposure duration. This transmission also triggers the laser irradiation. The transmitted exposure duration is used to calculate the `TIMERCOEFF2` value that determines the software triggering of the TIMERA0 to ensure ceasing the laser irradiation. `TIMERCOEFF` ensures that the temperature measurement is conducted periodically with an interval of 56.8 ms. Sending a `0` character acts as a safety measure by immediately turning the laser irradiation off. This command also resets the microcontroller state machine for consequent operation.

```
while (1) {
   if (rxIFG) {
// receives the transmission from the software buffer
// into dummy and returns its length
      rxLen = rxUart(dummy);
// transmits a new line and a bell characters as a marker
      txUart("\n\a", 2);
      query = memcmp(dummy, "0", 1);
      if (query == 0) {
// this is used for resetting the system to initial state
// when a 0 character is transmitted
         fInput = 0;
         trigger = 0;
         timeFlag = 0;
         timerCoeff2 = 0;
         TIMERCOEFF2 = 0;
      } else {
// string to integer conversion of the exposure duration
         fInput = atof(dummy);
// calculates the TIMERCOEFF2 from the fInput (the exposure
// duration)
         TIMERCOEFF2 = (int) ((fInput * 32768) / TA0CCR0);
// raises the software interrupt variable trigger, that
// starts the count-up to the TIMERCOEFF2 value (the
// exposure duration)
         trigger = 1;
      }
      memset(dummy, 0, rxLen); // Clear dummy string
// converts the set exposure duration value back into a
// string, the new lines act as visual marker
      sprintf(str, "\n%.2f\n\n", fInput);
```

```
// echoes the received string back to UART as an ACK signal.
        txUart(str, strlen(str));
    }
}
```

B.10.2 TIMERA0 Interrupt Service Routine

This code is used for the fixed-duration/energy laser applications (control group) conducted in the bovine liver coagulation study. TIMERA0 is triggered at every count-up to `TA0CCR0 = 310` which corresponds to 9.5 ms when ACLK is sourced from the external 32 768 Hz crystal. The software timer counters (`timerCoeff` and `timerCoeff2`) and the counter limit variables (`TIMERCOEFF` and `TIMERCOEFF2`) enable triggering at longer periods than the 16-bit timer counter permits. Normally, the maximum counts one can achieve is $2^16 = 65536$ corresponding to 2 s at 32 768 Hz. Using this trick it is possible to ensure triggering at longer durations that are a multiple of `TA0CCR0`. `timerCoeff` reaches `TIMERCOEFF` every 56.8 s triggering the segment of the code that periodically measures the tissue temperature and transmits its value and the laser control signal value to the computer. When the `trigger` software interrupt flag is raised by the main code as a response to receiving the exposure duration, the laser irradiation is initiated and `timerCoeff2` count-up is enabled. Once `timerCoeff2` reaches `TIMERCOEFF2`, `timeFlag` is raised terminating the laser irradiation. This code also has a segment acting as an emergency abort or system reset. For this purpose, the user has to transmit a `0` character via UART, turning the laser off.

```
#pragma vector=TIMER0_A0_VECTOR
__interrupt void TIMER0_A0_ISR(void) {
    float tempVal = 0;
    unsigned int tempRAW = 0;

    timerCoeff++;
// timerCoeff2 is not increased when the trigger flag
```

```
// marking the start of laser exposure is not up

    if (trigger) {
        timerCoeff2++;
    }

    if ( timerCoeff2 == TIMERCOEFF2 ) {
        timerCoeff2 = 0;
        if (trigger) {
// once the TIMERCOEFF2 is reached (intInpus seconds),
// timeFlag is raised to prevent laser emission
            timeFlag = 1;
        }
    }

    if ( timerCoeff == TIMERCOEFF ) {
        timerCoeff = 0;
        tempRAW = getTempRAW(&tempVal);

/* First timeFlag is checked to ensure that laserStatus
*  is not changed to 1 after the exposure is completed.
*  If the timeFlag is not up, then the system checks for
*  trigger. This is used for turning on laser when trigger
*  is up. If TIMERCOEFF2 = 0, it means that I sent a 0
*  character from the terminal, denoting emergency
*  shutdown or system reset. In this case laserStatus is
*  changed to 0, ceasing the laser exposure.
*/
        if (timeFlag) {
            laserStatus = 0;
        } else if (trigger) {
```

```
            laserStatus = 1;
        }

        if (TIMERCOEFF2 == 0) {
            laserStatus = 0;
        }
        laser(laserStatus);

// Used for Windows systems
//      sprintf(str,"%.2f\t%u\t%u\r\n",tempVal,laserStatus...
//      ...,tempRAW);
//      txUart(str, 16);

// Used for Mac systems
        sprintf(str,"%.2f\t%u\t%u\n",tempVal,laserStatus...
        ...,tempRAW);
        txUart(str, strlen(str));
    }
}
```

APPENDIX C. CONFERENCE PRESENTATION

The following presentation was delivered at Optical Interactions with Tissue and Cells XXVII conference of Photonics West 2016 Biomedical Optics.

BOĞAZİÇİ UNIVERSITY

SPIE. PHOTONICS WEST BIOS

The Moscone Center
San Francisco, CA, United States
13 - 18 February 2016

A non-contact temperature measurement system for controlling photothermal medical laser treatments

Özgür Kaya, MSc and Murat Gülsoy, PhD

Institute of Biomedical Engineering
Boğaziçi University, İstanbul, Turkey

BME INSTITUTE OF BIOMEDICAL ENGINEERING

BOĞAZİÇİ UNIVERSITY

Outline

- Photothermal effects & laser applications
- Clinical Problems
- Temperature Measurement & Laser Control System
- System Specs & Calibration
- Performance Evaluation
- Conclusion
- Future Work

BME INSTITUTE OF BIOMEDICAL ENGINEERING

Thermal Effects in Tissue

Temperature	Biological effect
37°C	Normal
45°C	Hyperthermia
50°C	Reduction in enzyme activity, cell immobility
60°C	Denaturation of proteins and collagen, coagulation
80°C	Permeabilization of membranes
100°C	Vaporization, thermal decomposition (ablation)
> 100°C	Carbonization
> 300°C	Melting

Niemz, M. H. , Laser-Tissue Interactions, p. 78, Springer-Verlag (2007)

BOĞAZİÇİ UNIVERSITY

Dosimetry Studies

- Laboratory
  - Determination of ideal laser parameters
  - Controlled environment
  - Uniformity of subjects
- Clinic (real life)
  - Non-uniform subjects
  - Ideal parameters?

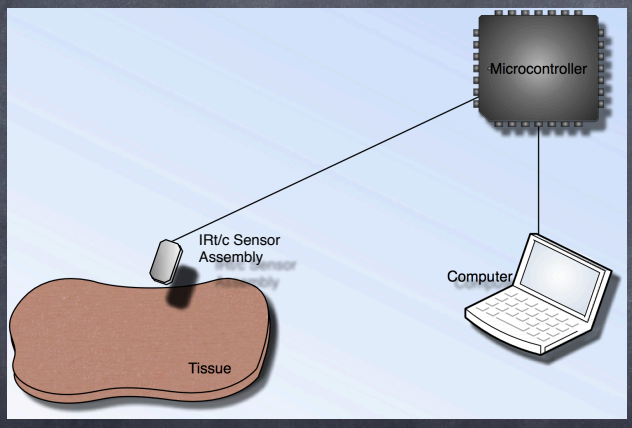
BME INSTITUTE OF BIOMEDICAL ENGINEERING

Clinical Problems

- Varying Optical Characteristics Among Subjects
  - skin color / pigmentation
  - hydration level
  - body composition
- Presence of Infection / Shock?
- Varying Thermal Characteristics Among Subjects
  - perfusion
  - body composition
- Repeatability and Reliability Issues

BOĞAZİÇİ UNIVERSITY

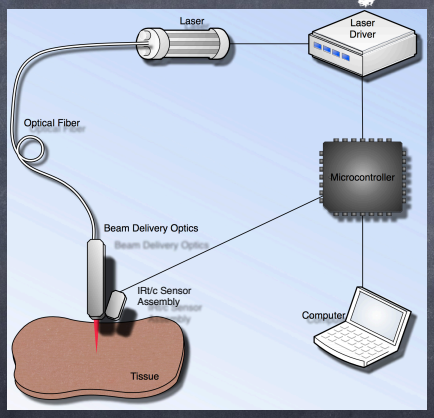
Temperature Measurement System



BME INSTITUTE OF BIOMEDICAL ENGINEERING

BOĞAZİÇİ UNIVERSITY

Tissue Temperature Controlled Medical Laser System



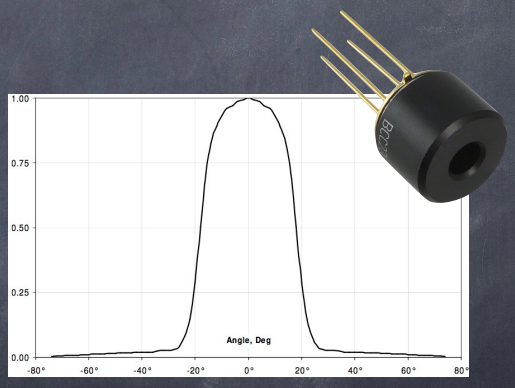
7 / 18

BME INSTITUTE OF BIOMEDICAL ENGINEERING

BOĞAZİÇİ UNIVERSITY

IR Temperature Sensor

- IR thermopile (5.5-12 µm)
- Signal conditioning, ADC
- Signal processing
- SMBUS communication
- 2x2 mm IC in TO can

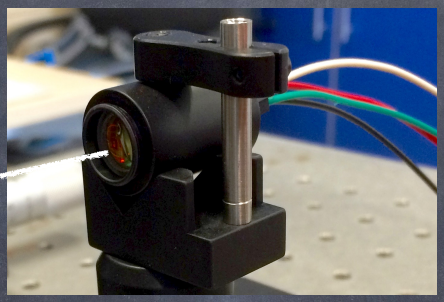


8 / 18

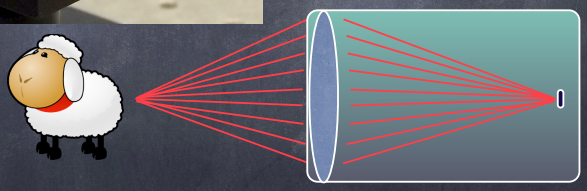
BME INSTITUTE OF BIOMEDICAL ENGINEERING

BOĞAZİÇİ UNIVERSITY

Temperature Sensor Assembly



AR coated
ZnSe Lens
(3-11 μm)

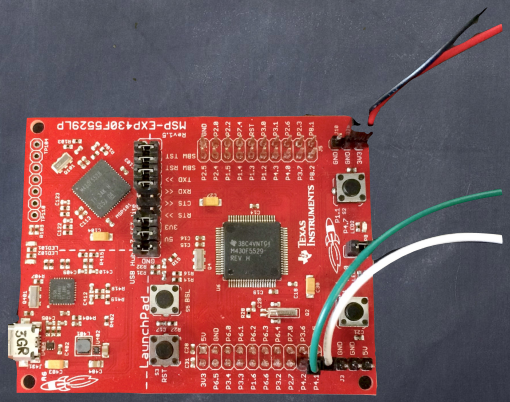


BME INSTITUTE OF BIOMEDICAL ENGINEERING

BOĞAZİÇİ UNIVERSITY

Microcontroller

- Temperature readout
- Laser control: TTL
  - Exposure modulation
- MSP430 launchpad
- Interface: I²C, UART
- Timer, PWM

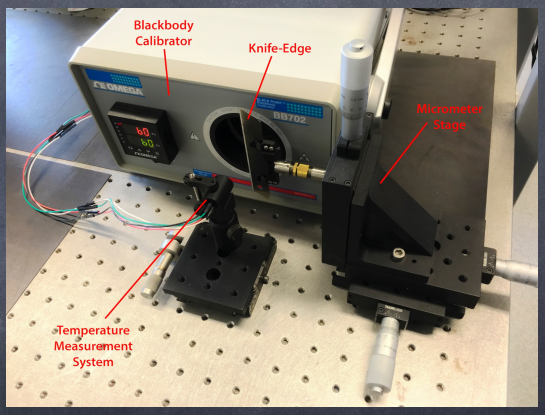


BME INSTITUTE OF BIOMEDICAL ENGINEERING

BOĞAZİÇİ UNIVERSITY

Calibration & Spatial Resolution

- Calibration: 30–150 °C
  - Conversion Formula
- Knife-edge test
  - 10/90 diameter: 3.6 mm
  - 20/80 diameter: 2.5 mm



BME INSTITUTE OF BIOMEDICAL ENGINEERING

BOĞAZİÇİ UNIVERSITY

Temporal Response

Settling time, ms	Min FIR (100b)	FIR 101b	FIR 110b	Max FIR (111b)
IIR 100%	55.615	67.903	92.479	141.631
IIR 80%	193.303	242.455	340.759	537.367
IIR 67%	376.887	475.191	671.799	1065.015
IIR 57%	422.783	533.375	754.559	1196.927
IIR 50%	468.679	591.559	837.319	1328.839

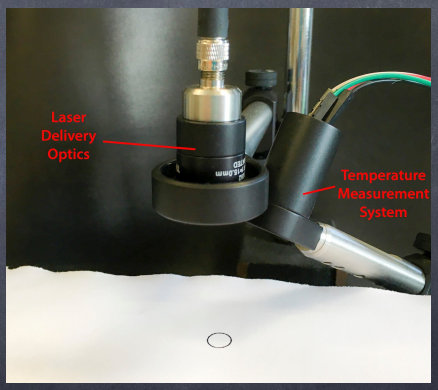
Process	t $[ms]$
Sensor Settling	55.516
Readout Interval	56
Temperature Acquisition, Data Conversion and Processing	0.87
Response Time	< 57

BME INSTITUTE OF BIOMEDICAL ENGINEERING

Laser System

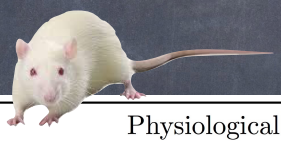
- Ytterbium fiber laser (1071 nm)
- Power: 8.3 W & Spot size: 7 mm





BOĞAZİÇİ UNIVERSITY

Performance Evaluation



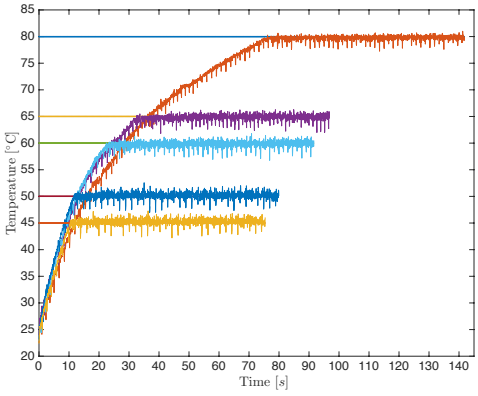
T_{target}	Physiological Effect / Laser Treatment
45°C	Hyperthermia, Treatment of Granulation Tissue
50°C	Reduction in Enzyme Activity, Cellular Immobilisation Thermal Treatment of Malignant Tissues
60°C	Denaturation of Proteins and Collagen, Coagulation, Surgical Haemostasis
65°C	Ideal Temperature for Laser Tissue Welding
80°C	Permeabilization of Membranes

BME INSTITUTE OF BIOMEDICAL ENGINEERING

Results

T_{target} [°C]	$T_{av.\ tissue}$ [°C]	σ [°C]
45	45.273	0.704
50	50.158	0.742
60	59.819	0.698
65	64.855	0.673
80	79.693	0.524

T [°C]	σ [°C]
45	0.504
50	0.488
60	0.500
65	0.483
80	0.435



BOĞAZİÇİ UNIVERSITY

Conclusion

- feasible candidate for controlling laser exposure for photothermal medical laser applications
- maintains target tissue temperature within a narrow range
- add-on for medical laser systems
- translation of novel laser treatment techniques into clinic
- safety of photochemical (non-thermal) laser treatments

BME INSTITUTE OF BIOMEDICAL ENGINEERING

Future Work

- Manufacturing robust prototype
- Investigating other control methods
- Performance tests with various tissues
- Photothermal Applications
  - Laser Tissue Welding



BOĞAZİÇİ UNIVERSITY

Acknowledgements

This research project was supported by Boğaziçi University Research Fund with grant number 8500 (14XM2).

Thank you to İnci Çilesiz and Adnan Kurt for their guidance!

Thank you for listening!

BME INSTITUTE OF BIOMEDICAL ENGINEERING

APPENDIX D. PUBLISHED CONFERENCE PROCEEDING

A non-contact temperature measurement system for controlling photothermal medical laser treatments

Özgür Kaya and Murat Gülsoy

Boğaziçi University, Institute of Biomedical Engineering,
Kandilli Campus, Çengelköy, 34684, İstanbul, Turkey

ABSTRACT

Photothermal medical laser treatments are extremely dependent on the generated tissue temperature. It is necessary to reach a certain temperature threshold to achieve successful results, whereas preventing to exceed an upper temperature value is required to avoid thermal damage. One method to overcome this problem is to use previously conducted dosimetry studies as a reference. Nevertheless, these results are acquired in controlled environments using uniform subjects. In the clinical environment, the optical and thermal characteristics (tissue color, composition and hydration level) vary dramatically among different patients. Therefore, the most reliable solution is to use a closed-loop feedback system that monitors the target tissue temperature to control laser exposure. In this study, we present a compact, non-contact temperature measurement system for the control of photothermal medical laser applications that is cost-efficient and simple to use. The temperature measurement is achieved using a focused, commercially available MOEMS infrared thermocouple sensor embedded in an off-axis arrangement on the laser beam delivery hand probe. The spot size of the temperature sensor is *ca.* 2.5 *mm*, reasonably smaller than the laser spot sizes used in photothermal medical laser applications. The temperature readout and laser control is realized using a microcontroller for fast operation. The utilization of the developed system may enable the adaptation of several medical laser treatments that are currently conducted only in controlled laboratory environments into the clinic. Laser tissue welding and cartilage reshaping are two of the techniques that are limited to laboratory research at the moment. This system will also ensure the safety and success of laser treatments aiming hyperthermia, coagulation and ablation, as well as LLLT and PDT.

Keywords: medical laser treatment, photothermal interactions, temperature measurement, laser control, temperature control

1. INTRODUCTION

A very common usage of lasers in medicine is to heat tissues. The optical energy delivered to the tissue is converted to heat which results in a temperature increase that leads to various effects depending on the final temperature: hyperthermia (45°C), reduction in enzyme activity and cell immobility (50°C), denaturation of proteins and collagen, coagulation (60°C), permeabilization of membranes (80°C), vaporisation, decomposition (thermal-ablation) (100°C), melting (>100°C), and carbonisation (>300°C).[1] Depending on the medical procedure, it is necessary to ensure that some of these effects are generated while preventing the others from happening. Laser welding of various tissues,[2–10] ablation of various soft and hard tissues,[11–14] angioplasty,[15,16] treatment of granulation tissues,[17] treatment of hemangioma,[18] cartilage regeneration[19] and reshaping[20,21] are among the possible medical laser treatments. All of these procedures are highly temperature dependent and will result in failure if a specific temperature value is not reached.[8,14] However, if a certain temperature value is exceeded, thermal damage is eminent in the target and proximal tissues, which causes prolongation of recovery time and in some cases even failure of the treatment.[4,7–9,14,16,18,22]

The achieved tissue temperature is a function of the generated heat due to laser irradiation and the thermal properties of the tissue (specific heat, thermal conductivity and diffusivity) including perfusion characteristics.[23]

Further author information: (Send correspondence to Özgür Kaya)
Özgür Kaya: E-mail: okaya04@gmail.com, Telephone: +90 532 224 9882
Murat Gülsoy: E-mail: murat.gulsoy@boun.edu.tr, Telephone: +90 216 516 3460

Optical Interactions with Tissue and Cells XXVII, edited by E. Duco Jansen
Proc. of SPIE Vol. 9706, 97060K · © 2016 SPIE · CCC code: 1605-7422/16/$18 · doi: 10.1117/12.2212254

Downloaded From: http://proceedings.spiedigitallibrary.org/ on 03/11/2016 Terms of Use: http://spiedigitallibrary.org/ss/TermsOfUse.aspx

The extent of the generated heat depends on the laser parameters (wavelength, power density, exposure time, operation mode) as well as the optical properties (absorption and scattering coefficients) of the target tissue.[24] The absorption of the tissue is defined by the tissue type (composition), thickness, vascularity, fat content and hydration level.[25] Pigmentation, hence the skin color, is an important factor for skin applications.

The most common method to prevent thermal damage and ensure temperature dependent treatment success is conducting tissue and treatment specific dosimetry studies.[3,11,16,26] Nonetheless, the controlled condition of the laboratory environment and uniformity of research animals can hardly be encountered in the clinic. In real life, the optical and thermal properties of the subjects may not only change interpersonally, but also within the same person depending on circadian rhythm, physiological condition (*e.g.* inflammation, tumors, circulatory shock, sepsis), environmental factors (*e.g.* heat stress, hypothermia) and diet (hydration level).[23,27] Thus, one cannot expect to end up with the same successful results in the clinical environment when using laser parameters only defined by dosimetry studies.

The current trend in photothermal laser treatments is to use a closed-loop feedback mechanism for safety and treatment success reasons. While some research groups focus on secondary effects of thermal damage on tissue optical properties (*e.g.* reflection and scattering coefficients),[19,28] others focus on the cause of thermal damage, namely, tissue temperature.[4,5,7–9,15,17,29–35] Non-contact measurement of surface temperature of the tissue by means of infrared (IR) radiometry is considered as the gold standard for clinical applications for its promising results and because it does not carry the risk of contaminating the treatment area as well as interfering/preventing laser exposure.

Unfortunately, many of the above mentioned medical laser techniques cannot be used in the clinical environment due to the lack of a commercially available, simple to operate, affordable and reliable tissue temperature controlled medical laser system. It is possible that such a system will enable the improvement of current and development of new photothermal treatment techniques that address other health conditions and their translation into the clinic. In this study, we present a non-contact tissue surface temperature measurement system for controlling photothermal medical laser treatments that makes use of a commercially available MOEMS IR thermocouple sensor (IRt/c). The realized system is simple to operate, small in size, affordable and does not require excessive maintenance.

2. MATERIALS & METHODS

The developed temperature measurement system consists of an IRt/c sensor within an optical imaging assembly that can be used off-axially in combination with a laser delivery setup. The readout of the temperature sensor is processed using a microcontroller board that also regulates the modulation of the laser system.

2.1 Temperature Sensor

The temperature sensor (MLX90614ESF-BCC, Melexis, Belgium) used for this system contains an IRt/c sensor, signal conditioning, A/D conversion, dedicated signal processing and communication circuits on the same $2 \times 2\ mm$ chip packaged hermetically in a TO can. The digital temperature data can be acquired using the SMBUS protocol. The spectral bandwidth of the sensor (5.5–12 μm) is suitable for the desired temperature measurement range of 20–150°C (corresponding to a maximum emission bandwidth of 6.9–10 μm). It is important to note that this sensor cannot be used with lasers operating within its spectral bandwidth in order to avoid interference with the measurement. The field of view (35°) of the sensor is feasible for achieving the desired optical system. The sensor has a maximum measurement error of ±1°C over temperature range of interest.

2.2 Optical Design & Analysis

The optical system was designed to image a small area of the target (tissue) surface onto the sensor surface using an IR lens. An anti-reflection coated (3–11 μm) ZnSe lens (Crystran Ltd., UK) was used for achieving maximum transmission over the measurement bandwidth. The distance between the optical system exit pupil and the measurement surface was a limiting factor for ensuring a small measurement spot diameter due to the magnification of the imaging system. The system was designed to realize a balanced compromise between operating distance and measurement spot size. The designed optical system was analyzed using an open source ray tracing software (Beam4, Stellar Software, CA, USA).

Downloaded From: http://proceedings.spiedigitallibrary.org/ on 03/11/2016 Terms of Use: http://spiedigitallibrary.org/ss/TermsOfUse.aspx

2.3 Control System Development

A microcontroller development board (MSP-EXP430F5529LP, Texas Instruments, TX, USA) operating at 24 MHz was used as a central component of this system: interfacing with the IRt/c sensor for temperature acquisition, processing the temperature information for laser control, and interfacing with a PC for user input and data output. This micro-controller supports I^2C and UART communication protocols with dedicated hardware peripherals. It is possible to modify the I^2C peripheral in software to emulate SMBUS protocol. Several hardware timer modules sourced by two reliable clock sources enable independent triggering of events as well as PWM output for modulated laser control.

Currently, the raw temperature data acquired with the SMBUS protocol is converted to a temperature value in the Celsius scale. The operation of the laser is controlled with a TTL signal using the simplest method, namely exposure modulation. In this method, the laser irradiation is turned on while the measured temperature is below the target temperature, and vice versa.

2.3.1 Hardware Stopwatch

Two functions (`tic()` and `toc()`) were developed for controlling one of the timer modules of the microcontroller as a hardware stopwatch to measure individual processes with a 10 μs precision. The stopwatch function operates independent of other processes because the timer module is a hardware peripheral.

2.3.2 Moving Average Temperature Acquisition

A moving average function for temperature acquisitions were developed for the spatial resolution measurement procedure. The window size of this function was dynamically adjustable (2, 4, 8, 16, 32, and 64 points) by pressing a pushbutton.

2.4 Measurement of System Specifications

2.4.1 Calibration & Accuracy

The temperature measurement system was calibrated using a blackbody calibrator (BB702, Omega Engineering, CT, USA) presented in Figure 1. The accuracy and the stability values of this device provided by the manufacturer are 0.5°C and 0.1°C, respectively. The blackbody calibrator was set to a temperature and the measurement system was directed at the calibration target. The raw temperature data was recorded for 60 seconds after the calibrator reached steady-state. The recorded data was averaged, and this process was repeated over the range of 30–150°C. The resulting raw data - real temperature values were used to calculate a mathematical formula for temperature conversion. Using this calibration technique, the average measurement error of the system was defined by the accuracies of the sensor and calibrator.

The temperature measurement suffers from noise to a small extent. This results in a transient measurement error which can be characterized by the standard deviation over a period of time (*i.e.* 60 seconds). The transient error was calculated for the temperatures listed in Table 1.

2.4.2 Temporal Response

The temporal response of the system was not measured using conventional methods because a commercial sensor was used. The settling time of the sensor, provided by the manufacturer, was used to determine the readout interval of the system. The readout duration, defined as the time required for completing the I^2C communication with the sensor for temperature acquisition and conversion of the acquired data, is partly a function of the microprocessor speed. This duration was measured using the `tic()` and `toc()` functions of the developed microcontroller code.

2.4.3 Spatial Resolution

The measurement of the spatial resolution was conducted using the knife-edge test as depicted in Figure 1. For this purpose, the blackbody calibrator was set to a temperature value 100°C higher than the ambient temperature. The temperature measurement system was set to operate in 64-point moving average window mode. It was pointed to the calibrator target; and a razor blade attached to a micrometer stage was scanned between them. The average temperature value for each increment of the micrometer stage was recorded. The acquired data was analyzed to reveal 20/80 and 10/90 knife-edge diameter of the measurement spot.

Downloaded From: http://proceedings.spiedigitallibrary.org/ on 03/11/2016 Terms of Use: http://spiedigitallibrary.org/ss/TermsOfUse.aspx

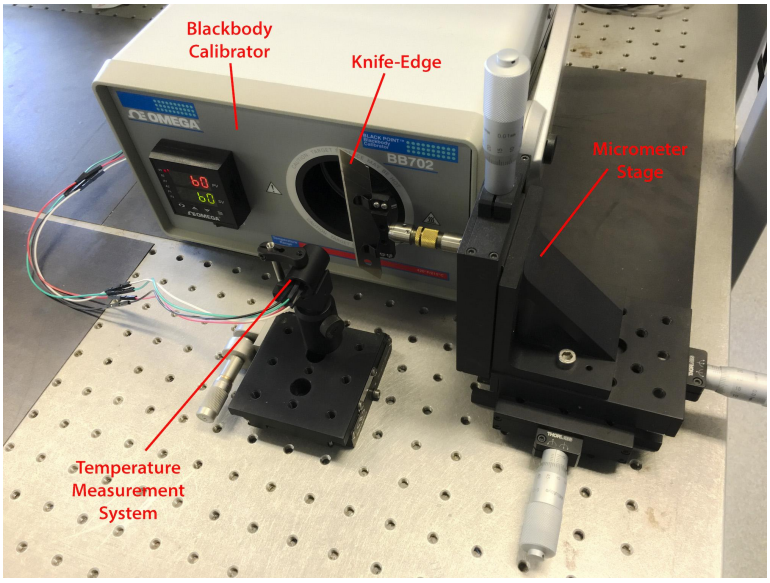


Figure 1. The blackbody calibrator and the knife-edge test setup.



Figure 2. Fiber coupling (top) and laser beam delivery (bottom) assemblies.

Table 1. Temperature values used for the performance evaluation of the system.

T_{target}	Physiological Effect / Laser Treatment
45°C	Hyperthermia, Treatment of Granulation Tissue
50°C	Reduction in Enzyme Activity, Cellular Immobilisation Thermal Treatment of Malignant Tissues
60°C	Denaturation of Proteins and Collagen, Coagulation, Surgical Haemostasis
65°C	Ideal Temperature for Laser Tissue Welding
80°C	Permeabilization of Membranes

Downloaded From: http://proceedings.spiedigitallibrary.org/ on 03/11/2016 Terms of Use: http://spiedigitallibrary.org/ss/TermsOfUse.aspx

2.5 Laser Irradiation System

For the purpose of demonstrating the performance of the developed temperature measurement system, a TTL signal controllable laser operating in the near IR region was selected ($\lambda = 1071\ nm$, Ytterbium Fiber Laser, YLM-20-SC, IPG Photonics, MA, USA). The collimated output of the laser was coupled to a low-OH optical fiber patch cable ($\varnothing = 1000\ \mu m$, NA = 0.39, M35L01, Thorlabs Inc., NJ, USA) using a lens tube assembly and a plano-convex N-BK7 lens (Thorlabs Inc., NJ, USA) and as depicted in Figure 2. The other end of the patch cable was connected to another lens tube assembly which functioned as the beam delivery hand piece. The hand piece was positioned to achieve a rather large laser spot diameter of *ca.* 7 mm for the sake of easy alignment. The laser spot of the had a Gaussian intensity profile due to the fiber coupling. The attenuation introduced by the optical assembly rendered the maximum achievable output power to a value of 8.3 W, which was also the set value for the performance evaluation of the developed temperature measurement and laser control system. The operation of the laser was modulated via a TTL signal generated by the microcontroller.

2.6 Performance Evaluation of Temperature Controlled Laser Irradiation

The practical performance criteria for this system was determined as its ability to maintain the tissue temperature at a set value by controlling the laser exposure. The target temperatures were chosen to emulate several of the thermo-physiological effects on tissues given in Table 1.

Full thickness skin tissues of Wistar albino rats recently sacrificed in course of another research project were harvested in flap form. The samples were placed on a lab jack fur side (epidermal side) down. The laser delivery assembly was positioned perpendicularly above the target area. The temperature measurement system was situated carefully above the target area with an oblique angle in order to perfectly match the laser spot with the measurement spot without blocking the laser beam. The experiment setup is exhibited in Figure 3. The laser exposure was initiated while the temperature measurement and laser control system was operational. The temperature data and laser control signal was recorded for analysis.

The average temperature value was calculated for 60 seconds after the target temperature was reached. The difference between the target and average temperature values provides a quantitative measure for the performance of the system for the set laser parameters and target temperature. The standard deviation of the same temperature data was also calculated for assessing the dynamic variation of the tissue temperature.

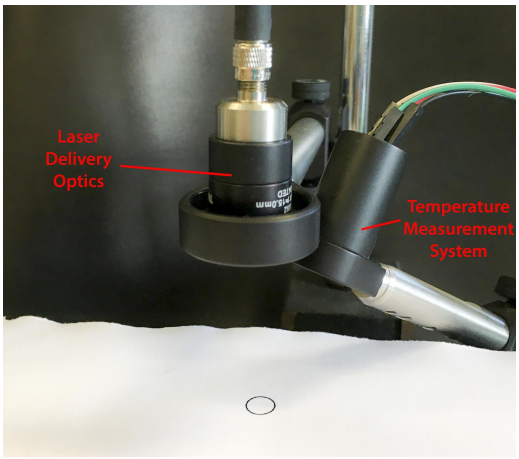


Figure 3. Temperature controlled laser irradiation setup.

Downloaded From: http://proceedings.spiedigitallibrary.org/ on 03/11/2016 Terms of Use: http://spiedigitallibrary.org/ss/TermsOfUse.aspx

3. RESULTS & DISCUSSION

3.1 System Specifications

Table 2. Transient error for thermo-physiologically important temperatures.

T [°C]	σ [°C]
45	0.504
50	0.488
60	0.500
65	0.483
80	0.435

3.1.1 Accuracy

The average accuracy of the system is expected to be ±1°C, considering the sensor and calibrator accuracy values. The transient error of the system defined as the standard deviation of the 60 second temperature recording is given in Table 2. The standard deviation is observed as approximately 0.5°C over a wide range of temperatures. Even though, the noise present in the measurement system may result in momentary excessive or insufficient laser exposure, the thermal characteristics of the tissue can compensate for this error. Therefore, the average and transient accuracy values are sufficient for the reliable operation of the temperature measurement and laser control system.

Table 3. Individual process durations of the temperature measurement system.

Process	t [ms]
Sensor Settling	55.516
Readout Interval	56
Temperature Acquisition, Data Conversion and Processing	0.87
Response Time	< 57

3.1.2 Temporal Response

The durations of individual processes of the system provided in Table 3 accounted for a response time of less than 57 ms. The response time of the system is satisfactory for preventing thermal damage in most medical laser treatments.

3.1.3 Spatial Resolution

The 20/80 and 10/90 knife-edge diameters of the temperature measurement spot were found out as 2.5 mm and 3.6 mm, respectively. These values correspond with the measurement spot diameter values computed using the ray tracing software. Even though a smaller measurement spot diameter is preferable, the spatial resolution of the system is sufficient for many medical laser applications such as laser tissue welding, cartilage reshaping, and treatment of granulation tissues.

3.2 Performance Evaluation

The temperature data of the skin tissues undergoing controlled laser irradiation with various target temperatures are represented with different colors in Figure 4. The target temperatures are marked with horizontal lines in the same graph for convenience. The 60 second average temperatures and standard deviation values after reaching the target temperatures are provided in Table 4.

The small differences between the target and average tissue temperatures reveal that the system is satisfactorily capable of maintaining the tissue temperature by controlling laser irradiation. The comparison of the

Downloaded From: http://proceedings.spiedigitallibrary.org/ on 03/11/2016 Terms of Use: http://spiedigitallibrary.org/ss/TermsOfUse.aspx

standard deviations given in Tables 2 and 4 reveal that the variation of the temperature after reaching the target value is significantly due to measurement noise. The noise certainly affected the laser exposure undesirably, nevertheless the thermal inertia of the tissue conveniently corrected for these momentary errors acting as a low pass filter.

The fact that temperature curves do not overlap in Figure 4 support the phenomena of non-homogenous optical/thermal characteristics even for the tissues of the same individual. This is a proof of the requirement for a temperature controlled medical laser system.

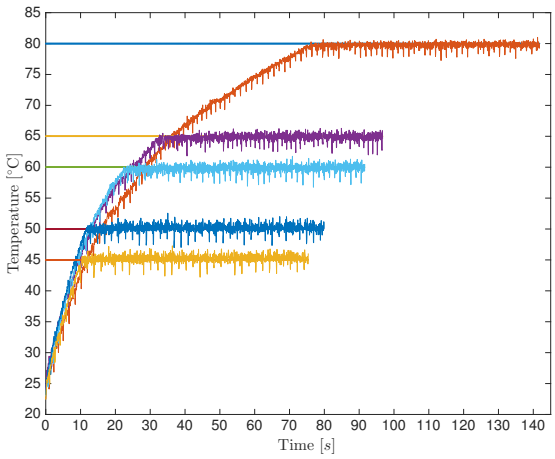


Figure 4. Temperature controlled laser irradiation.

Table 4. Performance characteristics for thermo-physiologically important temperatures.

T_{target} [°C]	$T_{av.\ tissue}$ [°C]	σ [°C]
45	45.273	0.704
50	50.158	0.742
60	59.819	0.698
65	64.855	0.673
80	79.693	0.524

4. CONCLUSION

The non-contact temperature measurement system presented in this paper is a feasible candidate for controlling laser exposure for photothermal medical laser applications. It is shown that the system is reliable for maintaining target tissue temperature within a narrow range even using the simplest laser control method (Exposure Modulation). This system is a promising candidate as an add-on for medical laser systems operating in UV, visible and near-IR region of the spectrum in order to ensure patient safety and treatment success during photothermal applications. The use of this system may enable the translation of novel laser treatment techniques (*e.g.* laser tissue welding, cartilage reshaping) into clinical use. This system will also ensure the safety of photochemical (non-thermal) laser treatments like low level laser therapy and photodynamic therapy.

Downloaded From: http://proceedings.spiedigitallibrary.org/ on 03/11/2016 Terms of Use: http://spiedigitallibrary.org/ss/TermsOfUse.aspx

The further development of this system will focus on improving the laser control method and producing a mechanically robust prototype that combines the off-axially placed temperature measurement system and beam delivery optics in a single hand piece. The performance of the total system will be tested using different laser wavelengths, power densities, and tissues for various photothermal medical laser treatment techniques.

ACKNOWLEDGMENTS

This research project was supported by Boğaziçi University Research Fund with grant number 8500 (14XM2).

REFERENCES

[1] Niemz, M. H., [*Laser-Tissue Interactions: Fundamentals and Applications*], Springer Science & Business Media, Berlin, third, enlarged ed. (2007).

[2] Poppas, D. P., Stewart, R. B., and Massicotte, J. M., "Temperature-Controlled Laser Photocoagulation of Soft Tissue: In Vivo Evaluation Using a Tissue Welding Model," *Lasers Surg. Med.* **18**, 335–344 (1996).

[3] Tabakoğlu, H. O. and Gülsoy, M., "In vivo comparison of near infrared lasers for skin welding.," *Lasers Med. Sci.* **25**(3), 411–21 (2010).

[4] Cilesiz, I., Springer, T., Thomsen, S., and Welch, a. J., "Controlled temperature tissue fusion: argon laser welding of canine intestine in vitro.," *Lasers Surg. Med.* **18**(4), 325–34 (1996).

[5] Spector, D., Rabi, Y., Vasserman, I., Hardy, A., Klausner, J., Rabau, M., and Katzir, A., "In vitro large diameter bowel anastomosis using a temperature controlled laser tissue soldering system and albumin stent.," *Lasers Surg. Med.* **41**(7), 504–8 (2009).

[6] Stewart, R. B., Benbrahim, a., LaMuraglia, G. M., Rosenberg, M., L'Italien, G. J., Abbott, W. M., and Kung, R. T., "Laser assisted vascular welding with real time temperature control.," *Lasers Surg. Med.* **19**(1), 9–16 (1996).

[7] Cilesiz, I., "Controlled Temperature Photothermal Tissue Welding," *J. Biomed. Opt.* **4**(3), 327–336 (1999).

[8] Cilesiz, I., Thomsen, S., Welch, a. J., and Chan, E. K., "Controlled temperature tissue fusion: Ho:YAG laser welding of rat intestine in vivo. Part two.," *Lasers Surg. Med.* **21**(3), 278–86 (1997).

[9] Cilesiz, I., Thomsen, S., and Welch, a. J., "Controlled temperature tissue fusion: argon laser welding of rat intestine in vivo. Part one.," *Lasers Surg. Med.* **21**(3), 269–77 (1997).

[10] Small IV, W., Celliers, P., Kopchok, G., Reiser, K., Heredia, N., Maitland, D., Eder, D., London, R., Heilbron, M., Hussain, F., White, R., Da Silva, L., and Matthews, D., "Temperature Feedback and Collagen Cross-Linking in Argon Laser Vascular Welding," *Lasers Med. Sci.* **13**(2), 98–105 (1998).

[11] Gülsoy, M., Durak, K., Kurt, a., Karamürsel, S., and Cilesiz, I., "The 980-nm diode laser as a new stimulant for laser evoked potentials studies.," *Lasers Surg. Med.* **28**(3), 244–7 (2001).

[12] Ishihara, M., Arai, T., Sato, S., Morimoto, Y., Obara, M., and Kikuchi, M., "Measurement of the Surface Temperature of the Cornea During ArF Excimer Laser Ablation by Thermal Radiometry With a 15-Nanosecond Time Response," *Lasers Surg. Med.* **30**(1), 54–59 (2002).

[13] Kang, H. W., Oh, J., and Welch, a. J., "Investigations on laser hard tissue ablation under various environments.," *Phys. Med. Biol.* **53**(12), 3381–90 (2008).

[14] Swanson, D. K., Smith, W. J., Ibrahim, T., and Wechsler, A. S., "Tissue temperature feedback control of power: the key to successful ablation.," *Innovations: Technology and Techniques in Cardiothoracic and Vascular Surgery* **6**(4), 276–82 (2011).

[15] Kopchok, G. E., White, R. a., Tabbara, M., Saadatmanesh, V., and Peng, S. K., "Holmium:YAG laser ablation of vascular tissue.," *Lasers Surg. Med.* **10**(5), 405–13 (1990).

[16] Singleton, D. L., Paraskevopulos, G., Taylor, R. S., and Higginson, L. A. J., "Excimer Laser Angioplasty : Tissue Ablation , Arterial Response , and Fiber Optic Delivery," *IEEE J. Quantum Electron.* **23**(10), 1772–1782 (1987).

[17] Landsberg, R., DeRowe, A., Katzir, A., Shtabsky, A., Fliss, D. M., and Gil, Z., "Laser-induced hyperthermia for treatment of granulation tissue growth in rats.," *Otolaryngol. Head. Neck Surg.* **140**(4), 480–6 (2009).

[18] Svaasand, L. O., Randeberg, L. L., Aguilar, G., Majaron, B., Kimel, S., Lavernia, E. J., and Nelson, J. S., "Cooling efficiency of cryogen spray during laser therapy of skin.," *Lasers Surg. Med.* **32**(2), 137–42 (2003).

Downloaded From: http://proceedings.spiedigitallibrary.org/ on 03/11/2016 Terms of Use: http://spiedigitallibrary.org/ss/TermsOfUse.aspx

[19] Sobol, E., Shekhter, A., Guller, A., Baum, O., and Baskov, A., "Laser-induced regeneration of cartilage," *J. Biomed. Opt.* **16**(8), 080902–080902 (2011).

[20] Wong, B. J. F., Milner, T. E., Anvari, B., Sviridov, a., Omel'chenko, a., Bagratashvili, V. V., Sobol, E., and Nelson, J. S., "Measurement of radiometric surface temperature and integrated backscattered light intensity during feedback-controlled laser-assisted cartilage reshaping," *Lasers Med. Sci.* **13**(1), 66–72 (1998).

[21] Wong, B. J., Milner, T. E., Harrington, a., Ro, J., Dao, X., Sobol, E. N., and Nelson, J. S., "Feedback-controlled laser-mediated cartilage reshaping.," *Arch. Facial Plast. Surg.* **1**(4), 282–7 (1999).

[22] Sriramoju, V. and Alfano, R. R., "Management of heat in laser tissue welding using NIR cover window material.," *Lasers Surg. Med.* **43**(10), 991–7 (2011).

[23] Valvano, J. W., "Tissue thermal properties and perfusion," in [*Optical-Thermal Response of Laser-Irradiated Tissue*], 455–485, Springer (2011).

[24] Welch, A. J., "The thermal response of laser irradiated tissue," *Quantum Electronics, IEEE Journal of* **20**(12), 1471–1481 (1984).

[25] Bass, L. S. and Treat, M. R., "Laser tissue welding: a comprehensive review of current and future applications," *Lasers Surg. Med.* **17**(4), 315–349 (1995).

[26] Geldi, C., Bozkulak, O., Tabakoglu, H. O., Isci, S., Kurt, A., and Gulsoy, M., "Development of a Surgical Diode-Laser System : Controlling the Mode of Operation," *Photomed. Laser Surg.* **24**(6), 723–729 (2006).

[27] Barton, J. K., "Dynamic changes in optical properties," in [*Optical-Thermal Response of Laser-Irradiated Tissue*], 321–349, Springer (2011).

[28] Zając, A., Podniesiński, D., Świderski, J., Kęcik, D., Kęcik, M., and Kasprzak, J., "Procedures of optical control dedicated for laser welding process of biological tissues," *Opto-Electronics Review* **18**(1), 48–55 (2010).

[29] Cohen, M., Ravid, A., Scharf, V., Hauben, D., and Katzir, A., "Temperature controlled burn generation system based on a CO2 laser and a silver halide fiber optic radiometer.," *Lasers Surg. Med.* **32**(5), 413–6 (2003).

[30] Simhon, D., Ravid, a., Halpern, M., Cilesiz, I., Brosh, T., Kariv, N., Leviav, a., and Katzir, a., "Laser soldering of rat skin, using fiberoptic temperature controlled system.," *Lasers Surg. Med.* **29**(3), 265–73 (2001).

[31] Eyal, O. and Katzir, A., "Thermal feedback control techniques for transistor-transistor logic triggered CO2 laser used for irradiation of biological tissue utilizing infrared fiber-optic radiometry," *Appl. Opt.* **33**(9), 1751–1754 (1994).

[32] Sade, S., Eyal, O., Scharf, V., and Katzir, A., "Fiber-optic infrared radiometer for accurate temperature measurements.," *Appl. Opt.* **41**(10), 1908–14 (2002).

[33] Simhon, D., Halpern, M., Brosh, T., Vasilyev, T., Ravid, A., Tennenbaum, T., Nevo, Z., and Katzir, A., "Immediate tight sealing of skin incisions using an innovative temperature-controlled laser soldering device: in vivo study in porcine skin.," *Ann. Surg.* **245**(2), 206–13 (2007).

[34] Simhon, D., Gabay, I., Shpolyansky, G., Vasilyev, T., Nur, I., Meidler, R., Hatoum, O. A., Katzir, A., Hasmonai, M., and Kopelman, D., "Temperature-controlled laser-soldering system and its clinical application for bonding skin incisions," *J. Biomed. Opt.* **20**(12), 128002 (2015).

[35] Alexiades-Armenakas, M., "Combination Laser-Assisted Liposuction and Minimally Invasive Skin Tightening with Temperature Feedback for Treatment of the Submentum and Neck," *Dermatologic Surg.* **38**(6), 871–881 (2012).

Downloaded From: http://proceedings.spiedigitallibrary.org/ on 03/11/2016 Terms of Use: http://spiedigitallibrary.org/ss/TermsOfUse.aspx

APPENDIX E. PUBLISHED ARTICLE

applied sciences

MDPI

Article

Controlling Laser Irradiation with Tissue Temperature Feedback Enhances Photothermal Applications: Ex-Vivo Evaluation on Bovine Liver

Özgür Kaya [1,*], İpek Düzgören [1], İnci Çilesiz [2] and Murat Gülsoy [1]

[1] Institute of Biomedical Engineering, Boğaziçi University, Kandilli Campus, Üsküdar, Istanbul 34684, Turkey
[2] Biomedical Engineering, Istanbul Technical University, Ayazağa Campus, Maslak, Istanbul 34469, Turkey
* Correspondence: ozgur.kaya1@boun.edu.tr

Abstract: Achieving repeatable and successful results without causing excessive collateral damage is of paramount importance for photothermal laser applications. Predetermined laser parameters cannot ensure patient safety and treatment success due to variance between optical and thermal characteristics among subjects. Controlling laser irradiation with tissue temperature feedback is the current gold standard for various photothermal treatments (PTT) which are rate processes described by the Arrhenius temperature integral. This study establishes the validity of our low-cost design that makes tissue surface temperature control during photothermal laser applications more accessible in resource limited clinical environments. We demonstrated the practical performance and potential of our system with ex-vivo bovine liver irradiation using an ytterbium fiber laser ($\lambda = 1071$ nm) with two independent variables: laser power (3.4 W, 6.8 W and 10.2 W) and target surface temperature (55 °C, 65 °C and 75 °C). Our system efficiently maintained tissue surface temperatures at target values in all laser power groups. In contrast, fixed-dose application groups displayed a high final temperature range and variation in the control experiment. Temperature–time responses of samples varied significantly, in agreement with a wide range of optical and thermal coefficients. Long exposure duration groups (lower power, higher target temperature) displayed more radical differences suggesting a dominance of optical and thermal characteristics over the response. The low-cost surface-temperature-controlled medical laser system we have developed is capable of ensuring the success and reproducibility of PTT modalities and patient safety.

Keywords: temperature regulation; laser control; medical laser treatment; photothermal interactions

check for updates

Citation: Kaya, Ö.; Düzgören, İ.; Çilesiz, İ.; Gülsoy, M. Controlling Laser Irradiation with Tissue Temperature Feedback Enhances Photothermal Applications: Ex-Vivo Evaluation on Bovine Liver. *Appl. Sci.* **2023**, *13*, 237. https://doi.org/10.3390/app13010237

Academic Editor: Hossam S. Abbas

Received: 30 November 2022
Revised: 19 December 2022
Accepted: 20 December 2022
Published: 24 December 2022

Copyright: © 2022 by the authors. Licensee MDPI, Basel, Switzerland. This article is an open access article distributed under the terms and conditions of the Creative Commons Attribution (CC BY) license (https://creativecommons.org/licenses/by/4.0/).

1. Introduction

Medical laser applications in the photothermal region rely heavily on heat generation to achieve desired thermo-physiological effects [1,2]. Achieved physiological effects are tissue temperature dependent. Tissue temperature, in turn, is a function of generated heat, optical, and thermal properties of the tissue including perfusion characteristics [3]. Depending on the medical procedure, it is necessary to ensure that some of these thermo-physiological effects are generated while preventing some others. Laser tissue welding (LTW) [4–8], ablation of soft tissues [9,10], photocoagulation and photothermal denaturation [11], angioplasty [12,13], treatment of granulation tissues [14], cartilage regeneration [15], and reshaping [16] are among possible medical photothermal laser treatments (PTT).

Thermo-physiological interactions occur within a narrow temperature range. Any deviation from this range may result in treatment failure or excessive thermal damage [6]. For instance, photothermal treatment of granulation tissue aims to trigger apoptosis by hyperthermia (45–50 °C) induced heat shock protein production without causing necrosis (>50 °C) [14]. Another example for a highly temperature sensitive application is LTW. Optimally, LTW requires temperatures between 65 °C and 70 °C (skin tissue) to ensure collagen denaturation (>63 °C for treatment success) [17]. Keeping the tissues at this

temperature range for a moderate duration of time (ranging from 0.06 s to minutes) also prevents excessive thermal damage (coagulative necrosis, heat fixation), which results in scarring and prolonged recovery time [18]. Currently, both treatment of granulation tissue and LTW are experimental procedures, not regularly used in clinical environment due to reproducibility and safety issues.

Thermal and optical characteristics of tissues vary among individuals and can change even within the same individual over time [3,19]. Dosimetry studies are widely used for determining laser parameters and exposure durations for PTT. While providing generally satisfactory laser parameters for treatments, dosimetry studies conducted in controlled environments of laboratories (using rather uniform research animals) do not ensure optimal results for all subjects. A predetermined dose may result in successful treatments in the majority of subjects, but may also lead to treatment failure and/or excessive thermal damage in some subjects. Therefore, conducting PTT with real-time tissue temperature feedback control is necessary.

A tissue temperature controlled medical laser system ensures treatment success and standardization, as well as patient safety. It also compensates for inexperienced operators increasing reproducibility of results for current PTT modalities used in the clinic. Consequently, a temperature controlled system may endorse the translation of experimental laser techniques (e.g., LTW, granulation tissue treatment, cartilage reshaping), which currently are limited to the controlled environment of the laboratory, into regular clinical practice. Such a system may also be used in the research of thermal characteristics of tissues and development of new laser treatment techniques. Additionally, it can be used for preventing undesirable temperature increase during photochemical procedures (e.g., photodynamic therapy and low-level laser therapy), which are non-thermal processes by nature [20,21].

Various research groups utilized different techniques to develop temperature measurement and control systems for medical laser applications [4–7,9,11,12,16,22–25]. These systems excel at different aspects of temperature control (e.g., fast response time, high accuracy, high spatial resolution) but mostly share a common drawback: the requirement of multiple and costly apparatus that are complicated to use in the clinical environment.

Our aim was to design a low-cost, compact and simple to use non-contact temperature controlled medical laser system that can be easily implemented in a resource limited (lacking expensive control systems and the highly skilled technical staff to operate these systems) clinical environment. We have developed this limited-resource-compatible system using a high SNR infrared thermocouple (IRt/c) sensor to measure the blackbody radiation emanating from the surface of the tissue [26]. The total cost of this system including the microcontroller board, optical opto-electronical, and -mechanical components and excluding the laser source and driver is ca. 300 USD (single unit retail prices).

Building on Kaya and Gülsoy (2016), this study evaluates the practical performance of our tissue-temperature-controlled laser system in comparison to a fixed-dose laser application using higher power densities on the bovine liver tissue to provide an example for photothermal liver tumor treatments.

2. Materials and Methods

Apart from being a good model for human liver applications, using bovine liver as tissue sample provided several other advantages. Bovine liver is easy to acquire and conforms with other soft tissues regarding water content. Furthermore, using ex vivo tissue samples acquired from a slaughterhouse on different days enabled us to match clinical conditions (widely varying optical and thermal characteristics among subjects) in contrast to the more uniform properties among laboratory animals. Near-IR, and specifically Nd:YAG ($\lambda = 1064$ nm) lasers, are commonly used for photothermal aplications due to their ideally balanced tissue penetration and absorption characteristics [27,28]. For this purpose, we used a near-IR laser with a similar center wavelength ($\lambda = 1071$ nm).

2.1. Non-Contact Temperature Controlled Medical Laser System

The experimental setup is composed of a laser ($\lambda = 1071$ nm, Ytterbium Fiber Laser, YLM-20SC, IPG Photonics, Oxford, MA, USA), laser delivery optics designed for a converging beam with a Gaussian profile, providing a spot diameter of 3.5 mm ($1/e^2$) at the application distance (40 mm), and an IRt/c temperature measurement and laser control system as illustrated in Figure 1. We used a commercially available IRt/c sensor (MLX90614ESF-BCC, Melexis NV, Leper, Belgium) with a spectral bandwidth of 5.5–12 µm in our temperature measurement system; therefore, the system does not get affected by the laser irradiation. We also utilized a ½″ Lens Tube and an AR coated (3–11 µm) ZnSe lens (ZnSe10, Crystran Ltd., Dorset, UK) to house the IRt/c sensor and to convert the diverging measurement cone of the sensor into a converging measurement cone. We calibrated our temperature measurement system using a NIST certified blackbody source (BB702, Omega Engineering, Norwalk, CT, USA). The IRt/c system takes average surface temperature measurements from a center weighted 3.6 mm diameter spot at 41 mm focal distance. It operates at 57 ms refresh time with 1 °C accuracy and 0.02 °C resolution. Our previous work contains details on characterization methods for determining system specifications [26]. We assumed that the emissivity of the tissue is equal to the emissivity of water ($\epsilon = 0.96$). The IRt/c sensor assembly is attached to the side of the laser delivery optics at an oblique angle to perfectly coincide laser application and temperature measurement spots without interfering with the laser beam as depicted in Figure 1. We have used an ON-OFF feedback control mechanism for ensuring fast response of the system. The laser exposure is modulated using a TTL signal generated by the TI MSP-EXP430F5529LP microcontroller board, which also reads out the IRt/c sensor via an I^2C interface. This microcontroller feeds the real-time temperature data and the laser control signal to a computer via a Bluetooth connection for display and storage.

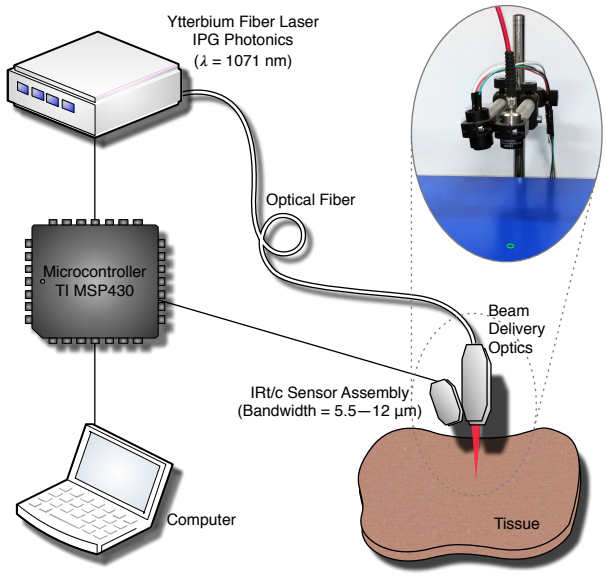


Figure 1. Schematic and photo of the experiment setup. The laser delivery optics (Gaussian profile, $\varnothing_{laser} = 3.5$ mm @ $d = 40$ mm) and the temperature measurement system ($\varnothing_{measurement} = 3.6$ mm @ $f = 41$ mm) are in an off-axis alignment configuration.

2.2. Photothermal Irradiation of Bovine Liver Tissue

2.2.1. Groups

We used 3 different laser powers and 3 different target temperatures (55 °C, 65 °C and 75 °C), corresponding to 9 experiment groups ($n = 16$), in surface temperature controlled mode. We also conducted a fixed-dose application as a control experiment which, additionally, enabled us to show the difference between tissue surface temperatures reached at the end of the exposure within the same group. We used the same 3 power levels in the fixed-dose application. The fixed-dose of each group ($n = 16$) in the control experiment was determined from the temperature controlled application data. We have computed the total exposure duration for each sample using the recorded laser control signal data and averaged this value within each application group to compute the fixed exposure duration, hence the fixed-dose (by multiplying the duration with the laser power) for each control group as provided in Table 1. The power levels 3.4 W, 6.8 W and 10.2 W correspond to average power densities of 35 W/cm^2, 71 W/cm^2, and 106 W/cm^2, respectively, for the Gaussian profile laser spot.

Table 1. Average dose delivered in the temperature controlled (experiment) groups and their equivalent exposure duration for the given power setting in fixed-dose (control) groups.

	55 °C	**65 °C**	**75 °C**
3.4 W	83.4 J (24.54 s)	142.5 J (41.91 s)	215.1 J (63.26 s)
6.8 W	53.5 J (7.87 s)	74.3 J (10.93 s)	104.0 J (15.29 s)
10.2 W	41.7 J (4.09 s)	64.5 J (6.32 s)	79.8 J (7.82 s)

2.2.2. Sample Preparation

Bovine livers were acquired from the slaughterhouse and stored at 4 °C until the procedure. On the experiment day, the liver of each animal was dissected to end up with 9 or 18 samples (corresponding to 1 or 2 samples from the same animal for each experiment group) of ca. 3 cm × 3 cm × 1.5 cm. This size was sufficient for providing a smooth and even surface for the target area, away from fascia and veins. The samples were packaged in aluminum foil for preventing desiccation and assigned randomly to groups. After reaching room temperature (ca. 23 °C), they were placed on a lab jack for irradiation.

2.2.3. Irradiation Procedure

The lab jack height was adjusted for aligning the top surface of the tissue sample with the laser spot and temperature measurement spot in order to ensure perfect overlapping of irradiation spot center with the temperature measurement spot center. The sample was positioned with the help of a visible guide beam to target a locus away from veins and fascia. Laser irradiation procedure was initiated from the computer by first starting the temperature data recording and then turning CW laser exposure on. In the temperature-controlled applications, once the tissue surface temperature reached the target value, the microcontroller modulated the laser exposure to maintain the target temperature for 5 s and then ceased the irradiation. The 5 s duration was chosen because it provides sufficient time at the target temperature for thermal effects to be manifested without causing significant dessication. In the fixed-dose applications (control experiment), the CW laser irradiation was maintained until the end of the predetermined duration for each fixed-dose group.

3. Results

Figures 2 and 3 reveal the raw (unfiltered) and superimposed temperature measurement data of all samples within each application group in temperature-controlled and fixed-dose applications, respectively. Further descriptive quantitative data are provided in Table 2 for the temperature-controlled application and in Table 3 and Figure 4 for the fixed-dose application.

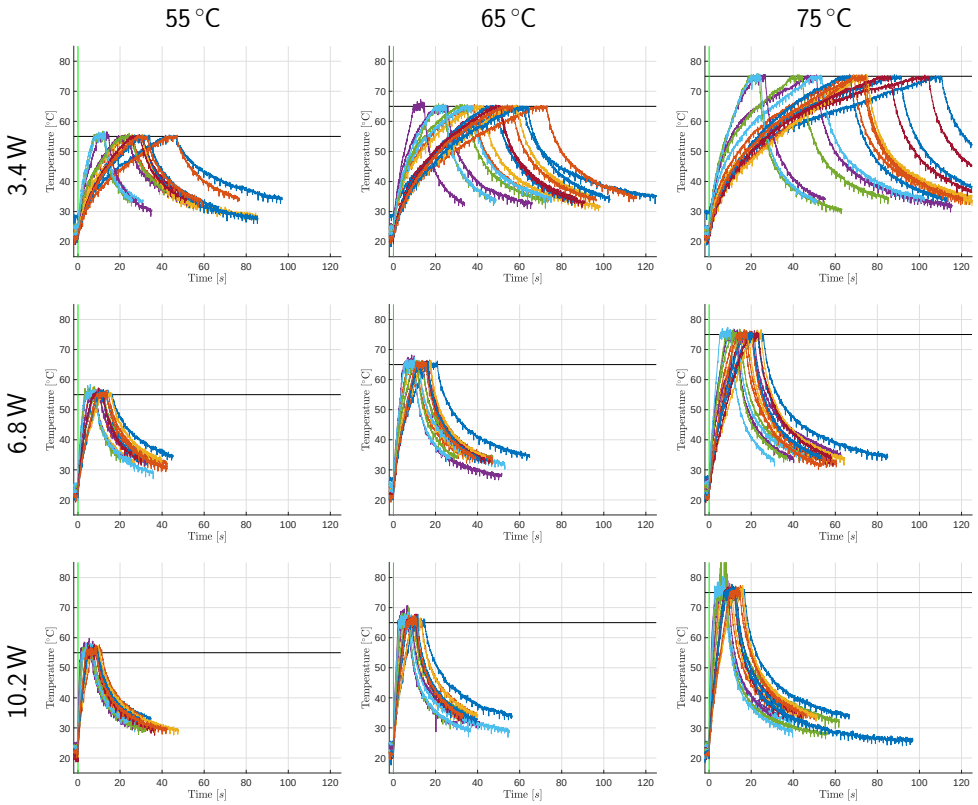


Figure 2. Temperature monitorization data of surface temperature controlled laser irradiation. The temperature–time response graphs (each individual sample represented with a different curve color) within each group are superimposed. The horizontal black lines and the vertical green lines represent the target temperature values and the laser emission commencement marks, respectively.

Table 2. Descriptive temperature values for the surface temperature controlled application: The mean (μ) and standard deviation (σ) values of maximum (T_{max}), minimum (T_{min}), mean (μ_T) and standard deviation (σ_T) values of the tissue surface temperature during the 5 s-period at the target value.

P_{laser}	T_{target}	$\mu_{T_{5s}}(\mu \pm \sigma)$ [°C]	$\sigma_{T_{5s}}(\mu \pm \sigma)$ [°C]	$T_{\text{min}}(\mu \pm \sigma)$ [°C]	$T_{\text{max}}(\mu \pm \sigma)$ [°C]
3.4 W	55 °C	54.6 ± 0.1	0.6 ± 0.1	52.8 ± 0.4	55.8 ± 0.5
	65 °C	64.5 ± 0.1	0.5 ± 0.1	62.8 ± 0.4	65.6 ± 0.5
	75 °C	74.4 ± 0.1	0.6 ± 0.1	72.6 ± 0.7	75.5 ± 0.2
6.8 W	55 °C	55.0 ± 0.2	0.7 ± 0.1	52.9 ± 0.5	57.0 ± 0.6
	65 °C	64.8 ± 0.2	0.8 ± 0.2	62.6 ± 0.6	66.6 ± 0.6
	75 °C	74.6 ± 0.1	0.8 ± 0.1	72.4 ± 0.5	76.4 ± 0.5
10.2 W	55 °C	55.3 ± 0.2	1.0 ± 0.2	52.8 ± 0.5	57.8 ± 0.9
	65 °C	65.1 ± 0.3	1.1 ± 0.3	62.3 ± 0.7	67.8 ± 1.2
	75 °C	74.9 ± 0.8	1.3 ± 0.8	71.8 ± 1.3	77.5 ± 1.1

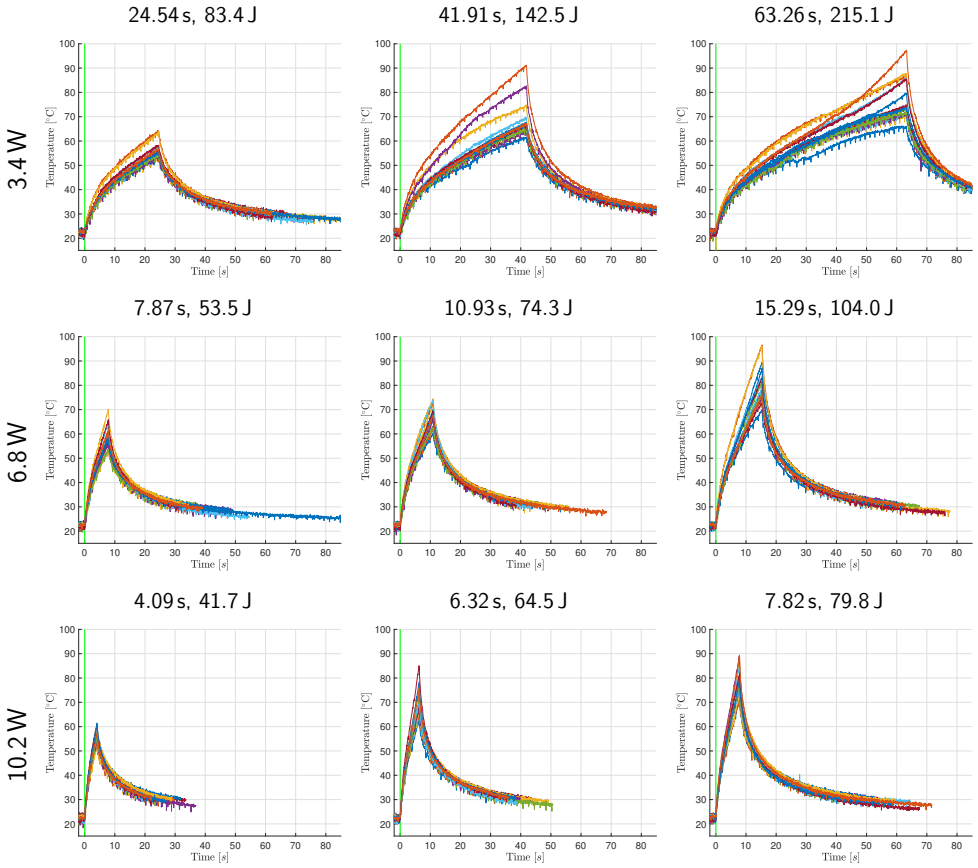


Figure 3. Temperature monitorization data of the fixed-dose application. The temperature–time response graphs (each individual sample represented with a different curve color) within each group are superimposed. The vertical green lines represent the laser emission commencement marks.

Table 3. Descriptive temperature values for the fixed-dose application: The mean (μ), standard deviation (σ), range ($max - min$), maximum (max) and minimum (min) values of the achieved tissue surface temperature at the end of laser exposure (T_{final}).

P_{laser}	$t_{exposure}$	E	$T_{final}\,(\mu \pm \sigma)$ [°C]	$T_{final\,(max)}$ [°C]	$T_{final\,(min)}$ [°C]
3.4 W	24.54 s	83.4 J	56.5 ± 3.2	64.3	53.8
	41.91 s	142.5 J	69.5 ± 7.5	91.2	61.6
	63.26 s	215.1 J	77.5 ± 8.7	97.4	66.2
6.8 W	7.87 s	53.5 J	59.0 ± 4.6	70.1	53.1
	10.93 s	74.3 J	67.8 ± 4.3	74.5	60.2
	15.29 s	104.0 J	81.0 ± 7.9	96.6	70.0
10.2 W	4.09 s	41.7 J	57.5 ± 2.9	61.4	52.2
	6.32 s	64.5 J	70.9 ± 5.5	85.1	63.0
	7.82 s	79.8 J	79.3 ± 6.1	89.4	71.0

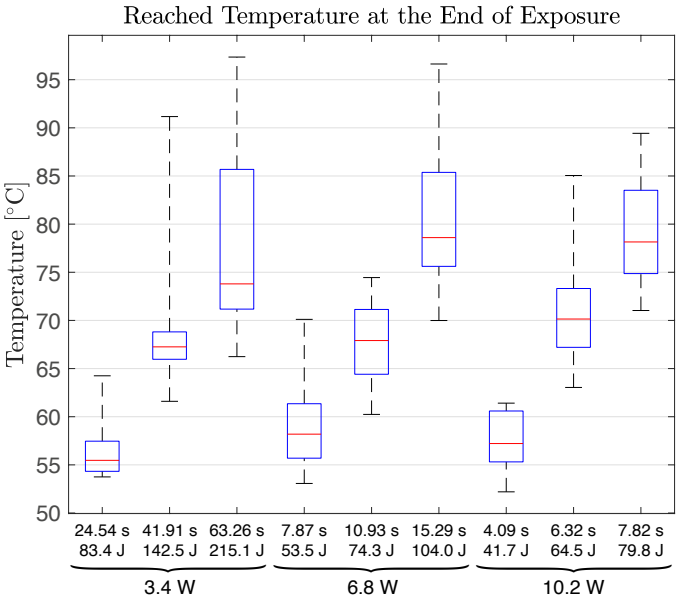


Figure 4. Box and whiskers plot of the tissue surface temperature reached at the end of exposure in the fixed-dose application. The red horizontal lines are the group medians. The blue boxes mark the interquartile ranges. The whiskers indicate the whole data range.

4. Discussion

Temperature–time responses of samples vary significantly within the same application group as depicted in Figures 2 and 3. These results confirm our initial assumptions regarding the non-uniformity of optical and thermal characteristics among subjects and show that temperature control is necessary for photothermal medical laser applications. As illustrated in Figure 2, our system can successfully control the tissue surface temperature during laser exposure. Mean tissue surface temperatures during the 5 s temperature controlled period do not deviate from the target value more than 0.6 °C on average. The maximum and minimum temperatures observed during this period also remain within a narrow range (4.1 °C on average) demonstrating the temperature stability our system can provide. This finding is also supported by the small magnitudes of the standard deviation values in Table 2.

Among a total of 144 samples in the temperature-controlled applications, only two samples of $P_{laser} = 10.2\,W$ & $T_{target} = 75\,°C$ group displayed anomalies. One sample contained fascia tissue underneath the target area, and the temperature increase caused it to contract, moving the laser irradiated surface in and out of the measurement spot. The fact that our system is a confocal *but* not a coaxial optical setup caused measurement errors due to the alteration of the target surface distance to the probe. Off-axis alignment requires a precise and constant application distance. Use of a mechanical spacer or another technology (e.g., a distance sensor) to ensure the required target to probe distance is necessary for handheld operation. The other sample experienced a high rate of temperature change (>20 °C/s) and has undergone partial carbonization at the center of the laser spot, even though the highest measured temperature was below 90 °C. Considering the Gaussian laser beam generates higher temperatures at the center of the spot, partial carbonization at that location is natural.

On the other hand, fixed-dose application results display increasing tissue surface temperatures until the end of the procedure (cessation of irradiation), as shown in Figure 3, resulting in a wide range of final temperatures within each group, as presented in Figure 4. These results prove that a fixed-dose cannot be relied upon to ensure treatment success (reaching desired temperature) while preventing excessive thermal damage in the clinical conditions due to the high temperature sensitivity of physiological effects generated in PTT.

Arrhenius temperature integral suggests that the progression of thermal damage is linear for constant tissue temperatures and exponential for linearly increasing tissue temperatures [6]. As a consequence, swiftly reaching a target value (depending on the desired physiological effect) and maintaining the tissue temperature at that value renders the progression of thermal damage a linear function of time. Our system can be used to constrain tissue surface temperature during laser exposure to control progression of thermal damage while guaranteeing the induction of desired physiological effects and preventing undesirable outcomes (e.g., carbonization, heat fixation, coagulative necrosis).

As the tissue is exposed to laser light, its temperature increases and a multitude of phenomena occur simultaneously [29]. Coagulation and denaturation of proteins change the optical properties of the tissue [6,19,30]. Moreover, the absorption coefficient of water at the ytterbium fiber laser wavelength ($\lambda_{center} \approx 1070\,\text{nm}$) decreases with increasing temperature [31]. The water content of the tissue may change due to evaporation induced dehydration (in conditions with very high temperatures or extended exposure durations). As water content decreases, thermal conductivity of tissue reduces [32]. Optical and thermal properties of the tissue dynamically change with its temperature and hydration level during laser irradiation [3,6,19].

In Figure 2, the lower laser power groups display a higher variation in their temperature increase curves. It seems that optical and thermal differences of samples dominate the temperature–time response of tissue when laser power is low. In addition, low power groups require longer to reach the target temperature. Thus, the tissue has more time to undergo the optical and thermal property changes elaborated above. The same observation and deduction are also valid, albeit to a lesser extent, for higher target temperature groups corresponding to longer exposure durations. Low power and longer duration groups in the fixed-dose application also display a higher variation in their temperature–time response curves. This resulted in higher final temperature ranges as presented in Table 3.

It is important to note that the emissivity, ϵ, can be a source of error in infrared temperature measurements. The accuracy and thus the performance of this system rely on the assumption of constant tissue emissivity that is equal to the emissivity of water. However, there is a linear relationship between the measured temperature and the fourth root of $1/\epsilon$ (inverse of emissivity), which corresponds to negligible measurement errors unless the change in emissivity is dramatic.

Another important point is that the infrared temperature measurement systems collect blackbody radiation only from the top 25–30 µm and the laser wavelength we have used ($\lambda = 1071$ nm) has a penetration depth of ca. 2–6 mm similar to Nd:YAG. This phenomenon may reduce the effectiveness of IR thermometrical laser control systems like ours and should be taken into consideration when using different irradiation wavelengths (This IR temperature measurement system should not be used with irradiation wavelengths close to or within the measurement bandwidth of 5.5–12 µm to avoid significant measurement errors). However, in the clinical setting, the perfusion of the tissue should have a cooling effect mainly below the tissue surface and we expect that the deeper tissue temperature would be lower than the surface temperature, practically eliminating the technical limitation of our system especially for laser wavelengths with less tissue penetration (until the 25 µm limit).

We have even conducted a thermal denaturation area study (available in the supplementary material) which supports our findings reported here.

Study Limitations

Even though our IRt/c system is calibrated, one limitation of this study is the lack of a secondary temperature measurement system for confirming our results. We abstained from using a contact requiring temperature measurement method to avoid changing the thermal dissipation characteristics of the tissue and interfering with the laser exposure. Unfortunately, a high resolution thermal camera with a fast temperature response was not available at hand.

5. Conclusions

The surface-temperature-controlled medical laser system developed in our laboratory is capable of ensuring the success and reproducibility of PTT modalities and patient safety even when using a sample population representative of wide optical and thermal property ranges encountered in clinical conditions. Our system successfully maintains tissue surface temperatures at required target values to induce desired thermo-physiological effects and prevents excessive thermal damage even when using different laser powers. It comprises relatively inexpensive components that perform efficiently even when using the simplest control method. It has an easy to operate, simple design that can be set up and used in the clinical environment in an appropriate enclosure without requiring complicated training. Thus, it may accelerate and enable the translation of novel photothermal laser applications currently confined to the controlled and uniform conditions of the laboratory (e.g., laser-tissue welding, PTT of granulation tissue, cartilage reshaping) into the clinic by rendering them more successful, reproducible, and safe even for a wide range of subjects which cannot be provided by manual dosimetry (surgeon's decision) or fixed-dosimetry. Additionally, researchers may use our system for investigating and developing new, and improving pre-existing, photothermal laser applications on various biological tissues by monitoring tissue surface temperature, controlling laser exposure, and facilitating gathering of information of related parameters (*i.e.*, thermal characterization of tissues).

Using the temperature monitorization capability of our system, we noticed that low laser power values accentuate the effect idiosyncratic differences of optical and thermal properties of tissues have on their temperature–time responses. This interaction between low laser power and idiosyncratic properties of tissues led to a wider range of exposure durations (required to reach target temperatures) in temperature-controlled laser irradiation.

Regulating photothermal medical laser applications by tissue temperature feedback is currently the gold standard of the trade. Our future work will focus on implementing laser power modulation and improving the control algorithm to monitor and manipulate the rate of tissue surface temperature increase. We will also conduct experiments to demonstrate the in vivo effectiveness of our system. Investigation of methods for determining tissue emissivity to ensure measurement accuracy and reliability is another course of further research.

Supplementary Materials: The following supporting information can be downloaded at: https://www.mdpi.com/article/10.3390/app13010237/s1, Figure S1: Box and whiskers plot of thermal denaturation diameters and depths; Figure S2: Exemplary bovine liver photothermal denaturation photographs; Table S1: Results of post hoc tests using Scheffe's procedure after one-way ANOVA of thermal denaturation diameter and depth values. References [33–36] are cited in the supplementary materials.

Author Contributions: Conceptualization, Ö.K. and M.G.; methodology, Ö.K. and M.G.; software, Ö.K.; formal analysis, Ö.K. and İ.D.; investigation, Ö.K. and İ.D.; resources, Ö.K. and M.G.; data curation, Ö.K.; writing—original draft preparation, Ö.K.; writing—review and editing, İ.Ç. and M.G.; visualization, Ö.K.; supervision, İ.Ç. and M.G.; project administration, Ö.K. and M.G.; funding acquisition, Ö.K. and M.G. All authors have read and agreed to the published version of the manuscript.

Funding: This research was funded internally by the Boğaziçi University Research Fund Grant No. BAP-8500 14XM2.

Institutional Review Board Statement: Ethical review and approval were waived for this study because ex vivo tissues were acquired from an abattoir.

Informed Consent Statement: Not applicable.

Data Availability Statement: The data presented in this study are available on request from the corresponding author.

Acknowledgments: The authors would like to thank Esin Öztürk Işık for guidance on statistical analysis in the study and Mehmet Emre Hatipoğlu for constructive criticism of the manuscript.

Conflicts of Interest: The authors declare no conflict of interest.

Abbreviations

The following abbreviations are used in this manuscript:

PTT	Photothermal therapy
LTW	Laser tissue welding
IRt/c	Infrared thermocouple
SNR	Signal to noise ratio
USD	United States Dollar
Near-IR	Near infrared
Nd:YAG	Neodymium-doped yttrium aluminum garnet
ZnSe	Zinc selenide
NIST	National Institute of Standards and Technology
TTL	Transistor–transistor logic
I^2C	Inter-Integrated circuit
CW	Continuous wave

References

1. Niemz, M.H., Laser-Tissue Interactions: Fundamentals and Applications. In *Laser-Tissue Interactions: Fundamentals and Applications*; 3rd ed.; Springer Science & Business Media: Berlin/Heidelberg, Germany, 2007; pp. 58–80. https://doi.org/10.1007/978-3-540-72192-5.
2. Thomsen, S.; Pearce, J.A. Thermal Damage and Rate Processes in Biologic Tissues. In *Optical-Thermal Response of Laser-Irradiated Tissue*, 2nd ed.; Welch, A.J., Van Gemert, M.J., Eds.; Springer: Dordrecht, The Netherlands, 2011; pp. 487–549. https://doi.org/10.1007/978-90-481-8831-4.
3. Valvano, J.W. Tissue thermal properties and perfusion. In *Optical-Thermal Response of Laser-Irradiated Tissue*, 2nd ed.; Welch, A.J., Van Gemert, M.J., Eds.; Springer: Dordrecht, The Netherlands, 2011; pp. 455–485. https://doi.org/10.1007/978-90-481-8831-4.
4. Poppas, D.P.; Stewart, R.B.; Massicotte, J.M.; Wolga, A.E.; Kung, R.T.; Retik, A.B.; Freeman, M.R. Temperature-controlled laser photocoagulation of soft tissue: In vivo evaluation using a tissue welding model. *Lasers Surg. Med.* **1996**, *18*, 335–344. https://doi.org/10.1002/(SICI)1096-9101(1996)18:4<335::AID-LSM2>3.0.CO;2-T.
5. Stewart, R.B.; Benbrahim, A.; LaMuraglia, G.M.; Rosenberg, M.; L'Italien, G.J.; Abbott, W.M.; Kung, R.T. Laser assisted vascular welding with real time temperature control. *Lasers Surg. Med.* **1996**, *19*, 9–16. https://doi.org/10.1002/(SICI)1096-9101(1996)19:1<9::AID-LSM2>3.0.CO;2-W.
6. Çilesiz, İ. Controlled Temperature Photothermal Tissue Welding. *J. Biomed. Opt.* **1999**, *4*, 327–336. https://doi.org/10.1117/1.429934.
7. Spector, D.; Rabi, Y.; Vasserman, I.; Hardy, A.; Klausner, J.; Rabau, M.; Katzir, A. In vitro large diameter bowel anastomosis using a temperature controlled laser tissue soldering system and albumin stent. *Lasers Surg. Med.* **2009**, *41*, 504–508. https://doi.org/10.1002/lsm.20799.
8. Tabakoğlu, H.Ö.; Gülsoy, M. In vivo comparison of near infrared lasers for skin welding. *Lasers Med. Sci.* **2010**, *25*, 411–421. https://doi.org/10.1007/s10103-009-0739-3.
9. Ishihara, M.; Arai, T.; Sato, S.; Morimoto, Y.; Obara, M.; Kikuchi, M. Measurement of the Surface Temperature of the Cornea During ArF Excimer Laser Ablation by Thermal Radiometry With a 15-Nanosecond Time Response. *Lasers Surg. Med.* **2002**, *30*, 54–59. https://doi.org/10.1002/lsm.10021.
10. Kopchok, G.E.; White, R.A.; Tabbara, M.; Saadatmanesh, V.; Peng, S.K. Holmium:YAG laser ablation of vascular tissue. *Lasers Surg. Med.* **1990**, *10*, 405–413. https://doi.org/10.1002/lsm.1900100502.
11. Schlott, K.; Koinzer, S.; Ptaszynski, L.; Bever, M.; Baade, A.; Roider, J.; Birngruber, R.; Brinkmann, R. Automatic temperature controlled retinal photocoagulation. *J. Biomed. Opt.* **2012**, *17*, 061223. https://doi.org/10.1117/1.JBO.17.6.061223.
12. Small IV, W.; Celliers, P.; Kopchok, G.; Reiser, K.; Heredia, N.; Maitland, D.; Eder, D.; London, R.; Heilbron, M.; Hussain, F.; et al. Temperature Feedback and Collagen Cross-Linking in Argon Laser Vascular Welding. *Lasers Surg. Med.* **1998**, *13*, 98–105. https://doi.org/10.1007/s101030050061.

13. Singleton, D.; Paraskevopoulos, G.; Taylor, R.; Higginson, L. Excimer laser angioplasty: Tissue ablation, arterial response, and fiber optic delivery. *IEEE J. Quantum Electron.* **1987**, *23*, 1772–1782. https://doi.org/10.1109/JQE.1987.1073231.
14. Landsberg, R.; DeRowe, A.; Katzir, A.; Shtabsky, A.; Fliss, D.M.; Gil, Z. Laser-induced hyperthermia for treatment of granulation tissue growth in rats. *Otolaryngol.—Head Neck Surg.* **2009**, *140*, 480–486. https://doi.org/10.1016/j.otohns.2008.12.004.
15. Sobol, E.; Shekhter, A.; Guller, A.; Baum, O.; Baskov, A. Laser-induced regeneration of cartilage. *J. Biomed. Opt.* **2011**, *16*, 080902. https://doi.org/10.1117/1.3614565.
16. Wong, B.J.F.; Milner, T.E.; Anvari, B.; Sviridov, A.; Omel'chenko, A.; Bagratashvili, V.V.; Sobol, E.; Nelson, J.S. Measurement of radiometric surface temperature and integrated backscattered light intensity during feedback-controlled laser-assisted cartilage reshaping. *Lasers Med. Sci.* **1998**, *13*, 66–72. https://doi.org/10.1007/BF00592961.
17. Simhon, D.; Halpern, M.; Brosh, T.; Vasilyev, T.; Ravid, A.; Tennenbaum, T.; Nevo, Z.; Katzir, A. Immediate tight sealing of skin incisions using an innovative temperature-controlled laser soldering device: In vivo study in porcine skin. *Ann. Surg.* **2007**, *245*, 206–213. https://doi.org/10.1097/01.sla.0000232554.13719.10.
18. Coad, J.E. Thermal fixation: A central outcome of hyperthermic therapies (Invited Paper). In *Proceedings of the Thermal Treatment of Tissue: Energy Delivery and Assessment III*; Ryan, T.P., Ed.; SPIE: Bellingham, WA, USA, 2005. https://doi.org/10.1117/12.591175.
19. Barton, J.K. Dynamic changes in optical properties. In *Optical-Thermal Response of Laser-Irradiated Tissue*, 2nd ed.; Welch, A.J., Van Gemert, M.J., Eds.; Springer: Dordrecht, The Netherlands, 2011; pp. 321–349. https://doi.org/10.1007/978-90-481-8831-4.
20. Lim, H.S. Reduction of thermal damage in photodynamic therapy by laser irradiation techniques. *J. Biomed. Opt.* **2012**, *17*, 128001. https://doi.org/10.1117/1.JBO.17.12.128001.
21. Grandinétti, V.d.S.; Miranda, E.F.; Johnson, D.S.; de Paiva, P.R.V.; Tomazoni, S.S.; Vanin, A.A.; Albuquerque-Pontes, G.M.; Frigo, L.; Marcos, R.L.; de Carvalho, P.d.T.C.; et al. The thermal impact of phototherapy with concurrent super-pulsed lasers and red and infrared LEDs on human skin. *Lasers Med. Sci.* **2015**, *30*, 1575–1581. https://doi.org/10.1007/s10103-015-1755-0.
22. Çilesiz, İ.; Thomsen, S.; Welch, a.J. Controlled temperature tissue fusion: Argon laser welding of rat intestine in vivo, Part One. *Lasers Surg. Med.* **1997**, *21*, 269–277. https://doi.org/10.1002/(SICI)1096-9101(1997)21:3<269::AID-LSM7>3.0.CO;2-O.
23. Çilesiz, İ.; Thomsen, S.; Welch, A.J.; Chan, E.K. Controlled temperature tissue fusion: Ho:YAG laser welding of rat intestine in vivo, Part Two. *Lasers Surg. Med.* **1997**, *21*, 278–286. https://doi.org/10.1002/(SICI)1096-9101(1997)21:3<278::AID-LSM8>3.0.CO;2-N.
24. Tunç, B.; Gülsoy, M. Tm:Fiber laser ablation with real-time temperature monitoring for minimizing collateral thermal damage: Ex vivo dosimetry for ovine brain. *Lasers Surg. Med.* **2013**, *45*, 48–56. https://doi.org/10.1002/lsm.22114.
25. Simhon, D.; Gabay, I.; Shpolyansky, G.; Vasilyev, T.; Nur, I.; Meidler, R.; Hatoum, O.A.; Katzir, A.; Hasmonai, M.; Kopelman, D. Temperature-controlled laser-soldering system and its clinical application for bonding skin incisions. *J. Biomed. Opt.* **2015**, *20*, 128002. https://doi.org/10.1117/1.JBO.20.12.128002.
26. Kaya, Ö.; Gülsoy, M. A non-contact temperature measurement system for controlling photothermal medical laser treatments. *Proc. SPIE* **2016**, *9706*, 97060K. https://doi.org/10.1117/12.2212254.
27. Whelan, W.M.; Wyman, D.R. Dynamic modeling of interstitial laser photocoagulation: Implications for lesion formation in liver in vivo. *Lasers Surg. Med.* **1999**, *24*, 202–208. https://doi.org/10.1002/(SICI)1096-9101(1999)24:3<202::AID-LSM5>3.0.CO;2-8.
28. Jacques, S.L.; Rastegar, S.; Motamedi, M.; Thomsen, S.L.; Schwartz, J.A.; Torres, J.H.; Mannonen, I. Liver photocoagulation with diode laser (805 nm) versus Nd:YAG (1064 nm). *Proc. SPIE* **1992**, *1646*, 107–117. https://doi.org/10.1117/12.137451.
29. Diller, K.R. Laser generated heat transfer. In *Optical-Thermal Response of Laser-Irradiated Tissue*, 2nd ed.; Welch, A.J., Van Gemert, M.J., Eds.; Springer: Dordrecht, The Netherlands, 2011; pp. 353–397. https://doi.org/10.1007/978-90-481-8831-4.
30. Jaywant, S.M.; Wilson, B.C.; Patterson, M.S.; Lilge, L.D.; Flotte, T.J.; Woolsey, J.; McCulloch, C. Temperature-dependent changes in the optical absorption and scattering spectra of tissues: Correlation with ultrastructure. *Proc. SPIE* **1993**, *1882*, 218–229. https://doi.org/10.1117/12.148080.
31. Mullick, S.; Madhukar, Y.K.; Kumar, S.; Shukla, D.K.; Nath, A.K. Temperature and intensity dependence of Yb-fiber laser light absorption in water. *Appl. Opt.* **2011**, *50*, 6319–6326. https://doi.org/10.1364/AO.50.006319.
32. Spells, K.E. The Thermal Conductivities of some Biological Fluids. *Phys. Med. Biol.* **1960**, *5*, 139. https://doi.org/10.1088/0031-9155/5/2/304.
33. Anderson, R.R. Polarized light examination and photography of the skin. *Arch. Dermatol.* **1991**, *127*, 1000–1005. https://doi.org/10.1001/archderm.1991.01680060074007.
34. Beatty, C.J.; Thomsen, S.L.; Vos, J.A.; Coad, J. Practical pathology for thermal tissue applications. *Proc. SPIE* **2015**, *9326*, 932602. https://doi.org/10.1117/12.2082934.
35. Thomsen, S.; Pearce, J.; Cheong, W.F. Changes in birefringence as markers of thermal damage in tissues. *IEEE Trans. Biomed. Eng.* **1989**, *36*, 1174–1179. https://doi.org/10.1109/10.42111.
36. Sherwood, M.E.; Flotte, T.J. Improved staining method for determining the extent of thermal damage to cells. *Lasers Surg. Med.* **2007**, *39*, 128–131. https://doi.org/10.1002/lsm.20450.

Disclaimer/Publisher's Note: The statements, opinions and data contained in all publications are solely those of the individual author(s) and contributor(s) and not of MDPI and/or the editor(s). MDPI and/or the editor(s) disclaim responsibility for any injury to people or property resulting from any ideas, methods, instructions or products referred to in the content.

Appl. Sci. **2022**, *1*, 0. https://doi.org/10.3390/app1010000

Supplementary Materials: Controlling laser irradiation with tissue temperature feedback enhances photothermal applications: *ex-vivo* evaluation on bovine liver

Özgür Kaya [1]*, İpek Düzgören [1], İnci Çilesiz [2] and Murat Gülsoy [1]

Analysis of the Temperature-Time Responses

Generally, the temperature-time response of our samples showed a logarithmic characteristic during the irradiation phase. We observed regions with a more abrupt change of curvature in some of the low power groups (especially 3.4 W & 65 °C and 3.4 W & 75 °C groups, corresponding to longer exposure times) leading to slight deviations from the logarithmic model. We were not able to generalize the characteristics of these changes. The change of temperature-time response curves may be due to the modifications of optical and thermal characteristics the tissues undergo at these temperature values, which are also varying among samples.

In contrast, the optical characteristics of the tissue are not relevant in the temperature decrease phase. Consequently, this phase displays an exponential decay. We expect that the temperature decrease curves mainly depend on the total heat deposited to the tissue, the thermal conductivity and dissipation characteristics of the tissue, and the temperature gradient between the measurement spot, the surrounding tissue, and the ambient environment.

In the clinical setting, we expect that the perfusion of the tissue will have a cooling effect increasing the time constant of the heating phase and decreasing the time constant of the cooling phase. Hence, we expect that the heating phase photothermal tissue characteristic differences would be exacerbated and the cooling phase thermal tissue characteristic differences would be subdued further emphasising the requirement of a tissue temperature controlled irradiation system.

Further Discussion on Fixed-Dose Results

The analysis of the achieved tissue surface temperature values at the end of the laser exposure (T_{final}) is provided in Table 3. The average final temperature standard deviation and the average final temperature range ($T_{final\,(max)} - T_{final\,(min)}$) are 5.6 °C and 19.8 °C, respectively. These values are larger than the desired target temperature windows for all photothermal laser application modalities. Hence, these results suggest that dosimetry based clinical photothermal laser applications are not viable for ensuring patient safety and treatment success.

Thermal Denaturation Experiment

Evaluation of Thermal Denaturation Area & Statistical Analysis

The use of bovine liver tissue enabled us to gauge the thermal effect of laser exposure by evaluating the extent of thermal denaturation diameter and depth. We evaluated the thermal denaturation in our samples by macroscopical inspection of color change and opacification (whitening). We photographed thermal denaturation diameter and depth of the irradiated samples using cross polarization imaging technique to eliminate reflections that can complicate the evaluation process [33]. A camera fitted with a prime macro lens and a circular polarizer (linear polarizer and quarter-wave plate combination) was placed perpendicularly at a fixed distance above the sample. The light source (flash) combined with a linear polarizer was placed at an oblique angle (45°) to further avoid surface reflections. The thermal denaturation depth images were taken after dissecting the sample along the center of the thermal denaturation zone. We used fixed magnification, shutter speed, f-number, ISO, and flash intensity for all photographs; and aligned a scale to the sample surface as a reference. A MATLAB code was composed to facilitate the blinded acquisition of manual measurements by 3 evaluators by marking the perceived thermal denaturation boundary on displayed images on a computer. We averaged the measurements of all 3 evaluators for each sample.

We performed one-way analysis of variance (ANOVA) of thermal denaturation zone measurements for each set of 3 groups with a common parameter (3 laser powers + 3 target temperatures). Scheffe's procedure was used to determine statistical differences between groups in the *post hoc*

Appl. Sci. **2022**, *1*, 0. https://doi.org/10.3390/app1010000

multiple comparison test after the one-way ANOVA conducted in MATLAB. Two-way ANOVA was performed to evaluate the interaction between laser power and target temperature on thermal denaturation zone. Significance level was set at $p < .05$ for all statistical tests.

Results of Thermal Denaturation Experiment

The thermal denaturation diameter and depth values of temperature controlled laser irradiation are provided as a box and whiskers plot in Fig. S1. Additionally, Fig. S2 depicts corresponding representative thermal denaturation area photographs.

One-way ANOVA

One-way ANOVA results indicate that during surface temperature controlled laser irradiation target temperature has a statistically significant effect on denaturation diameter ($p < .001$) and depth ($p < .005$) in all three power groups. On the other hand, laser power has a statistically significant effect on denaturation diameter only in 55 °C ($p = .015$) and 65 °C ($p = .007$) target temperature groups. Additionally, laser power has no statistically significant effect on denaturation depth in any target temperature group.

Post Hoc Test Using Scheffe's Procedure

Figure S1 contains the *post hoc* tests conducted using Scheffe's procedure for denaturation diameter ($n = 16$) and depth ($n = 13$). The mean and standard deviation values for thermal denaturation diameter and depth are also incorporated in Table S1.

Target temperature creates statistically significant differences in denaturation diameters between all groups for all laser powers. Yet, we only observe significant differences in the denaturation diameters between lowest and highest laser power groups (3.4 W and 10.2 W) for target temperatures of 55 °C and 65 °C. There is no statistically significant difference between laser power groups for 75 °C target temperature in the surface temperature controlled application.

There are statistically significant differences in denaturation depths between 55 °C and 75 °C target temperature groups for all laser powers. Additionally, there is a statistically significant difference between 65 °C and 75 °C target temperature groups for 6.8 W. There is no statistically significant difference in denaturation depths between any laser power groups for any target temperature group.

Two-way ANOVA

Two-way ANOVA results reveal that there is no interaction between target temperature and laser power using our surface temperature controlled laser irradiation system with respect to thermal denaturation diameter ($p = .996$) and depth ($p = .897$).

Discussion of Thermal Denaturation Zone

As it can be deduced from Figs. S1 and S2, and Table S1, the thermal denaturation size clearly increases with rising target temperature values for all power groups. This is expected for two reasons. First, higher target temperatures require longer exposure durations allowing more thermal energy dissipation to surrounding tissues. Second, a high temperature at the measurement spot also corresponds to a high spatio-thermal gradient resulting in faster thermal energy dissipation and expansion of the thermal damage. There is also a trend for an increase in thermal denaturation size with decreasing laser power for all target temperature groups. A low laser power results in an extended exposure duration to reach target temperature. Thus, it provides more time for heat dissipation to surrounding tissues, increasing the thermal denaturation size.

One-way ANOVA results indicate that target (surface) temperature has a statistically significant effect on denaturation diameter and depth. But, there is no statistically significant effect of laser power on denaturation diameter in 75 °C target temperature groups and on denaturation depth in any of the target temperature groups. Evaluation of the *post hoc* (multiple comparison) tests using Scheffe's procedure reveals further insight into the capabilities of our system. The most crucial interpretation is that our surface temperature controlled medical laser system can successfully regulate thermal denaturation diameter (by creating significant differences between groups) using

Appl. Sci. **2022**, *1*, 0. https://doi.org/10.3390/app1010000

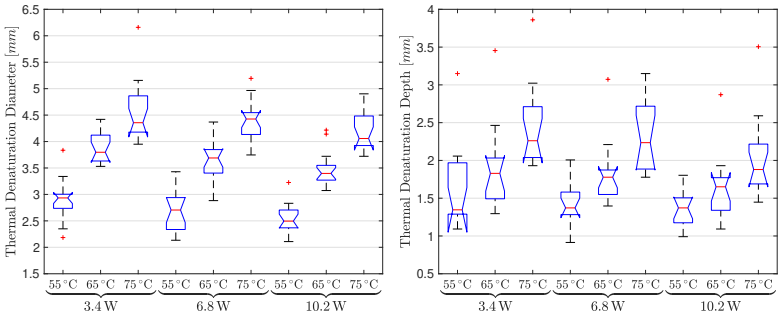


Figure S1. Box and whiskers plot of thermal denaturation diameters ($n = 16$) and depths ($n = 13$). Red horizontal lines are group medians. Blue boxes mark interquartile ranges. Red '+' signs represent outliers. Whiskers indicate most extreme data that is not an outlier.

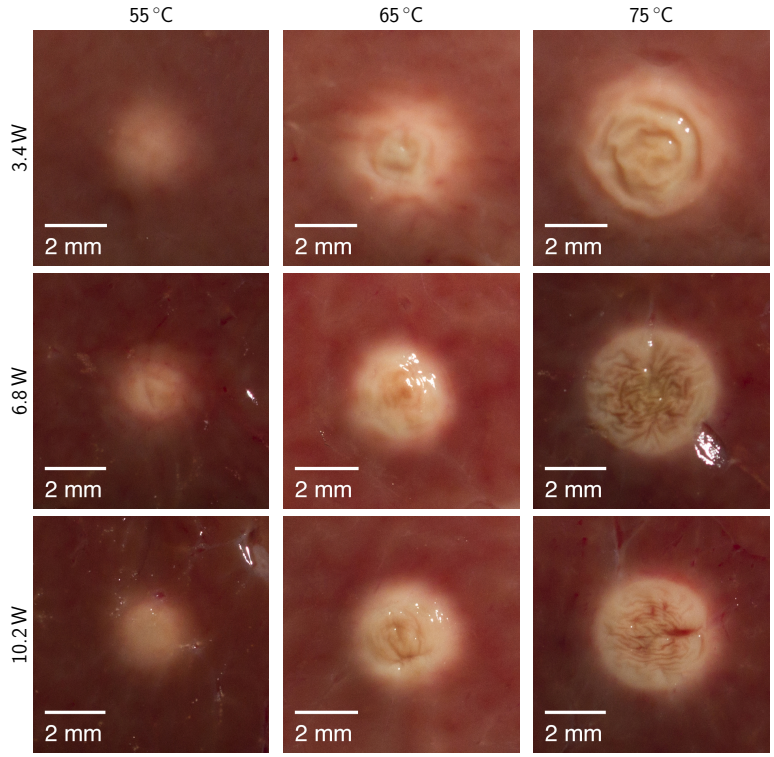


Figure S2. Exemplary bovine liver photothermal denaturation photographs.

Appl. Sci. **2022**, *1*, 0. https://doi.org/10.3390/app1010000

Table S1. Results of post hoc tests using Scheffe's procedure after one-way ANOVA of thermal denaturation diameter ($n = 16$) and depth ($n = 13$) values. Each row represents multiple comparisons conducted for the common parameter provided in the first column. Solid lines connecting two groups represent a statistically significant difference ($p < .05$).

Denaturation Diameter ($\mu \pm \sigma$) [mm]

	55 °C	65 °C	75 °C
3.4 W	2.90 ± 0.38 — $p < .001$	3.85 ± 0.28 — $p < .001$	4.52 ± 0.56
		$p < .001$	
6.8 W	2.68 ± 0.39 — $p < .001$	3.64 ± 0.38 — $p < .001$	4.37 ± 0.38
		$p < .001$	
10.2 W	2.53 ± 0.27 — $p < .001$	3.47 ± 0.32 — $p < .001$	4.18 ± 0.38
		$p < .001$	

Denaturation Depth ($\mu \pm \sigma$) [mm]

	3.4 W	6.8 W	10.2 W
55 °C	2.90 ± 0.38 — $p = .228$	2.68 ± 0.39 — $p = .454$	2.53 ± 0.27
		$p = .016$	
65 °C	3.85 ± 0.28 — $p = .216$	3.64 ± 0.38 — $p = .317$	3.47 ± 0.32
		$p = .007$	
75 °C	4.52 ± 0.56 — $p = .667$	4.37 ± 0.38 — $p = .473$	4.18 ± 0.38
		$p = .113$	

	55 °C	65 °C	75 °C
3.4 W	1.65 ± 0.56 — $p = .474$	1.93 ± 0.59 — $p = .063$	2.47 ± 0.55
		$p = .003$	
6.8 W	1.44 ± 0.28 — $p = .052$	1.85 ± 0.44 — $p = .013$	2.35 ± 0.48
		$p < .001$	
10.2 W	1.37 ± 0.23 — $p = .198$	1.68 ± 0.44 — $p = .107$	2.04 ± 0.55
		$p = .001$	

	3.4 W	6.8 W	10.2 W
55 °C	1.65 ± 0.56 — $p = .383$	1.44 ± 0.28 — $p = .897$	1.37 ± 0.23
		$p = .188$	
65 °C	1.93 ± 0.59 — $p = .918$	1.85 ± 0.44 — $p = .688$	1.68 ± 0.44
		$p = .446$	
75 °C	2.47 ± 0.55 — $p = .846$	2.35 ± 0.48 — $p = .341$	2.04 ± 0.55
		$p = .132$	

target temperature as a parameter. Additionally, it is capable of decreasing the effects of laser power on denaturation diameter and depth. Target temperature was less effective in regulating the denaturation depth. The reason for this phenomenon may be the fact that our system measures and controls tissue surface temperature.

Considering the two-way ANOVA results, we can irrefutably state that our temperature controlled laser irradiation system successfully eliminates the interaction between laser power and target temperature values (controlled variables) with respect to thermal denaturation diameter and depth. Conventional (fixed-dose) laser applications exhibit a strong interaction between these controlled variables.

The rate of temperature increase has a major role in controlling the resulting thermal effect successfully. Higher values of $^{dT}/_{dt}$ are associated with narrower gradients of thermal damage and provide more control over the denaturation area when using temperature feedback control [2,24]. The representative thermal denaturation area photographs depicted in Fig. S2 illustrate this phenomenon clearly. Higher laser power groups (corresponding to high $^{dT}/_{dt}$) exhibit a more defined thermal denaturation border than the lower laser power groups. A high $^{dT}/_{dt}$ also means reaching the target temperature faster, which enables us to minimize the exponential phase of the thermal damage progression. Conversely, a low $^{dT}/_{dt}$ allows the heat to diffuse into surrounding tissues for a longer duration (exponential phase), resulting in a less controlled thermal buildup due to the preponderate changes in optical and thermal characteristics. However, an extremely high $^{dT}/_{dt}$ value may prove hard to regulate thermally using a control system with limited response time. A momentary overshoot of tissue temperature may cause excessive thermal damage, especially when the target temperature value is high.

During surface temperature controlled application, tissues with different temperature increase curves receive different amounts of energy until the target temperature is reached. A difference in the delivered dose can lead to changes in the extent and size of thermal denaturation. The modulation of laser power to regulate the temperature-time response of tissue may be beneficial in controlling the thermal damage and the resulting denaturation zone. Dosimetry studies may reinforce efficiency and effectiveness of temperature- and temperature-change-rate-controlled medical laser systems, by providing feasible $^{dT}/_{dt}$ ranges and ideal initial laser power values specific to different tissues.

Study Limitations of Thermal Denaturation Experiment

Ideally, thermal damage is evaluated histologically with the help of staining techniques. Hematoxylin and eosin (H&E) or trichrome stains are commonly used to visualize thermally denatured collagen in tissues, which is a surrogate marker for thermal damage [34]. Collagen can also be utilized in polarization microscopy by observing loss of its birefringence due to thermal denaturation [35,36]. A recent trend for the evaluation of thermally treated tissues is viability staining methods. Tetrazolium based stains [*e.g.*, triphenyltetrazolium chloride (TTC) and nitroblue tetrazolium chloride (NBT)] interact with active cellular enzymes and mitochondrial cofactors to demarcate viable tissues [34,36]. Denaturation of these enzymes and disruption of mitochondrial processes due to thermal damage (non-viable tissues) will result in unstained (native colored) tissues.

Unfortunately, none of the above mentioned techniques were suitable for the evaluation of our samples. Liver tissues contain very little amounts of collagen ruling out H&E and trichrome staining as well as polarization microscopy techniques. Abattoir regulations in our country prevent acquisition of tissues at early stages of the process and render the tissues incompatible with viability staining methods (due to immediate cooling and prolonged acquisition time) as per the procedure described by Beatty *et al.* (2015). Therefore, we evaluated the thermal denaturation in our samples by macroscopical inspection of color change and opacification (whitening).

REFERENCES

1. Townes, C. H., *How the Laser Happened: Adventures of a Scientist*, Oxford University Press, USA, 1999.

2. Zaret, M. M., Breinin, G. M., Schmidt, H., Ripps, H., et al., "Ocular lesions produced by an optical maser (laser)," *Science*, Vol. 134, no. 3489, pp. 1525–1526, 1961.

3. Niemz, M. H., *Laser-Tissue Interactions: Fundamentals and Applications*, pp. 58–80. Berlin: Springer Science & Business Media, third, enlarged ed., 2007.

4. Cilesiz, I., Springer, T., Thomsen, S., and Welch, A. J., "Controlled temperature tissue fusion: argon laser welding of canine intestine in vitro.," *Lasers in Surgery and Medicine*, Vol. 18, pp. 325–34, Jan. 1996.

5. Poppas, D. P., Stewart, R. B., Massicotte, J. M., Wolga, A. E., et al., "Temperature-controlled laser photocoagulation of soft tissue: In vivo evaluation using a tissue welding model," *Lasers in Surgery and Medicine*, Vol. 18, no. 4, pp. 335–344, 1996. [doi:10.1002/(SICI)1096-9101(1996)18:4<335::AID-LSM2>3.0.CO;2-T].

6. Stewart, R. B., Benbrahim, A., LaMuraglia, G. M., Rosenberg, M., et al., "Laser assisted vascular welding with real time temperature control.," *Lasers in Surgery and Medicine*, Vol. 19, no. 1, pp. 9–16, 1996. [doi:10.1002/(SICI)1096-9101(1996)19:1<9::AID-LSM2>3.0.CO;2-W].

7. Cilesiz, I., Thomsen, S., Welch, A. J., and Chan, E. K., "Controlled temperature tissue fusion: Ho:YAG laser welding of rat intestine in vivo. Part two.," *Lasers in Surgery and Medicine*, Vol. 21, pp. 278–86, Jan. 1997.

8. Çilesiz, İ., Thomsen, S. and Welch, A. J., "Controlled temperature tissue fusion: argon laser welding of rat intestine in vivo, Part One," *Lasers in Surgery and Medicine*, Vol. 21, no. 3, pp. 269–277, 1997. [doi:10.1002/(SICI)1096-9101(1997)21:3<269::AID-LSM7>3.0.CO;2-O].

9. Small IV, W., Celliers, P., Kopchok, G., Reiser, K., et al. "Temperature Feedback and Collagen Cross-Linking in Argon Laser Vascular Welding," *Lasers in Surgery and Medicine*, Vol. 13, no. 2, pp. 98–105, 1998.

10. Çilesiz, İ., "Controlled temperature photothermal tissue welding," *Journal of Biomedical Optics*, Vol. 4, no. 3, pp. 327–336, 1999.

11. Bilici, T., Tabakoglu, O., Kalaycioglu, H., Kurr, A., et al., "Low-Power Skin Welding by Thulium (Tm : YAP) laser at 1980-nm," *Lasers and Electro-Optics 2009 and the European Quantum Electronics Conference. CLEO Europe - EQEC 2009. European Conference on*, Vol. 358, no. 2008, p. 34450, 2009.

12. Spector, D., Rabi, Y., Vasserman, I., Hardy, A., et al., "In vitro large diameter bowel anastomosis using a temperature controlled laser tissue soldering system and albumin stent," *Lasers in Surgery and Medicine*, Vol. 41, no. 7, pp. 504–508, 2009.

13. Tabakoğlu, H. Ö., and Gülsoy, M., "In vivo comparison of near infrared lasers for skin welding," *Lasers in Medical Science*, Vol. 25, no. 3, pp. 411–421, 2010.

14. Schlott, K., Koinzer, S., Ptaszynski, L., Bever, et al., "Automatic temperature controlled retinal photocoagulation," *Journal of Biomedical Optics*, Vol. 17, no. 6, p. 061223, 2012.

15. Ishihara, M., Arai, T., Sato, S., Morimoto, Y., et al., "Measurement of the Surface Temperature of the Cornea During ArF Excimer Laser Ablation by Thermal Radiometry With a 15-Nanosecond Time Response," *Lasers in Surgery and Medicine*, Vol. 30, no. 1, pp. 54–59, 2002.

16. Kang, H. W., Oh, J., and Welch, A. J., "Investigations on laser hard tissue ablation under various environments.," *Physics in Medicine and Biology*, Vol. 53, pp. 3381–90, June 2008.

17. Singleton, D., Paraskevopoulos, G., Taylor, R., and Higginson, L., "Excimer laser angioplasty: Tissue ablation, arterial response, and fiber optic delivery," *IEEE Journal of Quantum Electronics*, Vol. 23, pp. 1772–1782, Oct 1987.

18. Kopchok, G. E., White, R. A., Tabbara, M., Saadatmanesh, V., et al., "Holmium:yag laser ablation of vascular tissue," *Lasers in Surgery and Medicine*, Vol. 10, no. 5, pp. 405–413, 1990.

19. Landsberg, R., DeRowe, A., Katzir, A., Shtabsky, A., et al., "Laser-induced hyperthermia for treatment of granulation tissue growth in rats.," *Otolaryngology—Head and Neck Surgery*, Vol. 140, no. 4, pp. 480–486, 2009.

20. Svaasand, L., Randeberg, L., Aguilar, G., Majaron, B., et al., "Cooling efficiency of cryogen spray during laser therapy of skin," *Lasers in Surgery and Medicine*, Vol. 32, no. 2, pp. 137–142, 2003.

21. Sobol, E., Shekhter, A., Guller, A., Baum, O., "Laser-induced regeneration of cartilage," *Journal of Biomedical Optics*, Vol. 16, no. 8, p. 080902, 2011.

22. Wong, B. J. F., Milner, T. E., Anvari, B., Sviridov, A., et al., "Measurement of radiometric surface temperature and integrated backscattered light intensity during feedback-controlled laser-assisted cartilage reshaping," *Lasers in Medical Science*, Vol. 13, no. 1, pp. 66–72, 1998.

23. Wong, B. J., Milner, T. E., Harrington, A., Ro, J., et al., "Feedback-controlled laser-mediated cartilage reshaping," *Archives of Facial Plastic Surgery*, Vol. 1, no. 4, pp. 282–287, 1999.

24. Simhon, D., Halpern, M., Brosh, T., Vasilyev, T., et al., "Immediate tight sealing of skin incisions using an innovative temperature-controlled laser soldering device: in vivo study in porcine skin.," *Annals of Surgery*, Vol. 245, no. 2, pp. 206–13, 2007.

25. Coad, J. E., "Thermal fixation: a central outcome of hyperthermic therapies (invited paper)," in *Thermal Treatment of Tissue: Energy Delivery and Assessment III* (Ryan, T. P., ed.), SPIE, apr 2005.

26. Valvano, J. W., *Tissue Thermal Properties and Perfusion*, pp. 455–485. Springer, second ed., 2011.

27. Tabakoğlu, H. O., *Skin Tissue Welding with Near Infrared Lasers: Investigation of Optimal Parameters*. PhD thesis, Boğaziçi University, 2010.

28. Barton, J. K., *Dynamic Changes in Optical Properties*, pp. 321–349. Springer, second ed., 2011.

29. Sriramoju, V., and Alfano, R. R., "Management of heat in laser tissue welding using NIR cover window material.," *Lasers in Surgery and Medicine*, Vol. 43, pp. 991–7, Dec. 2011.

30. Zając, A., Podniesiński, D., Świderski, J., Kęcik, D., et al "Procedures of optical control dedicated for laser welding process of biological tissues," *Opto-Electronics Review*, Vol. 18, no. 1, pp. 48–55, 2010.

31. Cohen, M., Ravid, A., Scharf, V., Hauben, D., et al., "Temperature controlled burn generation system based on a CO2 laser and a silver halide fiber optic radiometer.," *Lasers in Surgery and Medicine*, Vol. 32, pp. 413–6, Jan. 2003.

32. Eyal, O., and Katzir, A., "Thermal feedback control techniques for transistor-transistor logic triggered CO2 laser used for irradiation of biological tissue utilizing infrared fiber-optic radiometry," *Applied Optics*, Vol. 33, no. 9, pp. 1751–1754, 1994.

33. Simhon, D., Ravid, A., Halpern, M., Çilesiz, İ., et al. "Laser soldering of rat skin, using fiberoptic temperature controlled system.," *Lasers in Surgery and Medicine*, Vol. 29, no. 3, pp. 265–73, 2001.

34. Sade, S., Eyal, O., Scharf, V., and Katzir, A.. "Fiber-optic infrared radiometer for accurate temperature measurements.," *Applied Optics*, Vol. 41, pp. 1908–14, Apr. 2002.

35. Lim, H. S., "Reduction of thermal damage in photodynamic therapy by laser irradiation techniques," *Journal of Biomedical Optics*, Vol. 17, no. 12, p. 128001, 2012.

36. Grandinétti, V. d. S., Miranda, E. F., Johnson, D. S., de Paiva, P. R. V., et al., "The thermal impact of phototherapy with concurrent super-pulsed lasers and red and infrared leds on human skin," *Lasers in Medical Science*, Vol. 30, no. 5, pp. 1575–1581, 2015.

37. Swanson, D. K., Smith, W. J., Ibrahim, T. and Wechsler, A. S., "Tissue temperature feedback control of power: the key to successful ablation.," *Innovations (Philadelphia, Pa.)*, Vol. 6, pp. 276–82, July 2011.

38. Tunç, B., and Gülsoy, M., "Tm:fiber laser ablation with real-time temperature monitoring for minimizing collateral thermal damage: ex vivo dosimetry for ovine brain," *Lasers in Surgery and Medicine*, Vol. 45, no. 1, pp. 48–56, 2013.

39. Çilesiz, İ., Thomsen, S., Welch, A. J., and Chan, E. K., "Controlled temperature tissue fusion: Ho:YAG laser welding of rat intestine in vivo, Part Two," *Lasers in Surgery and Medicine*, Vol. 21, no. 3, pp. 278–286, 1997. [doi:10.1002/(SICI)1096-9101(1997)21:3<278::AID-LSM8>3.0.CO;2-N].

40. Simhon, D., Gabay, I., Shpolyansky, G., Vasilyev, T., et al., "Temperature-controlled laser-soldering system and its clinical application for bonding skin incisions," *Journal of Biomedical Optics*, Vol. 20, no. 12, p. 128002, 2015.

41. Shah, J., Park, S., Aglyamov, S., Larson, T., "Photoacoustic imaging and temperature measurement for photothermal cancer therapy," *Journal of Biomedical Optics*, Vol. 13, no. 3, pp. 034024–034024, 2008.

42. Prasad, P. N., *Fundamentals of Light–Matter Interactions*, ch. 4, pp. 92–128. John Wiley & Sons, Ltd, 2003.

43. Niemz, M. H., *Laser-Tissue Interactions: Fundamentals and Applications*, pp. 9–43. Berlin: Springer Science & Business Media, third, enlarged ed., 2007.

44. Duck, F. A., *Physical Properties of Tissues: A Comprehensive Reference Book*, ch. 2, pp. 9–37. Academic press, 2013.

45. Thomsen, S., and Pearce, J. A., *Thermal Damage and Rate Processes in Biologic Tissues*, pp. 487–549. Springer, second ed., 2011.

46. Whelan, W. M., and Wyman, D. R., "Dynamic modeling of interstitial laser photocoagulation: Implications for lesion formation in liver in vivo," *Lasers in Surgery and Medicine*, Vol. 24, no. 3, pp. 202–208, 1999. [doi:10.1002/(SICI)1096-9101(1999)24:3<202::AID-LSM5>3.0.CO;2-8].

47. Saccomandi, P., Schena, E., Di Matteo, F. M., Pandolfi, M., "Laser interstitial thermotherapy for pancreatic tumor ablation: Theoretical model and experimental validation," in *2011 Annual International Conference of the IEEE Engineering in Medicine and Biology Society*, pp. 5585–5588, IEEE, 2011.

48. Holste, K. G., and Orringer, D. A., "Laser interstitial thermal therapy," *Neuro-oncology Advances*, Vol. 2, no. 1, p. vdz035, 2020.

49. Pang, S., Kapur, A., Zhou, K., Anastasiadis, P., et al., "Nanoparticle-assisted, image-guided laser interstitial thermal therapy for cancer treatment," *Wiley Interdisciplinary Reviews: Nanomedicine and Nanobiotechnology*, Vol. 14, no. 5, p. e1826, 2022.

50. Spells, K. E., "The thermal conductivities of some biological fluids," *Physics in Medicine and Biology*, Vol. 5, no. 2, p. 139, 1960.

51. Jaywant, S. M., Wilson, B. C., Patterson, M. S., Lilge, L. D., et al., "Temperature-dependent changes in the optical absorption and scattering spectra of tissues: correlation with ultrastructure," *Proceedings of SPIE*, Vol. 1882, pp. 218–229, 1993.

52. Mullick, S., Madhukar, Y. K., Kumar, S., Shukla, D. K., et al., "Temperature and intensity dependence of yb-fiber laser light absorption in water," *Applied Optics*, Vol. 50, pp. 6319–6326, December 2011.

53. Diller, K. R., *Laser Generated Heat Transfer*, pp. 353–397. Springer, second ed., 2011.

54. Çilesiz, İ., *The Value of Infrared Radiometry to Medical Laser Applications with an Outlook to Temperature Feedback and Tissue Welding Options*, pp. 18–24. Springer Berlin Heidelberg, 2001.

55. Webster, J. G., *Medical Instrumentation: Application and Design*, pp. 69–74. John Wiley & Sons, 2009.

56. Webster, J. G., and Eren, H., *Measurement, Instrumentation, and Sensors Handbook: Spatial, Mechanical, Thermal, and Radiation Measurement*, CRC Press, 2 ed., 2014.

57. Palmer, J. M., and Grant, B. G., *The Art of Radiometry*, SPIE Press Bellingham, WA, USA, 2010.

58. Wikipedia Commons, "File:wiens law.svg - wikimedia commons," 2015.

59. Xiao, Y., Wan, C., Shahsafi, A., Salman, J., et al. "Depth thermography: Noninvasive 3d temperature profiling using infrared thermal emission," *ACS Photonics*, Vol. 7, no. 4, pp. 853–860, 2020.

60. Gabay, I., Abergel, A., Vasilyev, T., Rabi, Y., et al., "Temperature-controlled two-wavelength laser soldering of tissues.," *Lasers in Surgery and Medicine*, Vol. 43, pp. 907–913, Nov. 2011.

61. Lahiji, G., and Wise, K., "A batch-fabricated silicon thermopile infrared detector," *IEEE Transactions on Electron Devices*, Vol. 29, pp. 14–22, Jan. 1982.

62. "Melexis product datasheet." Retrieved from `http://www.melexis.com/`, on 14.06.2014.

63. "Standard optical filters: Wide band & uncoated," tech. rep., Dexter Research Inc., Retrieved from `http://dexterresearch.com/?module=Page&sID=technical-library`, on 09.06.2014, 2014.

64. "Thorlabs product calatog v.21." Retrieved from `http://www.thorlabs.de/`, on 09.06.2014.

65. Jacques, S. L., Rastegar, S., Motamedi, M., Thomsen, S. L., et al., "Liver photocoagulation with diode laser (805 nm) versus Nd:YAG (1064 nm)," *Proceedings of SPIE*, Vol. 1646, pp. 107–117, 1992.

66. Kaya, Ö., and Gülsoy, M., "A non-contact temperature measurement system for controlling photothermal medical laser treatments," *Proceedings of SPIE*, Vol. 9706, p. 97060K, 2016.

67. Beatty, C. J., Thomsen, S. L., Vos, J. A., and Coad, J., "Practical pathology for thermal tissue applications," *Proceedings of SPIE*, Vol. 9326, pp. 932602–932602–8, 2015.

68. Thomsen, S., Pearce, J., and Cheong, W.-F., "Changes in birefringence as markers of thermal damage in tissues," *IEEE Transactions on Biomedical Engineering*, Vol. 36, no. 12, pp. 1174–1179, 1989.

69. Sherwood, M. E., and Flotte, T. J., "Improved staining method for determining the extent of thermal damage to cells," *Lasers in Surgery and Medicine*, Vol. 39, no. 2, pp. 128–131, 2007.

70. Anderson, R. R., "Polarized light examination and photography of the skin," *Archives of Dermatology*, Vol. 127, no. 7, pp. 1000–1005, 1991.